Master's Thesis

Characterization and Analysis of Brazed Aluminum-Zinc Coated Steel Joints

A thesis in the field of Materials sciences for the

Degree in Master of Mechanical Engineering

Author: Farrukh Hussain

Student ID: s300779

Supervisor: Dr. Graziano Ubertalli

Co-Supervisor: Dr. Sara Ferraris

Date: 11 December 2023

Summary

The automotive industry constitutes an important pillar in the world economy and has drastically changed how people live and work in a way that was unimaginable in the past. Automotive industry in Italy as well plays a key role in its economic development given the jobs it provides in entire value chain from design of components to the manufacturing of finished products. Although critical and essential in today's world, industry is under tremendous pressure to optimize its performance and efficiency to keep up with high standards in terms of the environment and achieve fuel efficiency. One of the key factors affecting these indicators is the weight of a vehicle which consequently requires more fuel consumption and hence more harmful gases. The motivation to replace high strength heavy material with combination of lightweight aluminum with steel while keeping the strength and integrity of the components greatly solves these challenges. Additionally, this technique equally benefits the EV sector which would result in more efficient battery consumption. However, the challenge lies in optimal joining of lightweight aluminum to more heavy high strength steel without any compromises.

This thesis is an effort in the same sense to test joining zinc coated steel with aluminum alloys using brazing technique under different conditions of brazing. The experimental activity investigated the possibility of joining AL-6016 alloy with zinc coated steel and pure zinc as a brazing alloy with and without the application of aluminum flux. The Joining area and reaction side is investigated with optical microscope, SEM, EDS, and micro hardness test. XRD technique has also been exploited to find residual stresses in the materials and find phase constituents on the reaction side of samples. Joining was achieved in both cases, however discontinuities were observed which were different in each case. Better joining between aluminum side and brazing alloy was observed in case of flux while joining was more continuous towards zinc coated steel with brazing alloy when flux was not used.

Acknowledgement

As I approach the culmination of my master's degree, with the submission of this thesis, I am filled with the conviction that the quest for wisdom and knowledge is a perpetual journey, one that I am committed to pursuing beyond this degree. My gratitude extends deeply to the Department of Mechanical and Aerospace Engineering (DIMEAS) at the Politecnico di Torino, a prestigious institution that has not only facilitated my academic pursuits but has also been instrumental in the honing of my skills. The opportunity to be part of such a diverse and dynamic academic community has been transformative, which has enabled me to forge connections with some of the most innovative and inspiring minds.

I extend my profound gratitude to my esteemed supervisors, Dr. Graziano Ubertalli and Dr. Sara Ferraris of the Department of Applied Science and Technology (DISAT) at the Politecnico di Torino for their unwavering support and insightful guidance through challenging and learning phases of this thesis.

I am also indebted to my dear friends, Ubaid and Talal, whose encouragement and support have been a source of strength throughout this thesis and entire course of my degree. Above all, my heartfelt thanks go to my family whose boundless love and belief in me have been the guiding lights of my life's journey. It is to them that I dedicate the fruits of this work; for they have nurtured my aspirations and celebrated my achievements with an unwavering faith that has carried me through to this momentous milestone.

Table Of Contents

1. INTRODUCTION 12

1.1 MOTIVATION 12

1.2 OBJECTIVE 15

2. STATE OF THE ART 17

2.1 JOINING PROCESS OF DISSIMILAR MATERIALS 17

2.2 WELDING TECHNIQUES - ALUMINUM ALLOYS TO STEEL 18

2.2.1 FUSION WELDING 19

2.2.1.1 MIG TIG WELDING 20

2.2.1.2 RESISTANCE SPOT WELDING 22

2.2.1.3 LASER BEAM WELDING 24

2.2.2 SOLID STATE WELDING 26

2.2.2.1 MAGNETIC PULSE WELDING 27

2.2.2.2 ROLL BONDING 28

2.2.2.3 FRICTION STIR WELDING 28

2.2.2.4 ULTRASONIC WELDING 30

2.2.2.5 OTHER WELDING TECHNIQUES 32

2.3 MECHANICAL JOINING - ALUMINUM ALLOY TO STEEL 34

2.3.1 SELF-PIERCING RIVETS 34

2.3.1.1 ALUMINUM AND STEEL SHEETS JOINED BY SELF-PIERCING RIVETS. 35

2.3.2 MECHANICAL CLINCHING 36

2.3.2.1 ALUMINUM AND STEEL SHEETS JOINING BY CLINCHING. 36

2.3.3 HEMMING 38

2.4 BRAZING– ALUMINUM ALLOY TO STEEL. 39

2.4.1 ROLE OF SURFACE ACTIVATION OF ALUMINUM SUBSTRATE 40

2.4.2 ROLE OF ZINC AS BRAZING ALLOY 43

2.5 XRD TECHNIQUE FOR RESIDUAL STRESSES AND PHASE DETECTION 46

2.5.1 XRD METHODOLOGY 47

2.5.2 Residual Stresses 49
2.5.3 Phase Detection by XRD 50
3. EXPERIMENTAL WORK 52
3.1 Materials 52
3.1.1 Aluminum 6016 52
3.1.2 Low Carbon Zinc Coated Steel 53
3.1.3 Other Materials 53
3.2 Methodology 54
3.2.1 Samples Cutting 54
3.2.2 XRD Machine Setup for Calculation of Residual Stresses 55
3.2.3 Residual Stresses on Exterior side with XRD 58
3.2.3.1 Parameters Selection for Samples 58
3.2.4 Surface Preparation and removal of oxide layer 59
3.2.5 Etching of Aluminum Only (Without Flux Brazed Sets Only) 61
3.2.6 Ultrasonic cleaning in Ethanol and Drying 62
3.2.7 Application of Flux (With Flux Brazed Sets Only) 63
3.2.8 Stacking of samples for Brazing 64
3.2.9 Furnace Brazing 65
3.2.10 Evaluation of Residual Stresses 67
3.2.11 Resin Mounting and Traversal Cutting 67
3.2.12 Polishing Operations 68
3.2.13 Optical Microscopy 69
3.2.14 Micro Hardness Test 70
3.3 Other Experiments 71
3.3.1 Scanning Electron Microscopy / Energy Dispersive Spectrometry 71
3.32 Phase constituents by XRD 74
4. RESULTS AND DISCUSSIONS 74
4.1 Optical Microscopy 75
4.1.1 Sample 1-3 (Set 1: Samples with Flux) 76

4.1.2 Sample 5 (successful joint without flux from set 2) 78
4.1.3 Sample 4 (Failed sample without flux) 80
4.2 SEM and EDS Analysis 82
4.2.1 Joining Area Analysis 82
4.2.1.1 Sample 1 (With Flux) 82
4.2.1.2 Sample 2 (Without Flux) 88
4.2.2 Failed Sample Analysis 95
4.3 XRD Analysis of Residual Stresses 100
4.3.1 Residual Stresses in Al-6016 100
4.3.2 Residual Stresses in zinc coated steel. 104
4.4 Phase Detections by XRD (Failed Samples) 107
4.4.1 Phase Detection by XRD for Zn Coated Steel 108
4.4.2 Phase Detection by XRD for Aluminum 109
4.5 Micro Hardness test 110
4.5.1 Micro Hardness Test (Sample with Flux) 110
4.5.2 Microhardness Test (Sample without Flux) 111
CONCLUSION 113
BIBLIOGRAPHY 116

List Of Figures

FIGURE 1. AUTOMOTIVE COMPONENT WEIGHT STATISTICS [1]..... 12

FIGURE 2. MATERIAL DISTRIBUTION IN A LIGHT CAR BODY [6]..... 13

FIGURE 3: DISSIMILAR MATERIALS JOINING TECHNIQUES [5]..... 18

FIGURE 4: DUAL PHASE DIAGRAM OF FE-AL [12] 20

FIGURE 5: SCHEMATIC OF TIG BRAZED WELDING OF AL STEEL [14]..... 21

FIGURE 6: CRACK INITIATION AND PROPAGATION ON INTERFACIAL IMC LAYER [14] 21

FIGURE 7: MIG BRAZED WELDING WITH AL AND GALVANIZED STEEL [15]..... 22

FIGURE 8: SCHEMATIC OF RESISTANCE SPOT WELDING 22

FIGURE 9: AL-ZN BINARY PHASE DIAGRAM WITH EUTECTIC POINT [19]..... 23

FIGURE 10: PROCESS AND AES SCAN OF WELD ZONE [18] 23

FIGURE 11: (A) SCHEMATIC OF BIMETALLIC SPOT WELDING (B) SECTION WITH BIMETALLIC INTERLAYER 40 % AL ALLOY AND 60% STEEL [20]..... 24

FIGURE 12: SCHEMATIC OF KEYHOLE LASER WELDING SET UP [21]..... 25

FIGURE 13: (A) CONDUCTION MODE LASER WELDING (B) PROCESS DEPICTION AT CROSS SECTION 25

FIGURE 14: SCHEMATIC SETUP OF FILLER METAL LASER WELDING IN LAP CONFIGURATION [24] 26

FIGURE 15: MAGNETIC PULSE WELDING COIL DESIGN (A) T SHAPE (B) E SHAPE [25] 27

FIGURE 16: SCHEMATIC OF FRICTION STIR WELDING OF AL TO STEEL ALONG WITH CROSS SECTION VIEW OF PERPENDICULAR WELD SURFACE [30] 29

FIGURE 17: RELATIONSHIP BETWEEN PIN OFF SET AND SPEED AND TENSILE STRENGTH [30]..... 30

FIGURE 18: SETUP FOR ULTRASONIC WELDING OF ALUMINUM TO STEEL [32]..... 31

FIGURE 19: RELATIONSHIP BETWEEN WELD STRENGTH AND VIBRATION AMPLITUDE AND INPUT POWER [35] .. 32

FIGURE 20: SCHEMATIC OF EXPLOSIVE BONDING BETWEEN ALUMINUM AND STEEL [36] 33

FIGURE 21: CONFIGURATION OF FRICTION BIT JOINING TECHNIQUE [25] 33

FIGURE 22: JOINING PROCESS OF METALLIC SHEETS BY SELF-PIERCING RIVETS [38]..... 34

FIGURE 23: SPR JOINING OF MULTIPLE SHEETS [40] 35

FIGURE 24: MECHANICAL CLINCHING PROCESS OF METALLIC SHEETS JOINING [40] 36

FIGURE 25: FACTURES IN STEEL SHEETS WITH CONVENTIONAL DIE AND CLINCHING [42] 37

FIGURE 26: RELATION BETWEEN TENSILE STRENGTH OF LOWER PLACED STEEL SHEET AND INTERLOCK [43] 37

FIGURE 27: HEMMING STAGES [45] 38

FIGURE 28: REDUCTION OF TENSILE STRESS CRACKS DUE TO STOPPER 38
FIGURE 29: SCHEMATIC OF SETUP FOR SURFACE ACTIVATION OPTIMIZATION [51] 41
FIGURE 30: OPTICAL MICROSCOPE IMAGES OF THE TRANSVERSE SECTION OF THE SAMPLES (NO ETCHING): (A) ZN AS RAZING MATERIAL; (B) ZAMA AS BRAZING MATERIAL. [51] 42
FIGURE 31: SCHEMATIC VIEW OF LWB PROCESS [51] 44
FIGURE 32: SURFACE MORPHOLOGIES OF THE JOINTS PRODUCED BY LASER WELDING WITHOUT FILLER POWDER AND WITH FILLER POWDER [51] 45
FIGURE 33: DIFFRACTION OF X RAY BY A CRYSTALLINE STRUCTURE [52] 48
FIGURE 34: XRD SCAN FOR PEAK SHIFTING AT DIFFERENT PSI ANGLES. 50
FIGURE 35: RELATIONSHIP BETWEEN D AND $\sin^2\Psi$ 50
FIGURE 36: XRD FOR PHASE DETECTION 51
FIGURE 37: ALUMINUM FLUX AL6 54
FIGURE 38: CUTTING MACHINE AND ALUMINA BLADE. 54
FIGURE 39: SAMPLES AFTER CUTTING. 55
FIGURE 40: RIGAKU GEIGERFLEX XRD MACHINE 56
FIGURE 41: RELATIONSHIP BETWEEN SIN 2THETA AND THETA 56
FIGURE 42: SAMPLE HOLDER USING POLYMER CLAY FOR XRD MACHINE. 57
FIGURE 43: XRD SCAN OF STEEL FOR PEAK SELECTION 57
FIGURE 44: XRD PROCEDURE 58
FIGURE 45: P320 ABRASIVE PAPER 61
FIGURE 46: ETCHING OF AL-6016 WITH 12% HNO3 61
FIGURE 47: ULTRASONIC CLEANING IN ETHANOL 62
FIGURE 48: COMPRESSED AIR GUN FOR DRYING 63
FIGURE 49: SAMPLES BEFORE STACKING. 63
FIGURE 50: APPLICATION OF FLUX ON ALUMINUM 64
FIGURE 51: STACKING ORIENTATION OF SAMPLES 65
FIGURE 52: PRESSING OF STACK WITH MECHANICAL PRESSER 65
FIGURE 53: TUBULAR FURNACE WITH ATTACHMENT TO ARGON CYLINDER 66
FIGURE 54: PLACEMENT OF SAMPLES IN DIE FOR RESIN MOUNTING 67
FIGURE 55: RESIN MOUNTING AND TRAVERSE CUTTING PROCESS 68

FIGURE 56: POLISHING MACHINE 69
FIGURE 57: OPTICAL MICROSCOPE 70
FIGURE 58: MICROHARDNESS TEST MACHINE 71
FIGURE 59: SAMPLE PLACEMENT IN VACUUM CHAMBER OF SEM MACHINE 72
FIGURE 60: SCHEMATICS OF SEM WORKING [48] 73
FIGURE 61: XRAY SPECTRAL BY EDS 74
FIGURE 62: ZINC COATING THICKNESS ON STEEL OPPOSITE TO REACTION SIDE 76
FIGURE 63: OPTICAL MICROSCOPE IMAGE OF TRAVERSE SECTION OF SET 1 SAMPLES A) & B) SHOWING JOINING AREA WHILE C) & D) SHOWING DISCONTINUITY ON STEEL SIDE. 76
FIGURE 64: OPTICAL MICROSCOPE IMAGE OF TRAVERSE SECTION OF SET 1 AT HIGHER MAGNIFICATION. 77
FIGURE 65: LOCALIZATION OF BRAZING MATERIAL ON PERIMETER 78
FIGURE 66: OPTICAL MICROSCOPE SCAN OF TRAVERSAL SECTION SHOWING DISCONTINUITY. 78
FIGURE 67: OPTICAL MICROSCOPE SCAN OF TRAVERSAL SECTION SHOWING JOINING AT DIFFERENT MAGNIFICATIONS. 79
FIGURE 68: BRAZING ALLOY ZINC PHASES 79
FIGURE 69: RESIN MOUNTING AND POLISHING OF TRAVERSE CROSS SECTION OF FAILED SAMPLE 80
FIGURE 70: AL-6016 TRAVERSE CROSS SECTION SCAN AFTER FAILED JOINING (TOP SIDE REACTION LAYER) 80
FIGURE 71: ZN COATED STEEL TRAVERSE CROSS SECTION SCAN AFTER FAILED JOINING. 81
FIGURE 72: SCANNING ELECTRON MICROSCOPY-ENERGY DISPERSIVE SPECTROSCOPY (SEM-EDS) ANALYSIS OF JOINING AREA OF TRAVERSAL CROSS SECTION OF SAMPLE WITH FLUX. 82
FIGURE 73: SEM-EDS ANALYSIS OF JOINING AREA OF TRAVERSAL CROSS SECTION OF SAMPLE WITH FLUX. 83
FIGURE 74: SEM-EDS ANALYSIS OF JOINING AREA OF TRAVERSAL CROSS SECTION OF SAMPLE WITH FLUX SHOWING CONTINUITY OF REACTION LAYER. 83
FIGURE 75: SEM-EDS ANALYSIS OF JOINING AREA OF TRAVERSAL CROSS SECTION OF SAMPLE WITH FLUX. 84
FIGURE 76: SEM-EDS ANALYSIS OF JOINING AREA OF TRAVERSAL CROSS SECTION OF SAMPLE WITH FLUX SHOWING INTERFACE LAYER BETWEEN AL AND ZN. 84
FIGURE 77: SEM-EDS ANALYSIS OF JOINING AREA OF TRAVERSAL CROSS SECTION OF SAMPLE WITH FLUX SHOWING LOCAL CHEMICAL COMPOSITION OF BASE MATERIALS. 85
FIGURE 78: SEM-EDS ANALYSIS OF JOINING AREA OF TRAVERSAL CROSS SECTION OF SAMPLE WITH FLUX SHOWING LOCAL CHEMICAL COMPOSITION ON INTERFACES AND IN JOINING AREA. 85
FIGURE 79: SEM-EDS ANALYSIS OF JOINING AREA OF TRAVERSAL CROSS SECTION OF SAMPLE WITH FLUX SHOWING LOCAL COMPOSITION OF JOINING AREA WITH TWO DIFFERENT PHASES. 86

FIGURE 80: SEM-EDS ANALYSIS OF JOINING AREA OF TRAVERSAL CROSS SECTION OF SAMPLE WITH FLUX SHOWING CRYSTALLINE MORPHOLOGY IN JOINING AREA. 86

FIGURE 81: SEM-EDS ANALYSIS OF JOINING AREA OF TRAVERSAL CROSS SECTION OF SAMPLE WITH FLUX SHOWING LOCAL CHEMICAL COMPOSITION ON INTERFACE LAYER BETWEEN STEEL AND ZN. 87

FIGURE 82: SEM-EDS ANALYSIS OF JOINING AREA OF TRAVERSAL CROSS SECTION OF SAMPLE WITHOUT FLUX SHOWING CONTINUITY OF REACTION LAYER. 89

FIGURE 83: SEM-EDS ANALYSIS OF JOINING AREA OF TRAVERSAL CROSS SECTION OF SAMPLE WITHOUT FLUX SHOWING LOCAL CHEMICAL COMPOSITION ON INTERFACE BETWEEN STEEL AND ZN. 89

FIGURE 84: SEM-EDS ANALYSIS OF JOINING AREA OF TRAVERSAL CROSS SECTION OF SAMPLE WITHOUT FLUX SHOWING LOCAL CHEMICAL COMPOSITION ON INTERFACE BETWEEN AL AND ZN. 90

FIGURE 85: SEM-EDS ANALYSIS OF JOINING AREA OF TRAVERSAL CROSS SECTION OF SAMPLE WITHOUT FLUX. 90

FIGURE 86: SEM-EDS ANALYSIS OF JOINING AREA OF TRAVERSAL CROSS SECTION OF SAMPLE WITHOUT FLUX AT HIGHER MAGNIFICATION OF AL AND ZN INTERFACE. 91

FIGURE 87: SEM-EDS ANALYSIS OF JOINING AREA OF TRAVERSAL CROSS SECTION OF SAMPLE WITHOUT FLUX AT HIGHER MAGNIFICATION OF AL AND ZN INTERFACE. 91

FIGURE 88: SEM-EDS ANALYSIS OF JOINING AREA OF TRAVERSAL CROSS SECTION OF SAMPLE WITHOUT FLUX SHOWING INTERFACE LAYER THICKNESS BETWEEN STEEL AND ZN. 92

FIGURE 89: SEM-EDS ANALYSIS OF JOINING AREA OF TRAVERSAL CROSS SECTION OF SAMPLE WITHOUT FLUX SHOWING LOCAL CHEMICAL COMPOSITION AT DIFFERENT AREAS AROUND AL-ZN INTERFACE. 92

FIGURE 90: SEM-EDS ANALYSIS OF JOINING AREA OF TRAVERSAL CROSS SECTION OF SAMPLE WITHOUT FLUX SHOWING LOCAL CHEMICAL COMPOSITION IN AL-ZN INTERFACE. 93

FIGURE 91: SEM-EDS ANALYSIS OF JOINING AREA OF TRAVERSAL CROSS SECTION OF SAMPLE WITHOUT FLUX SHOWING LOCAL CHEMICAL COMPOSITION AL-ZN INTERFACE. 93

FIGURE 92: SEM-EDS ANALYSIS OF JOINING AREA OF TRAVERSAL CROSS SECTION OF SAMPLE WITHOUT FLUX SHOWING LOCAL CHEMICAL COMPOSITION OF JOINING AREA. 94

FIGURE 93: SEM EDS SCAN OF ALUMINUM SUBSTRATE (1) 96

FIGURE 94: SEM EDS SCAN OF ALUMINUM SUBSTRATE (2) 96

FIGURE 95: SEM EDS SCAN OF ALUMINUM SUBSTRATE (3) 97

FIGURE 96: SEM EDS SCAN OF ZINC COATED STEEL SUBSTRATE (1) 98

FIGURE 97: SEM EDS SCAN OF ZINC COATED STEEL SUBSTATE (2) 98

FIGURE 98: SEM EDS SCAN OF ZINC COATED STEEL SUBSTRATE (3) 99

FIGURE 99: SEM EDS SCAN OF ZINC COATED STEEL SUBSTRATE (4) 99

FIGURE 100: XRD SCAN OF ALUMINUM SAMPLE 2 AT PHI-0 AND PHI-90 101
FIGURE 101: RELATIONSHIP BETWEEN D AND SIN Φ^2 FOR ALUMINUM (STRAIGHT LINE APPROXIMATION) 101
FIGURE 102: RELATIONSHIP BETWEEN D AND SIN Φ^2 FOR ALUMINUM (ELLIPTIC APPROXIMATION) 102
FIGURE 103: RESIDUAL STRESSES AL-6016 103
FIGURE 104: XRD SCAN OF ZINC COATED STEEL SAMPLE 1 WITH ZINC PEAK 105
FIGURE 105:RELATIONSHIP BETWEEN D AND SIN Φ2FOR ZINC COATED STEEL (LINE APPROXIMATION) 105
FIGURE 106: RELATIONSHIP BETWEEN D AND SIN Φ^2 FOR ZINC COATED STEEL (ELLIPTIC APPROXIMATION) . 106
FIGURE 107: RESIDUAL STRESSES IN ZINC COATED STEEL 107
FIGURE 108: XRD SCAN OF ZN COATED STEEL REACTION SIDE AFTER FAILED BRAZING 108
FIGURE 109: XRD SCAN OF ZINC COATED STEEL BEFORE BRAZING. 109
FIGURE 110: XRD SCAN OF ALUMINUM REACTION SIDE AFTER FAILED BRAZING 109
FIGURE 111: MICRO HARDNESS TEST ON SAMPLE WITH FLUX 110
FIGURE 112: MICRO HARDNESS TEST WITH SAMPLE WITHOUT FLUX 111
FIGURE 113: TREND OF MICROHARDNESS IN JOINING CROSS SECTION. 112

1. Introduction

1.1 Motivation

In recent decades, harmful emissions from vehicles have had a negative impact on the environment and human health. Increased air pollution due to traffic in the automotive industry has prompted many government agencies to enact strict car regulations on manufacturers to reduce harmful emissions below the permitted limits.

Strict regulations and severe penalties imposed by government agencies put tremendous pressure on automakers to explore different methods and technologies that help reduce emissions. Weight reducing is a popular strategy used by various automakers and OEMs which can significantly reduce fuel consumption and CO_2 emissions. A lighter car uses less fuel because there is less power required to overcome its inertia, hence achieving better fuel efficiency, and resulting in lower carbon emissions. Generally, around 80% of vehicle weight is contributed by chassis, powertrain, body, and exterior components [1] . Hence these parts call for more research to make them lightweight while keeping strength required.

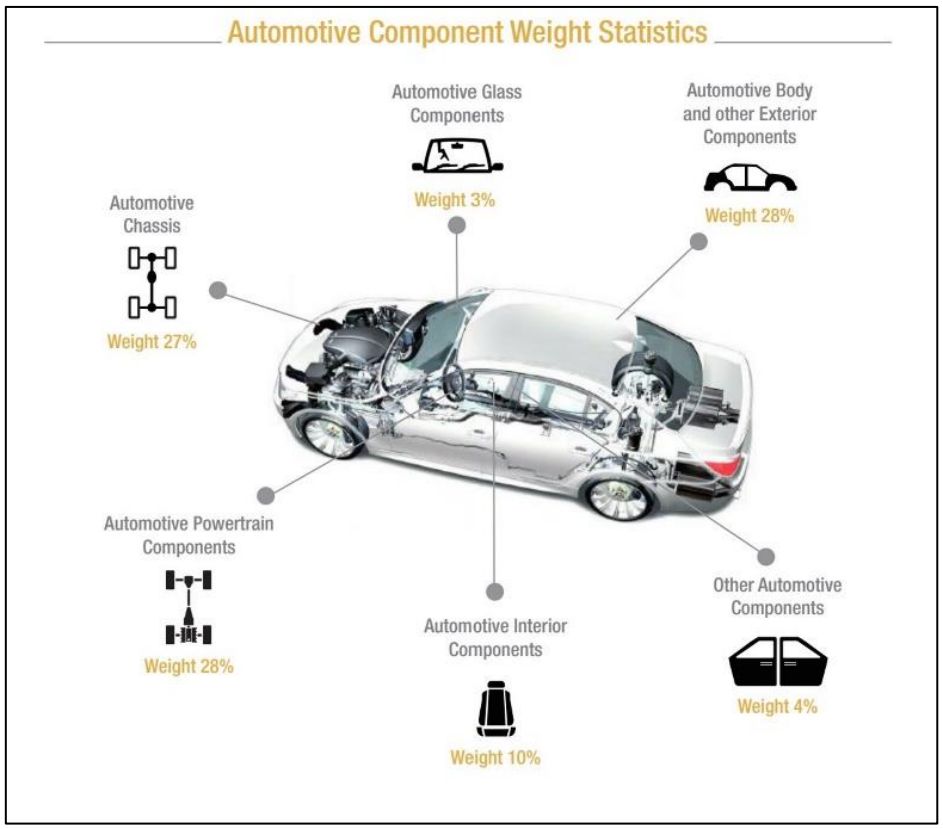

Figure 1. Automotive Component Weight Statistics [1]

While other research trying to combat environmental challenges like synthetic engineered fuel only finds application in fuel driven vehicles, weight reduction equally affects all types of vehicles whether fuel driven or electric vehicles. Generally, a 10% reduction in weight results in a 6% enhancement in fuel economy [1]. In electric vehicles the weight of many IC vehicles is offset by battery weights. Similarly, in the case of EV a 10% weight reduction can provide 14% increase in battery range [2].

At the start of the automotive industry many materials were considered for specific parts in vehicles. Steel was a prominent choice due to its low cost, high strength, ability to modify sheets at room temperature and robust spot welding. However, this technique incurred wight penalties and soon aluminum and magnesium found their ways into the manufacturing and replacing components. Now a days design is optimized for the right material in the right form for each part [3]. In modern car industry, multi material use is a common practice to gain the benefits of each material in a specific application such as structured steel in frames, aluminum alloys in bumper beams to ensure lightweight and provide support in crashworthiness, and composite sheets at some parts to provide high stiffness [5].

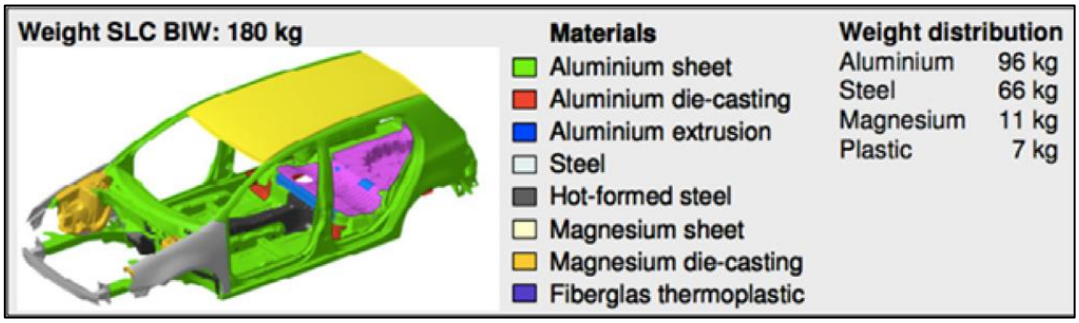

Figure 2. material Distribution in a light car body [5]

Engineering challenge lies in enabling optimum joining of dissimilar materials especially aluminum and steel in automotive industry which ensures guarantees required strength for mixed material structures. Dissimilar materials can be considered as materials combinations which pose challenges in joining mainly due to different elemental composition or high differences in physical properties [6]. However, joining dissimilar metals not only results in weight reduction but also provides product flexibility to use each material in an efficient and functional manner. Many technologies are in practice for joining dissimilar metals with their own advantages and limitations such as mechanical joints to include threaded fasteners, clinching, friction stir blind

riveting and self-piercing rivets etc. Chemical joining process includes adhesion while thermal fusion processes account for electric arc welding, plasma sintering, high energy beam welding, brazing, and soldering [4].

This thesis investigates the methodologies of joining aluminum alloys with steel with focus on joining zinc coated low carbon steel with aluminum alloy using Al-6016 with the help of pure zinc as a brazing alloy and provide recommendation for its application at industrial level.

1.2 Objective

Improvement of fuel consumption dictates reduction in weight while at the same time collision safety requires enhanced thickness of sheets which inherently requires more weight. To satisfy both needs, aluminum alloy sheets along with high strength steels are increasingly being integrated in the automotive industry. These trends such as lightness, greater performance and functionality dictate the use of multi-material constructions. The properties of each material are utilized to achieve desired product performance. This process also poses many challenges due to the same or different chemical and physical properties of each material. Conventional methods have been in use, but they have their shortcomings in extreme operational conditions. Brazing is one such method which has promising capabilities as it does not involve base material to change their state or characteristics and joint is a result of metallic bonds between base material and brazing alloy.

Brazing is a joining process and distinguishes from soldering in the sense that it requires above 450°C temperature for melting of filler material. This filler material is responsible for wetting the base and forms liquidus however temperature must not exceed the melting point of base materials [8]. This characteristic gives brazing a unique prospect as base material does not deform as in case of welding where base material melts because of intensive local heating and which causes thermal distortion. Another strong aspect of brazing is its ability to form joints between potentially different materials with significant strength. These characteristics make brazing a promising technique to be employed in automotive and aerospace industry to provide a better lightweight structure of multi hybrid materials. Filler material selection is a critical factor in brazing and depends on the materials joint and operating environment of the joint and more such. Several filler materials have been standardized in form of families which can be adopted for a particular base material joint however search for a more direct and effective filler material is always received in engineering realms [9].

Steel and aluminum being prime materials in study cannot be easily joined through traditional welding techniques due to large differences in thermal and physical properties and melting temperatures. The resulting joint would be susceptible to distortions and would not have structural integrity as steel and aluminum both have different expansion rates. Brazing promises optimal joint between steel and aluminum

using a filler material and hence the complete procedure is done below the melting temperatures of both base material this gives good structural integrity to the joint while keeping the inherent properties of both base materials.

This thesis aims at evaluating experimentally the joining of low carbon zinc coated steel with aluminum alloys using brazing. As brazed joints are formed due to formation of intermetallic bonds between base and filler material, Scanning Electron Microscopy (SEM) and optical microscopy would be employed to characterize the bonding. Furthermore, as this thesis aims at developing a sustainable method for employing at industrial level, X-ray diffraction (XRD) technique would be applied to evaluate residual stresses in the steel and aluminum sample before and after brazing to compare and get information about reaction. XRD was also used to check presence of elemental composition and intermetallic compounds which would be supported by EDS scan on reaction sides of samples.

2. State of the Art

This chapter of thesis would focus on summarizing different techniques of joining dissimilar materials with special focus on joining aluminum alloys with steel. Many research articles and review papers have been carefully read and cited throughout.

Use of hybrid structures in industry provides not only product flexibility but also enhances product effectiveness by carefully tailoring desired properties of each material.

2.1 Joining Process of Dissimilar Materials

Hybrid structures are a combination of two or more materials in each configuration and size, they optimally serve a specific technical purpose. These components and parts made of different materials are connected by different possible methods of joining. Each has a unique strength and the limitations of joining characteristics. However, significant challenges arise when the materials are of different chemical, mechanical, thermal, or electrical properties. Chemical, thermal, and physical attributes (thermal expansion, ductility, fatigue/fracture mechanics, Young's modulus, etc.) can both cause problem of the bonding process itself, but also for structural integrity during the operational life of joint or the product. To achieve an optimal and functional joint, these challenges need to be addressed. These differences of materials should be minimized through selection of similar materials however this choice quickly becomes difficult when atomic structures, micro and macrostructures of material are widely different [10].

Generally keeping automotive sector in focus, following types of joining techniques are employed in practice considering type of materials involved, cost effects, operational conditions, and engineering constraints:

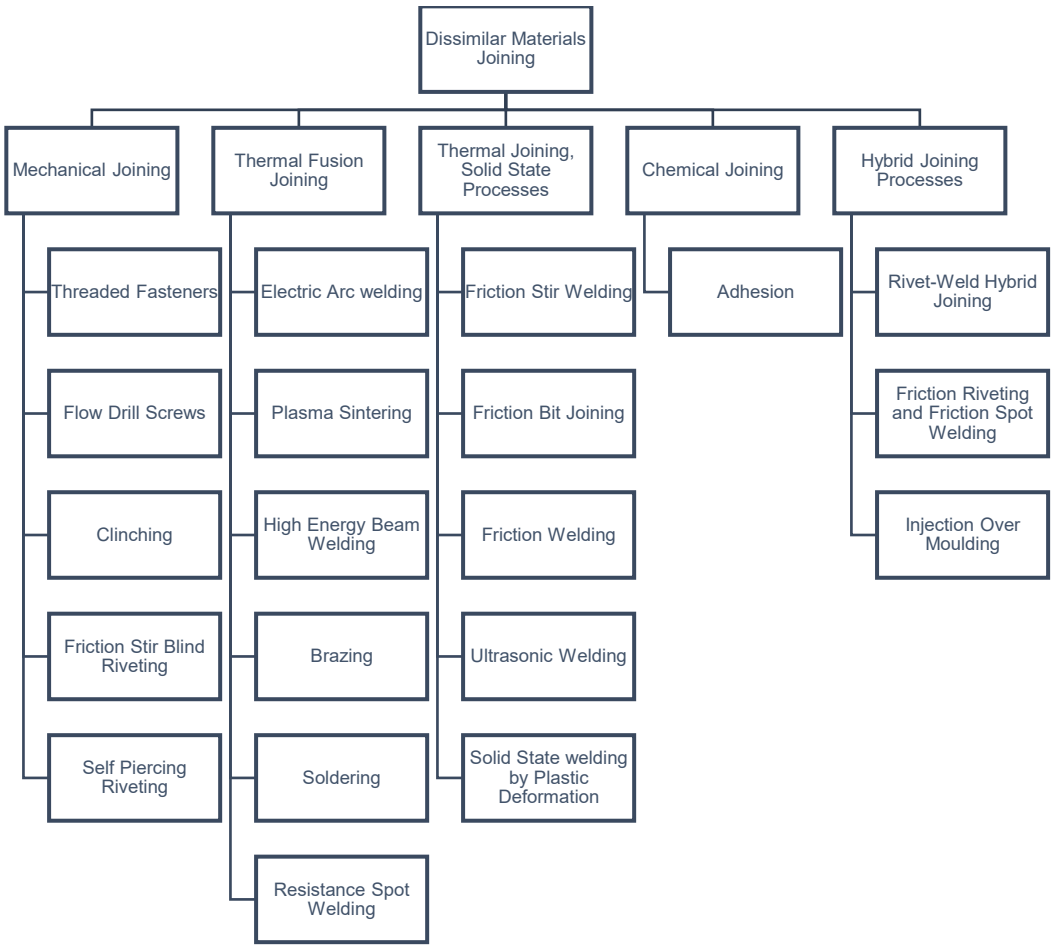

Figure 3: Dissimilar Materials Joining Techniques [4]

2.2 Welding Techniques - Aluminum Alloys to Steel

So far joining of dissimilar materials techniques have been highlighted keeping in view the automotive industry. Most conventional and common methodologies when joining metals are welding techniques and scientific research in this field is continuous to develop or improve already established welding methods for better joining of dissimilar metals such as aluminum alloys to steel. Most generic resistance welding is not the most effective technique for both materials for brittle microstructures leading to crack for highly resistive steel sheets and aluminum characteristics such as high conductivity, low melting point and stable natural oxide layers poses severe difficulties. In this section prevalent welding technologies and their strengths and drawbacks would be studied keeping in view aluminum alloy to low carbon steel.

2.2.1 Fusion Welding

Aluminum due to its high heat and electrical conductivity and low melting point is difficult for welding operation and some techniques are more preferred compared to others. Seam welding is preferrable because of strength and sealing effect, however spot welding is considered more suitable due to low weldability. Aluminum alloys are increasingly being used in the car industry due to their light weight and effectiveness in absorbing crash energy while steel having high strength, cost effective, robust, and easily weldable remains a primary material in automotives. Joining of these two materials with welding without loss of joint strength has been a major engineering challenge due to large electrochemical difference of 1.2 volts, different thermal expansions, different lattice transformation, heat capacity, melting points (660°C for Al and 1497°C for steel) and negligible solid solubility [11]. Critical factors of control and effectiveness of different welding technologies have always been to reduce size and quantity of intermetallic formation of Al/Fe.

Generally welding is categorized in fusion and solid-state streams. In fusion, heat source cause variation in temperature field which is not uniform. These thermal variation in and around the heat affected zone causes variation in microstructures of bonds and on solidification with inhomogeneous phase changes can lead to many issues such as intermetallic formation, weld shrinkage and shape distortion, significant residual stresses and formation of brittle fragile fracture and stress corrosion cracking. Intermetallic (Fe_xAl_y) responsible for brittleness of joint are result of different welding parameters such as temperature time pressure and atmospheric conditions. Intermetallic compounds are formed due to atomic diffusion of atoms which is a time dependent process however time is reduced at higher temperature. Intermetallic compounds (IMC) pose immense challenges in fusion welding due to their negligible plastic deformation and increased thickness of this layer results in fragile joints.

Al rich IMC are more brittle in nature while at the same time solubility of Al in Fe is far greater than Fe in Al. Therefore, generally, the critical area is closer to Al side which results in brittle IMC. However, Meco et al. [13] demonstrated that IMC layer with less than 10 μm does not affect ductility and strength of joints while thicker layers become critically more brittle. Thermodynamically, chemical potential difference, phase nucleation in mobility of elemental composition of both materials result in intermetallic

formation of different possible combinations. As per Fe-Al phase diagram (Figure 4) [11], formation of IMC is evident in pursuit of metallic junction between Aluminum and Steel.

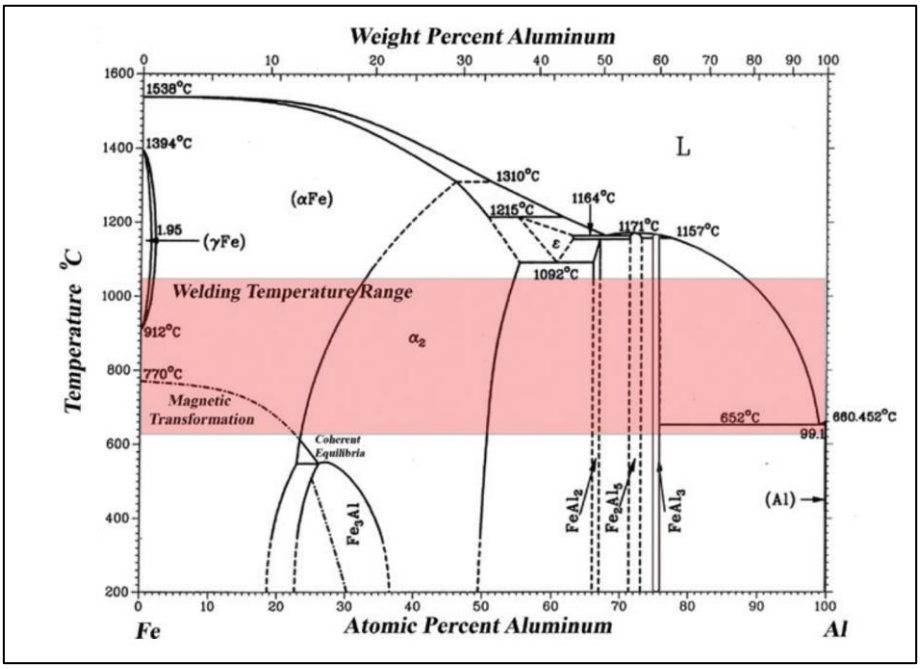

Figure 4: Dual Phase Diagram of Fe-Al [11]

Some of the important welding techniques are being presented here with focus to Aluminum and steel joining while investigating in terms of intermetallic formations and other problems:

2.2.1.1 MIG TIG Welding

Known to work at higher temperatures and without the use of flux and in presence of shielding gas gives good result in terms of slug formation and shielding gas helps protect joint and spread of alloying elements. However, High thermal gradients significantly raise the formation of IMC with considerable layers.

TIG welding brazing was carried out on Aluminum alloy 5A06 and stainless steel SUS321 with filler metal along with modified aluminum flux was used on steel side in butt configuration. The joint resulted in molten weld joint on aluminum side while brazed weld on steel side. The schematic of the experiment is illustrated in figure 5 with interfacial layer with crack propagation scan at figure 6. Results concluded formation of three different types of IMC with layer thickness from 5 μm to 35 μm which resulted in fracture upon tensile test at 120 MPa [13]. XRD scan confirmed presence

of the η-Fe2Al5 IMC and FeSi2 phases and fracture occurred due to brittle nature of IMC.

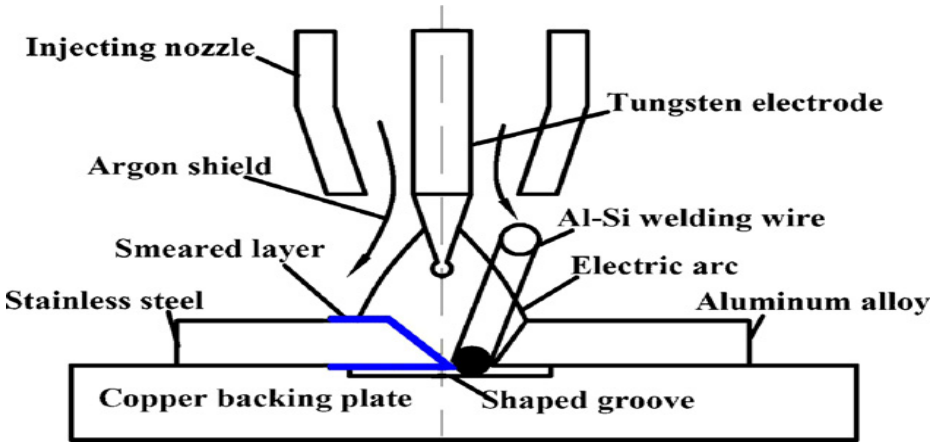

Figure 5: Schematic of TIG brazed Welding of Al Steel [13]

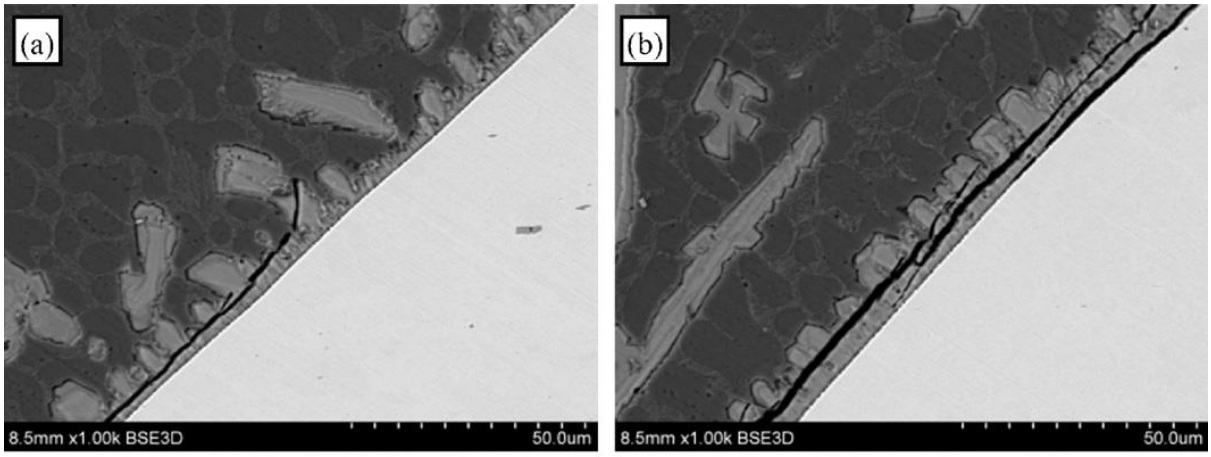

Figure 6: Crack initiation and propagation on interfacial IMC layer [13]

When Aluminum 2B50 and stainless steel were joined with MIG technique with aluminum coated on steel surface to enhance brazed welding of steel surface. Results concluded presence of lot of IMCs on steel surface and cracks appearing on interfacial surface between steel and weld resulted in failure at 60 MPa. Same experiment but with galvanized steel showed three different regions including zinc rich zone, reaction layer and fusion zone (figure 7) and tensile test showed better results with fracture occurred due to crack in heat affected zone at 193.6 MPa [14].

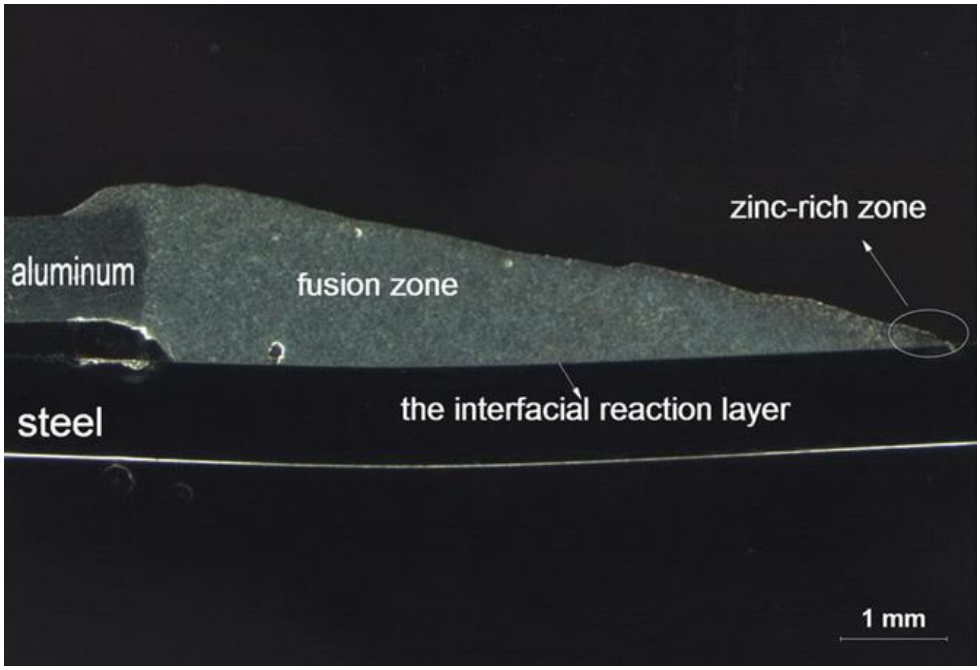

Figure 7: MIG brazed welding with Al and Galvanized Steel [14]

2.2.1.2 Resistance Spot Welding

Resistance spot welding is one of the oldest welding processes; still dominates the field of car assembly. This technique is robust and cost effective in the case of homologues material. However, procedure is not so straightforward and easy when joining dissimilar materials like Aluminum and steel. Aluminum alloys show low resistivity and higher thermal conductance which requires high amount of current energy to achieve desired heat making it less cost attractive [15]. Additionally, presence of stable oxide layer on Aluminum further aggravates the problem. A typical schematic of the resistance spot welding is depicted in figure 8.

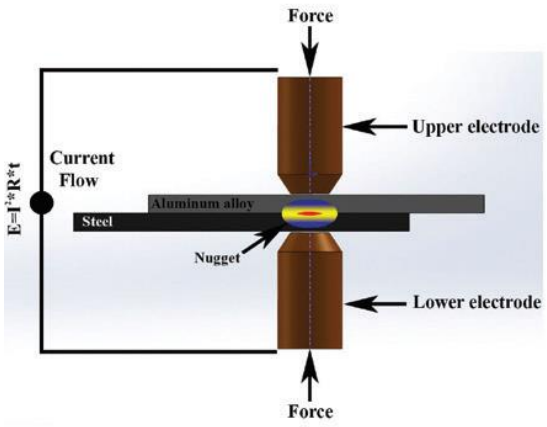

Figure 8: Schematic of Resistance Spot Welding

Two major issues are faced when Aluminum alloys are joined together with zinc coated steel through this technique is the presence of oxide layer which when removed at higher temperatures result in thick layer of IMC which compromises the strength of the joint. Another issue is the electrochemical corrosion in presence of any moisture due to large difference in ionization tendency of bother materials. Experimental study by Kenji Miyamoto [17] utilized eutectic reaction of Al and zinc to remove oxide layer at lower temperatures and formation of uniform and thin layer (around 2 μm) of Intermetallic compounds at the interface which gave a significant joint strength. Use of epoxy sealant optimally kept the moisture out to avoid risk of corrosion. Al-Zn binary phase diagram [18] at figure 9 shows eutectic reaction at 382°C. Results indicated successful removal of oxides and their expulsion to the sides and thin layer of IMC at figure 10.

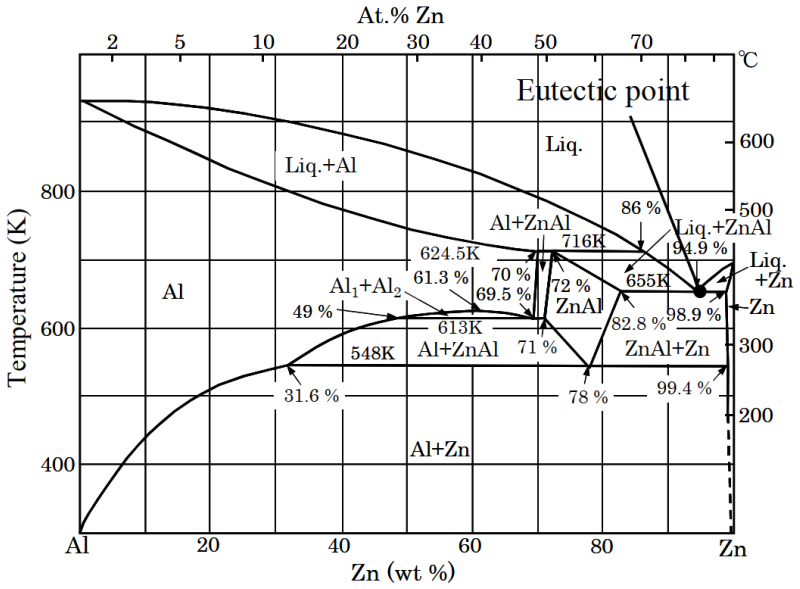

Figure 9: Al-Zn binary phase Diagram with eutectic point [18]

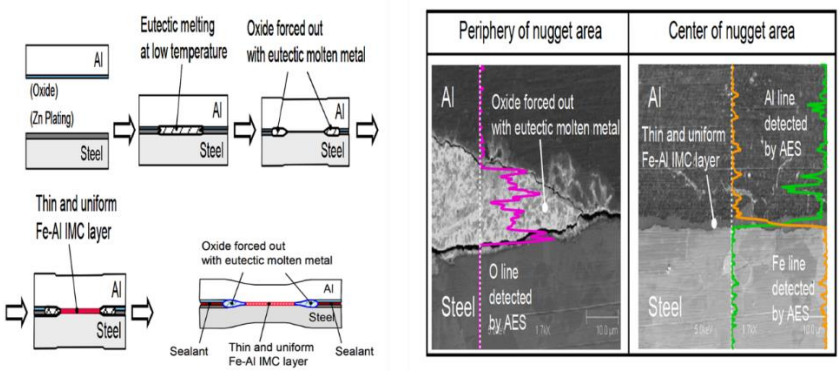

Figure 10: Process and AES scan of weld zone [17]

Studies have shown that nugget diameter correlates with welding current during Al alloy and steel spot welding. Resistance spot welding with interlayer is frequently supported to provide a thin layer of IMC. Even bimetallic layers have been found to provide reasonable strength however cracks were still resulted in IMC layer. Bimetallic strips however reduced the chances of corrosion due to presence of steel-steel and Aluminum- Aluminum crevices [20]. The schematic of bimetallic layer is depicted in figure 11.

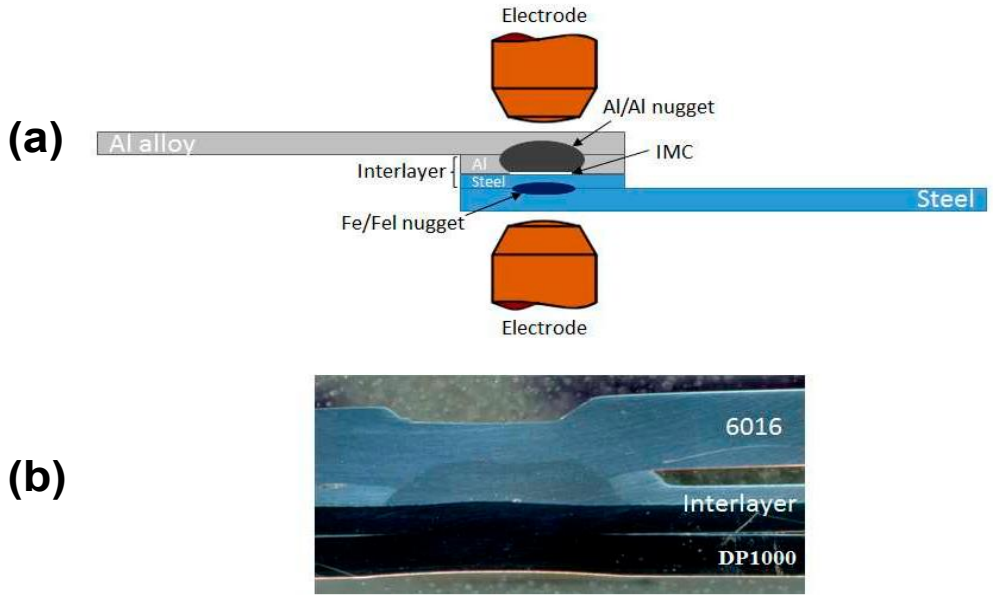

Figure 11: (a) Schematic of Bimetallic spot Welding (b) Section with bimetallic interlayer 40 % Al alloy and 60% steel [20]

2.2.1.3 Laser Beam Welding

A laser beam from remote source can be employed to concentrate on workpiece resulting in less heat effected zone giving smooth surface finish while maintaining high productivity speed. Generally, this technique of welding is sophisticated approach and is used in automotive industry for homogenous materials joining. Considering materials in question zinc coated steel with aluminum alloys, this technique has been highlighted in some scientific papers with following laser beam techniques are focused:

a. Keyhole Welding
b. Conduction mode welding
c. Reactive Wetting
d. Braze Filler Metal Welding

Reported by Sierra [20], keyhole configuration was tested with overlap configuration with steel on top. Variable penetration of laser beam was used to develop a relation between penetration to aluminum concentration in the weld and strength of weld. Results showed defect free welds when penetration was limited to under 500 μm and IMC on weld aluminum interface composed of Fe_2Al_5 and $FeAl_3$ with thickness layer varying from 5 μm to 20 μm. The peculiarity of this technique is that both metals are melted and then solidified with either aluminum or iron rich fractions with changing parameters. The schematic of the configuration is illustrated at figure 12. Thin metallic strips of copper and nickel showed better strength in tensile shear test.

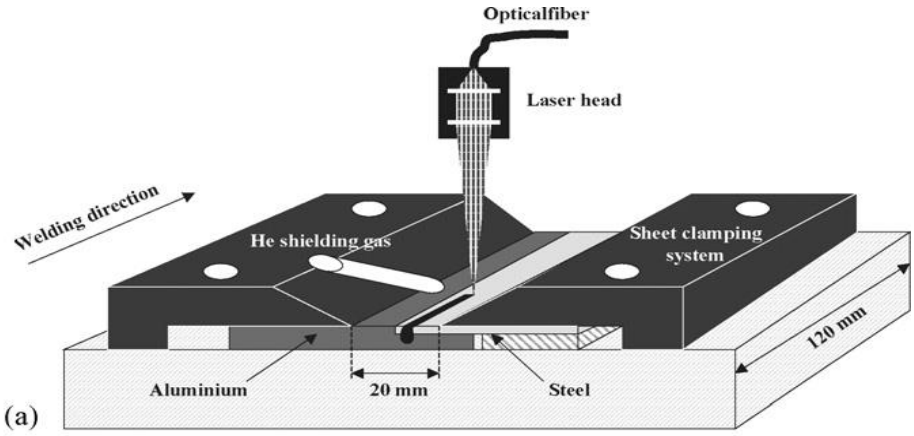

Figure 12: Schematic of keyhole laser welding set up [20]

Conductive mode of welding as name suggested use thermal phenomena of conduction to melt aluminum while steel remains in solid state at the interface of weld. Fan reported [21] relationships of this technique between peak temperature, thermal cycle and cooling rate with the thickness of IMC phases. While thermal cycle and peak temperature show inverse relation (higher the temperature and cycle thinner the IMC layer), Cooling rate being most important showed direct relation with larger cooling rate resulting in large thickness of IMC. The schematic of the process is depicted in figure 13.

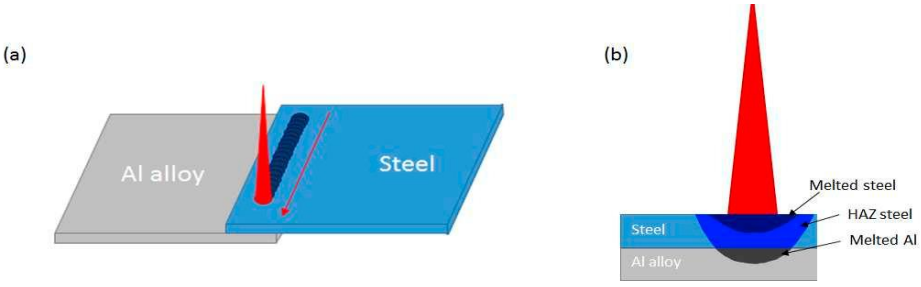

Figure 13: (a) Conduction mode laser welding (b) Process depiction at cross section

Reactive wetting in overlap configuration resorts to focusing laser onto Aluminum side to melt it and then react to solid steel. Sierra at [22] observed that use of brazing flux significantly improved mechanical strength while without the flux failure occurred at considerable low values. Also, although zinc coated on steel helps in wetting process, it also induces porosities due to evaporation with higher temperatures involved which considerably lowers the strength. IMC mainly Fe_2Al_5 was founded on with aluminum rich phases with cracks with thickness layer higher than 10 μm.

In braze filler metal laser beam welding, a thin metal wire of brazing alloy is used to form bonding. Sierra at [23] experimented joining Al 6016 with low carbon DC04 steel with Al-12Si filler wire. The schematic of lap joint set up is illustrated in figure 14. The study showed considerable tensile strength of the joint (190 N mm^{1}) which is comparable to UTS of parent AL 6016. While the Al to filler interface showed regular bonding, a thin Fe-Al-Si intermetallic was formed toward steel weld interface which ultimately resulted in failure of the joint at higher loads.

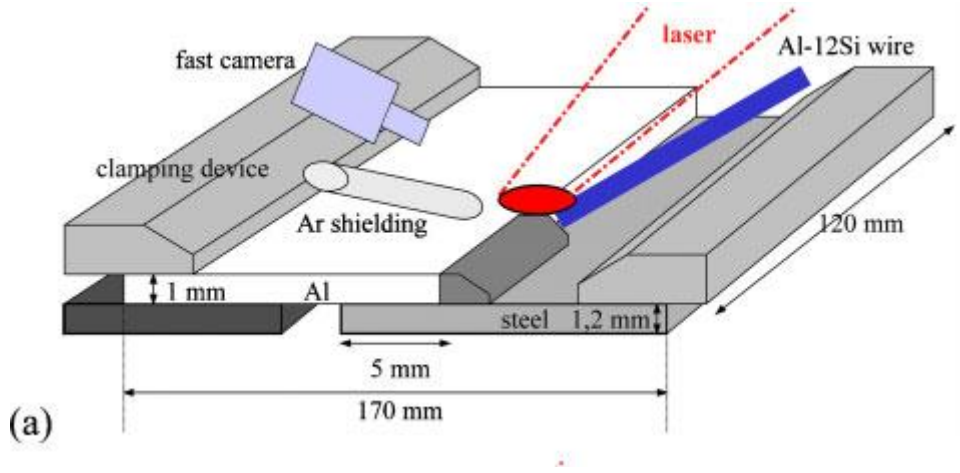

Figure 14: Schematic setup of Filler metal Laser Welding in Lap Configuration [23]

2.2.2 Solid State Welding

With solid state welding there is no liquid or molten phase in the joint. The principle is illustrated as when two clean surfaces come into close contact under sufficient pressure, they form a joint. To form a strong bond, it is important that the interface be free of oxide films, scale, metalworking fluids, other contaminants, and even absorbed gas layers. Welding is accomplished by one of the following phenomena. Diffusion is

the movement of atoms across an interface; therefore, applying external heat improves the strength of the bond between bonding surfaces as in diffusion bonding. Pressure influences the interface; higher pressure would result in plastic deformation to occur making resulting joint strong. Lastly, relative Interface Movements occur when contacting surfaces move relative to one another even a very low amplitudes will affect mating surfaces, breaking up the oxide films and creating new, clean surfaces, improving bond strength.

Considering Aluminum alloy and low carbon steel joining, solid state welding is most attractive as no molten phase is involved, intermetallic compound can be reduced which are the prevalent reason of failure of these joints. Several techniques of solid state are present in literature relating to joining of Aluminum and steel. Some of them are expressed here.

2.2.2.1 Magnetic Pulse Welding

In magnetic pulse welding, magnetic energy is focused on a small area using coil generator and field shapers. Pulsed current is passed in the coil which generates magnetic field in the aluminum sheet due to its conductivity which produces pressure in the sheet and metallic bonding occurs when this pressure exceeds the UTS of the material. Thickness of the sheets and size of the coil are also limiting factors in this technique. Optimal configuration illustrated in figure 15 has been reported in literature about type and design of coils for aluminum and steel sheets [24].

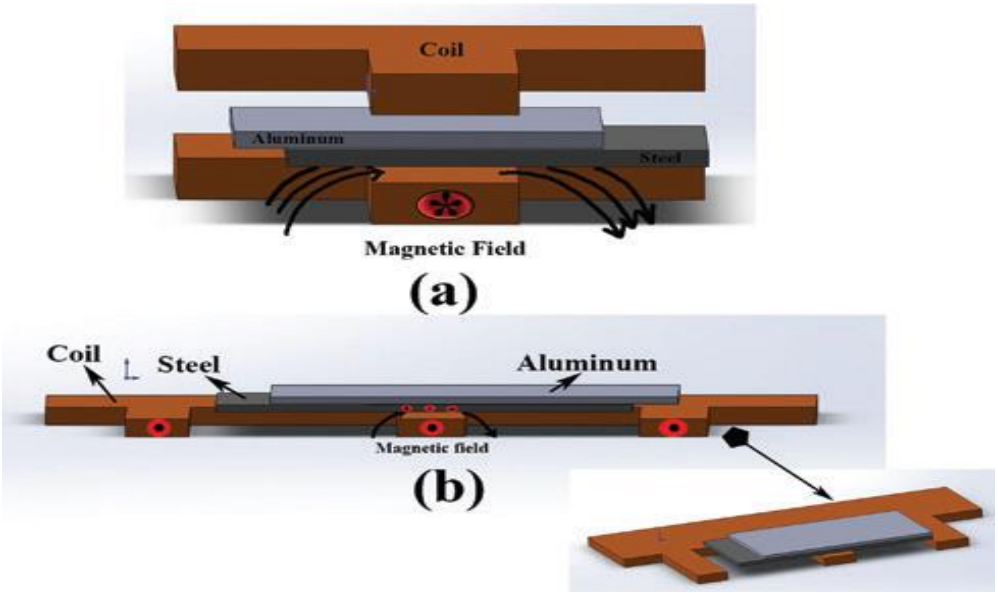

Figure 15: Magnetic Pulse welding coil design (a) T shape (b) E shape [24]

Another critical parameter of this technique is the presence of an optimal gap between both sheets for good welding joint. Literature has reported that in absence of this gap, twice electrical energy maybe needed for same set of pre cleaned surfaces [25]. The morphology of the joints appears to have a wavy interface with very thin IMC layers and higher shear strength is in center of the joining area while low strength at the edges due to weakness of the bonds.

2.2.2.2 Roll Bonding

Roll Bonding technique makes use of pressure to form metallic bonds between inner metals. Therefore, surfaces are required to be cleaned and removed from oxides which is always a difficult task for aluminum and requires a special atmosphere. Upon pressure micro crack appears in the strain hardened brittle surface, through these cracks the base metals meet each other forming bimetallic joints through formation of atomic bonds. In the case of aluminum and steel joining, these brittle surfaces are major cause of failure for this type of joining technique.

As the bond is directly related with pressure, normally reduction in thickness is required for formation of sufficient joint. Pre annealed aluminum (AA1050) 1mm sheet with AISI 304L 1.2 mm sheet were roll bonded at room temperature and at 100°C to get different microstructures at the core of stainless steel mainly martensitic-austenitic and austenitic in Al/304L/Al configuration. Paper concluded that strength of Al was attained with only 38% reduction of thickness which was quite promising [26]. It has been found that annealing after cold rolling generally helps strengthen the joint due to better atomic diffusion and makes it ductile. However annealing temperature must not be higher due to formation of brittle IMC [27].

Main parameters effecting this technique that have been elaborated in literature are rolling speed, pre and post heat treatment and rolling strip friction.

2.2.2.3 Friction Stir Welding

Friction stir welding is a comparatively newer solid state welding technique which employs a cylindrical tool with a rotating pin and a specially designed shoulder. The technique used both heat and pressure as driving energies to form a bond. It provides almost IMC free joints as the working temperature is below melting point of both

metals. The rotating pin is responsible for softening the material below its melting point through heat of friction and then stirring action provides mechanical force of joining in plasticized materials. The motion of pin and toll can be translated along the seam to provide conventional friction stir weld or can be focused in a limited area to provide friction stir spot weld. Heat is localized in small areas below the melting point of parent material and resultantly heat affected zone is also narrow and generally joints are free of distortions and with refined microstructures.

Even though zinc coated steel and aluminum joining through this technique suffers because of low melting eutectic point of aluminum zinc, several studies have been successfully conducted in joining steel with aluminum. Schematics of the technique are illustrated in figure 16. Kimapong at [29] studied the effects of pin speed, rotating direction and offset in joining magnesium containing aluminum to steel. Study concluded that there was an optimal speed giving highest strength whereas low speed was unable to produced desired frictional heat and too large speed resulted in high temperatures which formed unstable joint due to magnesium getting oxidized as shown in the figure below. An optimal diameter of the pin along with its offset toward steel (given at figure 17) gave the highest tensile strength although aluminum had to be in the retreating side of the pin to achieve any success. Lastly, IMC were not found in the joint while a very thin layer was observed towards the top region due to additional heat from shoulder.

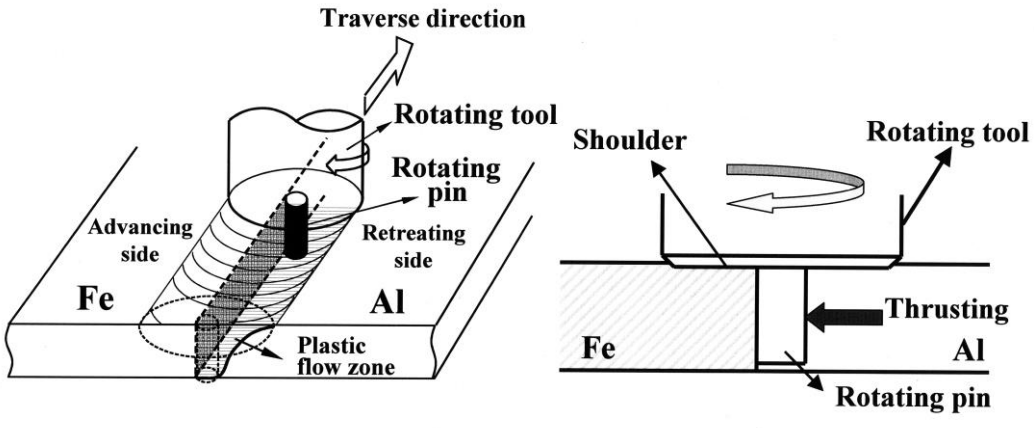

Figure 16: Schematic of friction stir welding of Al to steel along with cross section view of perpendicular weld surface [29]

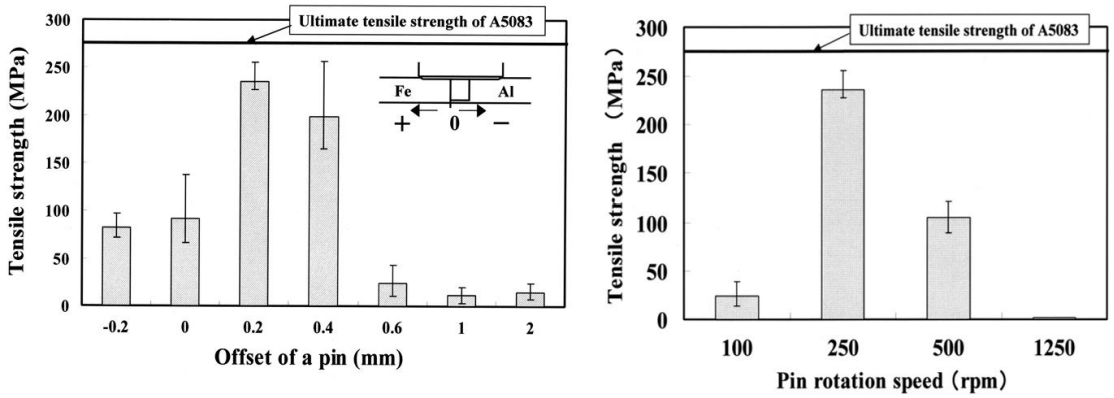

Figure 17: Relationship between pin off set and speed and tensile strength [29]

Friction stir spot weld is similar except for rotating tool is either stationary or move over a very small region to form a spot like welding. Several techniques of this kind have been reported in literature like tool only penetrating Al top sheet, or steel bottom sheet and even tool motion can be linear or even abrasive circles as reported at [30].

2.2.2.4 Ultrasonic Welding

Ultrasonic welding is a solid-state thermomechanical and energy efficient technique generally adopted for spot welding. This technique finds it difficult to work on complex geometrical joints. It uses the frequency generator which produces energy which through piezoelectric transducer is converted in mechanical oscillatory motion. This motion is transformed from two sonotrode tips to the welding sheets. It enables local deformation and heat generation to form the joint. Additionally, to be welded sheets are clamped under the effect of the force. Major parameters of the process are frequency, process time and clamping force. Two types of mechanical vibrations can be transferred to metal sheets either linear or torsional through respective motion of sonotrodes. Schematic of the technique are illustrated in figure 18 employed for aluminum to steel joining [31].

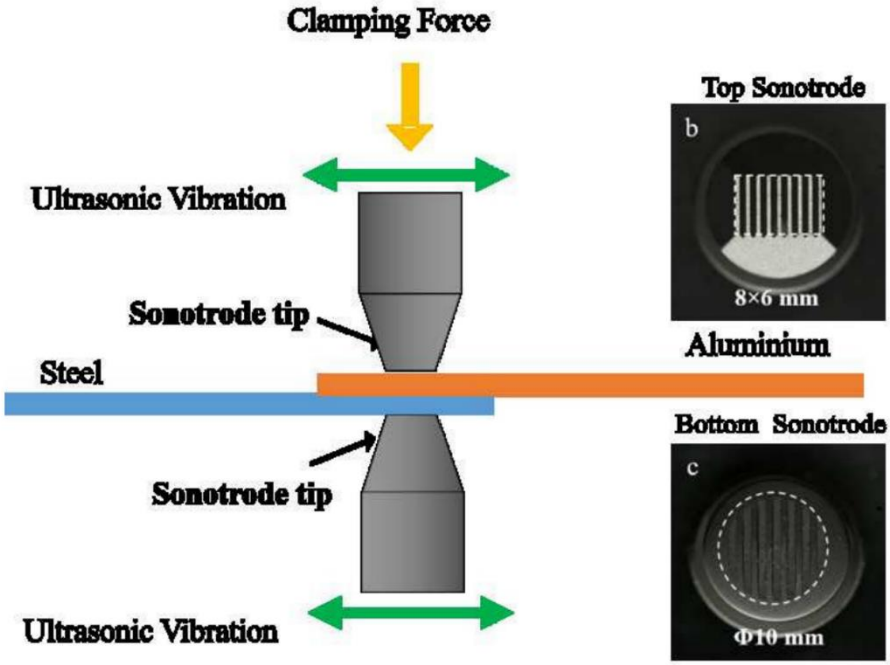

Figure 18: Setup for ultrasonic welding of aluminum to steel [31]

For aluminum to steel joining this technique has the added advantage of destroying oxides due to vibration and hence does not require surface preparation and cleaning in advance. 20 kHz frequency has been reported to be reasonable for both aluminum to aluminum and aluminum to steel joining [32]. And for clamping force, higher force would result in lower process time and lower frequency amplitude but at the cost of higher energy input. Literature has further elaborated the use of flat tips for aluminum and dome shaped tips for steel side sonotrodes [33].

An important consideration is joining of aluminum to zinc coated steel as at high process time temperature range goes above critical range of IMC formations like 500°C and due to low melting of eutectic Al-Zn strength of the joint decreases considerably [31].Low temperatures of up to 380°C and process time varying from 1 to 3 seconds offer optimal joint with sufficient strength between aluminum and steel.

Tsujino at [34] developed a relation between frequency amplitude, input power and weld strength while keeping process time of 2 seconds and static pressure of 20 MPa while joining pure aluminum and stainless steel in butt configuration. It was shown that joint strength is close to aluminum strength under large vibration amplitude.

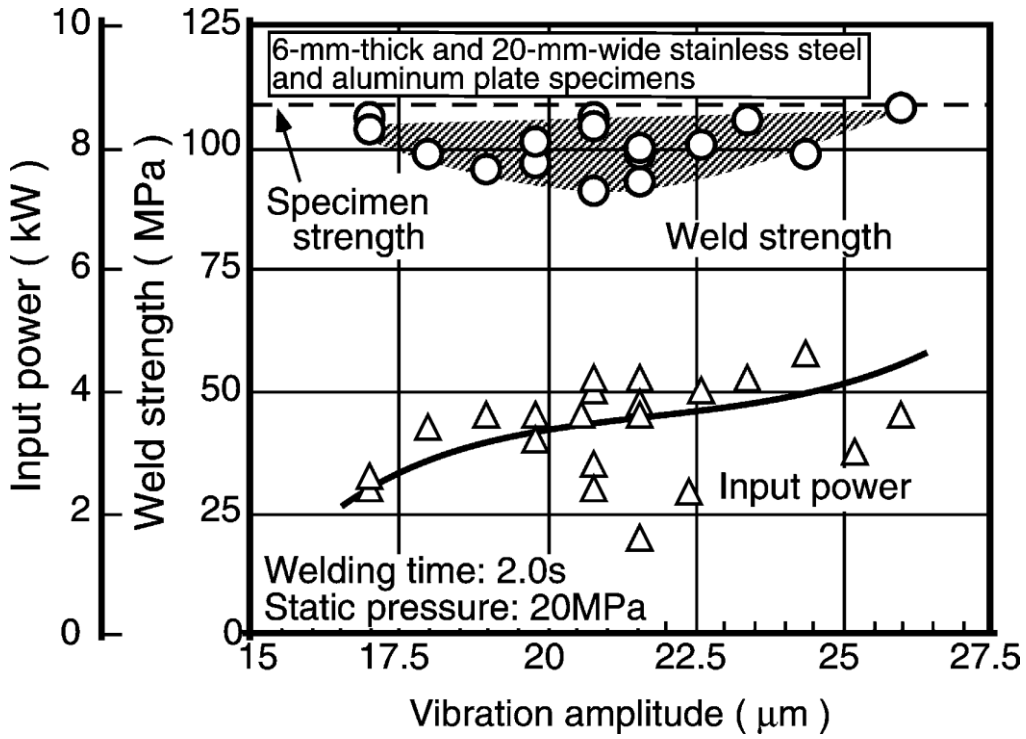

Figure 19: relationship between weld strength and vibration amplitude and input power [34]

2.2.2.5 Other Welding Techniques

There are many other welding techniques reported in literature with regards to joining aluminum to steel such as explosive welding, Friction bit joining, diffusion bonding and other hybrid joints.

Explosive welding can be employed to variable thickness of sheets in dissimilar metals without much heat affecting zone however it requires use of explosives which is problematic in industrial storage. Basic principle of technique uses high speed of flyer metal driven by explosive energy which collides with other stationary metal and collision energy result in breakage of oxide layer and direct atomic bonding. Almost IMC free joints can be formed between aluminum and steel using this technique. Schematic of explosive bonding process is illustrated in figure 20 [35].

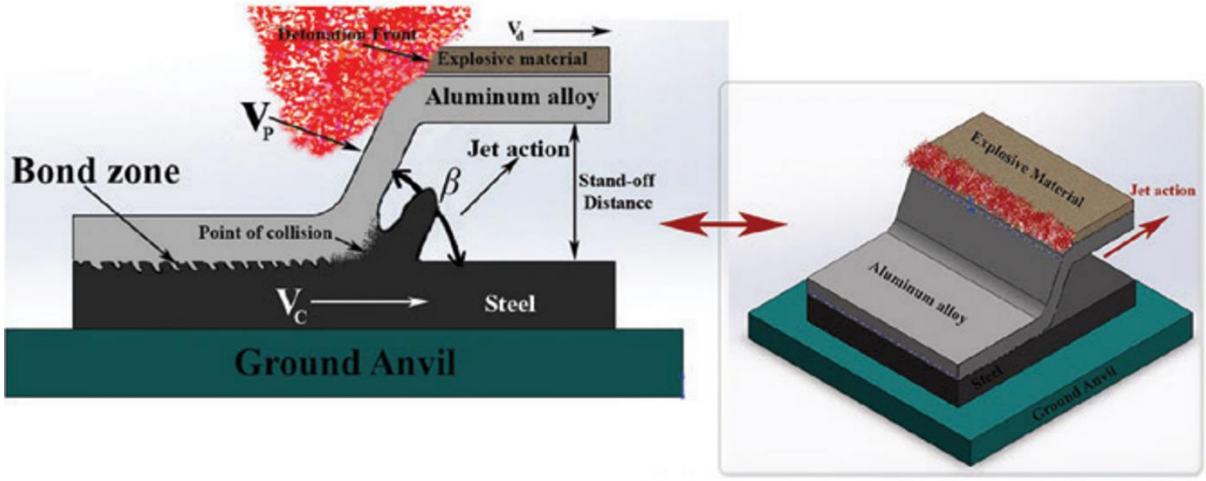

Figure 20: Schematic of explosive bonding between aluminum and steel [35]

In friction bit joining, junction is achieved not only due to mechanical lock but also a solid-state weld between bit and steel sheet. Generally, aluminum sheet is placed on top through which a bit made of carbon or tool steel is cut through top sheet under rotational axial load until it penetrates the aluminum and reaches the steel sheet. In the second stage higher rotational speed of bit caused bit to join with steel due to heat of friction and plastic deformation. Schematic of the technique is illustrated in figure 21[24].

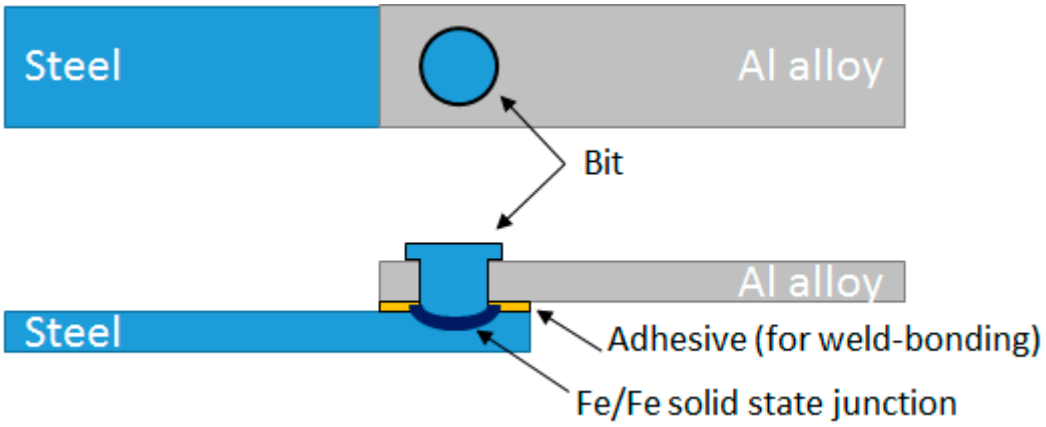

Figure 21: Configuration of Friction Bit Joining technique [24]

Hybrid or mixed welding joints are on the rise when aluminum to steel joining is studied. Advantages of both techniques are acquired to reach higher tensile strength with minimum defects. Friction stir welding was combined with TIG welding between

stainless steel and Aluminum 6061 to reach 93% tensile strength of aluminum material which was difficult to acquire in friction stir joint alone [36].

2.3 Mechanical Joining - Aluminum Alloy to steel

Fusion Welding techniques are solely dependent on mettalurgical bonding of metals while mechanical process use plastic deformation as a joining technique and hance have comparatively low cost, high productivity and low effect to metallurgical properties of both materials. Plastic deformation is generally used for shape forming in manufacturing industry but can be employed for joining purposes of dissimlar metals as in this study and also they are attractive techniques due to no involvememt of heat. Although conventional mechanical tools such as nuts, screws and rivets are also used to join dissimilar metals in automotive sector, here other mechanical joining processes using plastic deformation for joining are discussed such as self piercing rivets, clinching and hemmeing etc.

2.3.1 Self-piercing Rivets

Self-piercing rivets are spot joining technique which does not require sheets to be predrilled. The schematic of the process for joining two generic metals is shown in figure 22. The process can be described as in three steps, first a rivet with enough strength to penetrate is punched into the top sheet. The rivet is then pushed inside the second sheet but not fully, lastly skirt or tip of the rivet makes flare which enables interlocking in the lower sheet. Rivet must also be ductile enough to undergo flaring and plastically deforming the lower sheet for good interlock. Interlock depends on plastic deformation of rivet and sheet but also on shape of rivet and die.

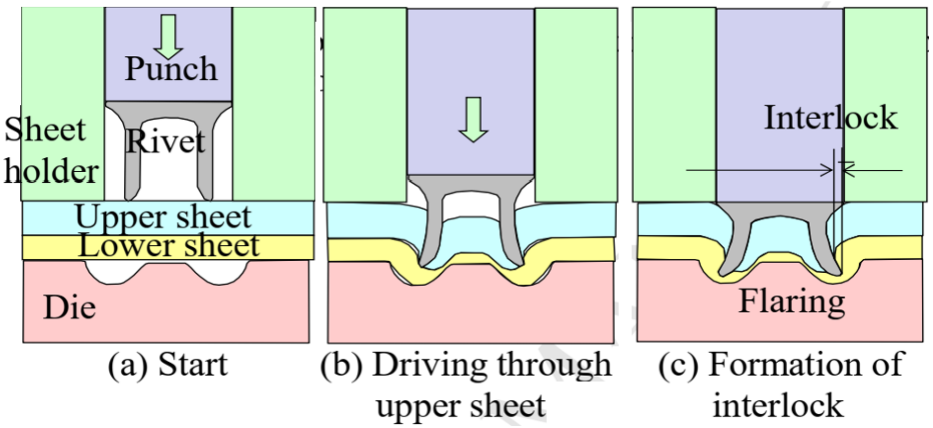

Figure 22: Joining process of metallic sheets by Self-piercing rivets [37]

The shape, dimension and diameter of the die is very critical for successful interlocking. Less depth would compromise penetration into the second sheet and a depth too long can cause rupture of the sheet.

2.3.1.1 Aluminum and steel sheets joined by Self-piercing rivets.

For joining aluminum sheets to aluminum sheets, rivets are normally made of boron steel which have sufficient strength to guarantee penetration and can flare for optimum interlock. But in case of aluminum to ultra-high strength steel, rivet strength is comparable to that of steel and hence self-piercing rivet technique becomes too difficult. When the steel sheet is at the top, rivet tip does not penetrate fully through the thickness of steel sheet and is not able to provide flaring for interlocking. While in case of bottom placed steel sheet, no flaring of rivet skirt in lower sheet happens and often leads to local rupture. K. Mori at [38] however optimized the die geometry and was able to achieve SPR joining between 980 MPa steel and aluminum sheet.

SPR technique has also been used for joining multiple sheets in automotive sector which generally requires three sheets with reinforced high strength steel at the bottom and steel or aluminum layers at the top. SPR treats all layers except the last one as top layer and rivet is driven through the complete layers except at the last where it forms flare for interlocking [39]. Zinc coated rivets are preferred for better protection against corrosion.

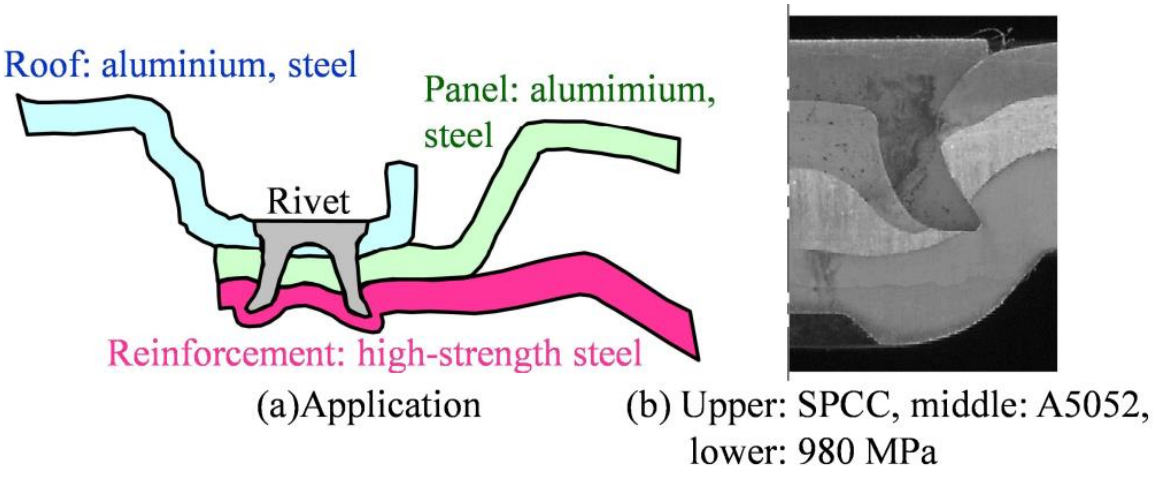

Figure 23: SPR joining of multiple sheets [39]

2.3.2 Mechanical Clinching

Mechanical clinching process is like that of self-piercing rivets however it does not use any rivets and only plastic deformation of both sheets is exploited for joining. Upper sheet thickness is a critical factor in joining as too low shrinkage at the neck of joint can lead to fracture. Interlock is achieved by different plastic deformations of both sheets and generally looks like a round button. The shape of die and groove ring inside helps develop the interlocking between both sheets. Process evolution is illustrated in figure 24 [39].

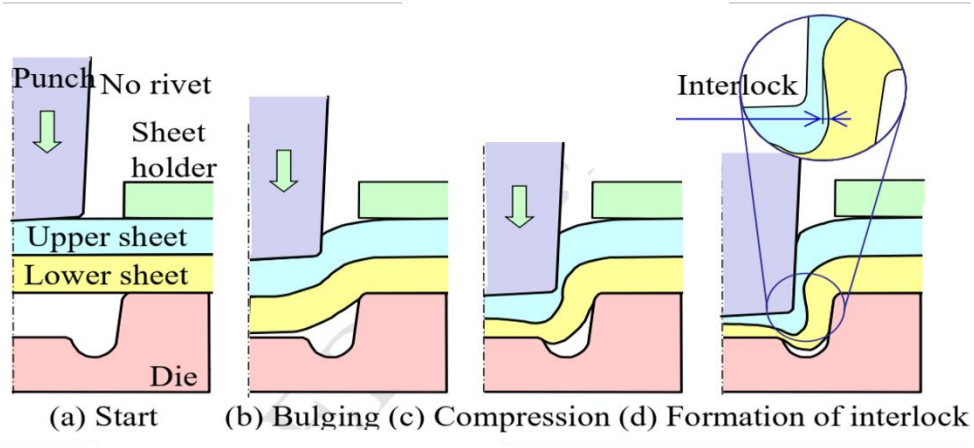

Figure 24: Mechanical clinching process of metallic sheets joining [39]

Generally round punch is used for clinching. However square punch have been reported to provide better strength [40] although less than one achieved with SPR. Some magnesium alloys which have less ductility have also been clinch joined at high tool temperatures.

2.3.2.1 Aluminum and steel sheets joining by clinching.

Like that of SPR process, with conventional die in case of joining high strength steel to aluminum sheets is very difficult due to high strength and low ductility of steel compared to aluminum. If placed at the top, the sheet tends to fracture due to deformation as clinching concentrates around the corner of the punch. If the steel sheet is placed at the lower side, it still fractured due to the tensile stress generated in bottom of the die and the groove [41].

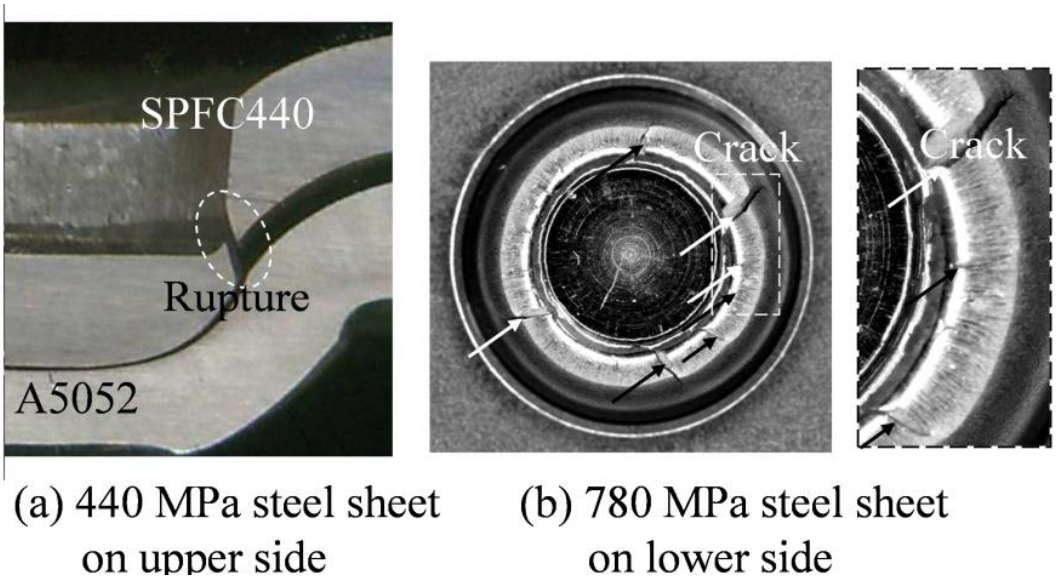

Figure 25: Factures in steel sheets with conventional die and clinching [41]

Y. Abe at [42] achieved successful clinching of high strength steel sheets placed at bottom with flat die without any cracks. Relationship (in figure 26) between conventional die and flat-bottomed die along with tensile strength of lower sheet showed, decreased interlocking with increasing strength of sheet. Same author in [43] used upper steel sheet configuration with aluminum sheet at the bottom, optimized shape of punch and die along with step punch was used to clinch thin steel sheet without any rupture along the shoulder.

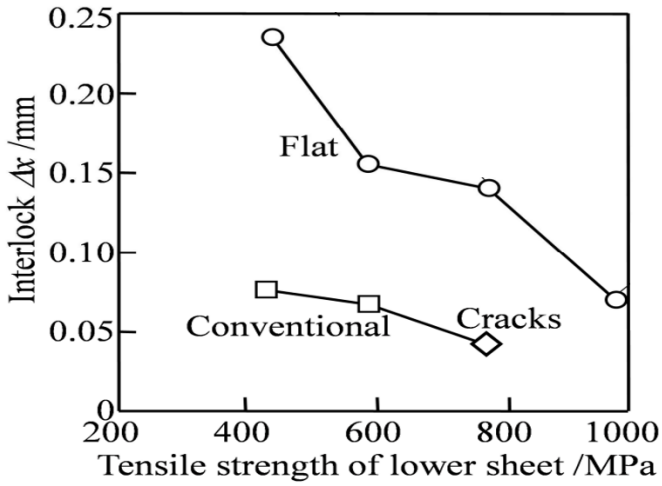

Figure 26: Relation between tensile strength of lower placed steel sheet and interlock [42]

2.3.3 Hemming

Hemming is another mechanical joining technique, in which the edge of one sheet is folded onto itself and when this folded edge is placed in a sandwich to another sheet it forms a joint. As joint is highly plastically deformed for a good joining, mild steel sheets with good ductility are normally used to avoid cracking. Sheets can be joined through press hemming or roller hemming for its high flexibility. Hemming is a three-stage process where the first stage involves flanging to make sheet edge at an angle to its flat surface, second is pre hemming and then final hemming with second sheet as a sandwich [44].

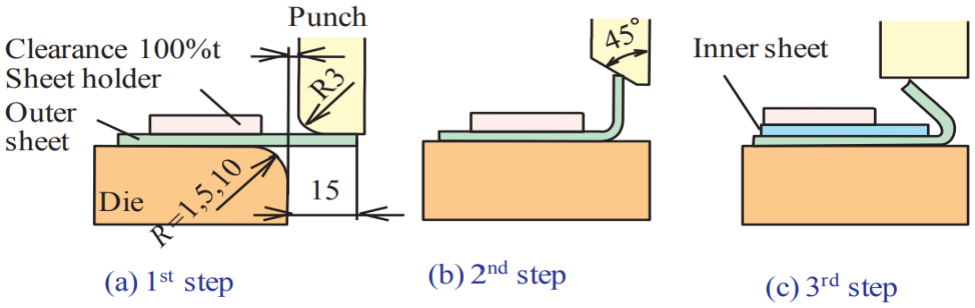

Figure 27: Hemming stages [44]

Several trends and optimizations have been studied and experimented in hemming process for joining for steel sheets such as placing of a stopper to avoid cracking which occur at the outer bend and a stopper provides a compressive force to avoid cracking in this region [44]. There is not much evidence of practical and efficient usage of this technique in joining aluminum and steel sheets.

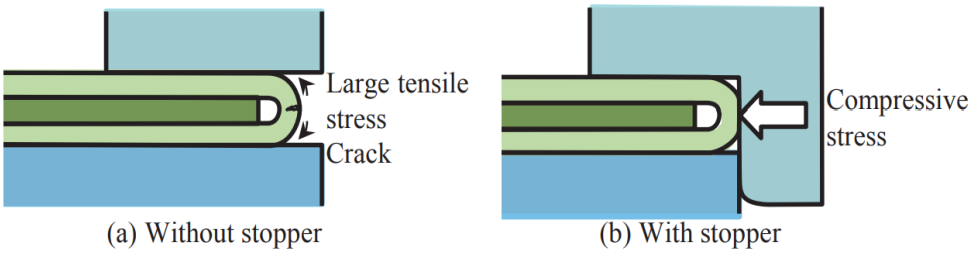

Figure 28: Reduction of tensile stress cracks due to stopper

2.4 Brazing– Aluminum alloy to Steel.

In the brazing process, a filler metal that melts above 450°C (842°F) but below the melting points of the metals being joined is used to join the metals. Filler metal is heated above melting point in the presence of an appropriate atmosphere, typically a flux. Then, by means of a capillary action, it flows over the base metals, or the metals being joined, and is drawn into the joint. The wetting and capillary action of molten filler metal is the foundation of the brazing process. The surfaces of the closely fitted base metals become wet when the filler metal is heated to its melting point. Through capillary action, the liquid filler metal enters the space between the base metals and, as it cools and solidifies, forms a bond.

As discussed previously, because of several metallurgical, thermal, and chemical incompatibilities, welding zinc-coated steel to aluminum alloys is particularly difficult. It is challenging to apply heat without either overheating the aluminum or underheating the steel due to the significant difference in melting points. Because aluminum has a higher thermal conductivity than steel, heat dissipation happens more quickly, which can cause uneven heating and cooling when welding. The different coefficients of thermal expansion of the materials add to the discrepancy by causing stress and possible distortion when the metals cool and contract at different rates. Brittle intermetallic compounds like FeAl3 and Fe2Al5 are also formed at the interface between steel and aluminum. These substances damage the integrity of the weld, resulting in a joint that is less ductile and weaker than the parent metals. In addition, zinc coating for corrosion resistance poses serious problems. Zinc vaporizes during welding at a high temperature, which increases weld porosity, spatter, and the production of harmful fumes. When aluminum is exposed to air at high temperatures, it oxidizes quickly and forms a stubborn oxide layer, which prevents proper fusion because its melting point is much higher than that of aluminum.

To overcome these difficulties, specialized welding techniques like brazing, the use of filler materials with lower melting points, or sophisticated procedures like laser brazing and Cold Metal Transfer (CMT) are frequently used. By controlling heat input, reducing the formation of IMC, compensating for thermal property differences, and addressing zinc evaporation, these techniques make joining zinc-coated steel and aluminum alloys easier. Despite their complexity, reliable welding of zinc-coated steel to

aluminum alloys is achievable with careful control over process parameters and joint design. This enables their use in a variety of applications where the desired combination of strength, light weight, and corrosion resistance is needed.

A strong and long-lasting joint must be ensured by following a few crucial steps when brazing aluminum alloy to zinc-coated steel. The surfaces that need to be joined are first meticulously cleaned to get rid of any impurities or oxides that can hinder the brazing procedure. The joint area is then treated with an appropriate flux to stop additional oxidation and make it easier for the filler metal to wet the base metals. The tight fit between the steel and aluminum components creates a small space that is ideal for capillary action. The assembly is heated to a temperature that melts the filler metal, which is typically an aluminum-silicon alloy or zinc-aluminum alloy but does not melt the base metals. This is typically accomplished with a torch or induction heating. Melting filler metal is pulled into the joint gap by capillary action, where it combines with the aluminum and zinc thin layer to create a metallurgical bond. Controlling the heat is crucial to avoid zinc vaporization and reduce the occurrence of brittle intermetallic compounds. The assembly is allowed to cool naturally after the filler metal has filled the joint space, solidifying the filler to form a robust, metallic bond. The brazing process is then finished by cleaning off any remaining flux or oxidation. Because this method can form a joint at lower temperatures, thereby reducing the risk of thermal distortion and maintaining the integrity of the metal, it is preferred for joining these dissimilar metals.

After briefly discussing brazing of aluminum alloy with zinc coated steel, some aspects of brazing alloy and parameters would be discussed.

2.4.1 Role of Surface Activation of Aluminum substrate

Oxide removal and surface preparation before brazing is a critical step to ensure proper reaction between filler material and base metals. Surface preparation often involves different steps to keep in view the type of base material to improve brazing operation. In the case of aluminum alloys, Graziano Ubertalli at [51] studied the effect of surface activation of aluminum alloys (Al5182 & Al6016) when pure zinc and ZAMA were used as brazing alloys. Three types of surface preparation were done:

1. All specimens were prepared by removing oxides mechanically with 320-grit abrasive paper, followed by ultrasonic cleaning in ethanol at 60°C for 10 minutes.
2. In addition to cleaning, aluminum flux containing cesium fluoroaluminate applied.
3. In addition to cleaning, each specimen's surface was etched using vacuum plasma with argon for 15 minutes at 200 W in radio frequency (RF) at an operating pressure of 1 Pa, and then coated with zinc by sputtering for 30 minutes at 100 W in direct current (DC) at a pressure of 6 × 10^-1 Pa, using the same instrument.

Brazing simulation was then carried out for both brazing alloys (Zn & ZAMA) in a tubular furnace at 10°C/min rate under Argon atmosphere to avoid oxidation. The temperature of 480°C was used for zinc as brazing alloy while temperature of 520 was used for ZAMA. Process is depicted in the following figure.

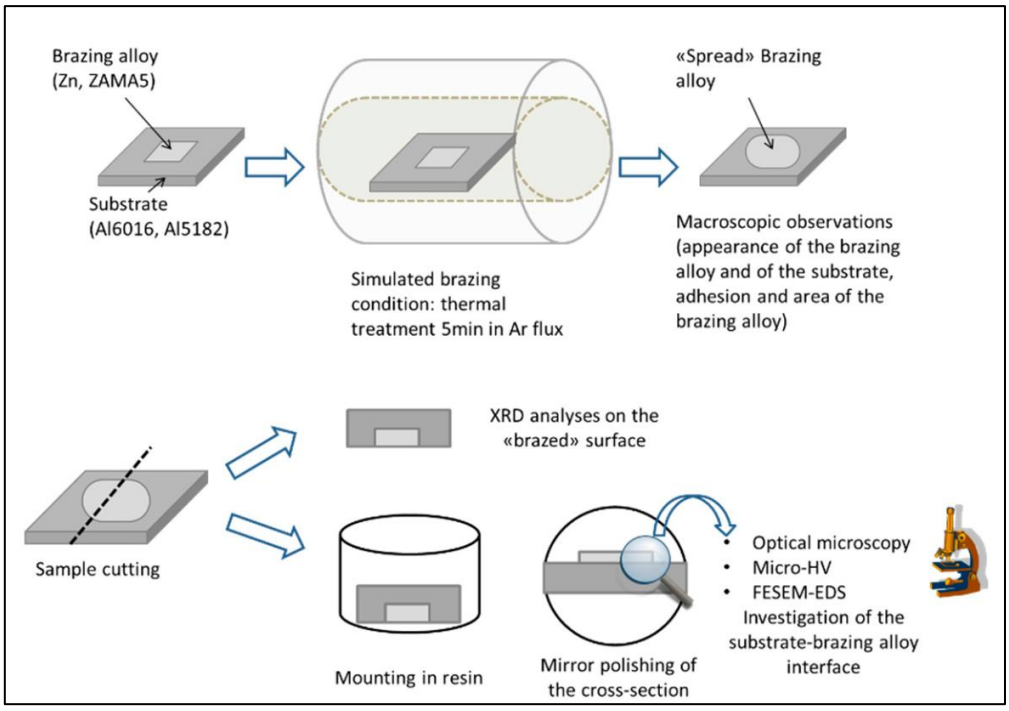

Figure 29: Schematic of setup for surface activation optimization [51]

Optically microscope observation of all samples were different and pointed to the fact that surface activation changes result of brazing and therefore must be optimized for materials under test.

The paper found that in simulated brazing tests, pure Zinc showed no visible reaction layers on clean Al6016 and Al5182 alloys. A moderate reaction layer under 100 µm was seen when pure Zinc and ZAMA were applied to Zn-sputtered Al6016. Conversely, on Al5182 treated with flux, pure Zinc and ZAMA formed drops with no continuous interface or clear reaction layer, while ZAMA on flux treated Al6016 resulted in a discontinuous reaction zone with visible brazing alloy remnants. Zinc on flux treated Al6016 created spread drops with a continuous interface and a thick reaction layer of several hundred microns. Significant reactions were also observed for Zinc on Zn-sputtered Al5182 and for ZAMA on clean Al5182, exhibiting a uniform reaction layer with a thickness of hundreds of microns, showing melting and solidification with visible grains and porosity. A continuous but thinner reaction layer was present for ZAMA on clean Al6016.

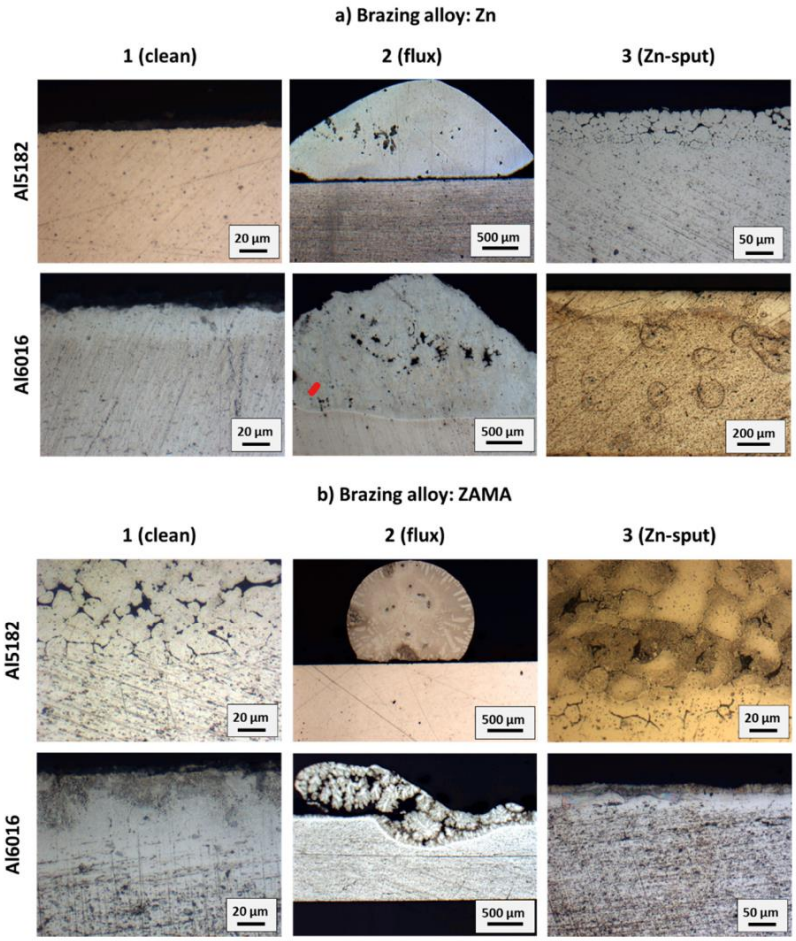

Figure 30: Optical microscope images of the transverse section of the samples (no etching): (a) Zn as razing material; (b) ZAMA as brazing material. [51]

2.4.2 Role of Zinc as Brazing Alloy

Zinc is a pivotal element in brazing applications, offering significant benefits such as the reduction of melting points and enhanced wetting of ferrous materials. Its affinity for aluminum enhances its suitability as a filler material, particularly in the automotive sector, where joining dissimilar metals like aluminum and steel is critical. The shift from heavier steel components to lighter aluminum alternatives is a strategic move towards lighter vehicle constructions, thereby contributing to lower emissions and improved fuel efficiency.

Current research is exploring the efficacy of Zn-based eutectic compositions (such as Zn-Al2, Zn-Al4, Zn-Al15, and Zn-Al22) and Al-based eutectics (including Al-Cu6, pure Al, Al-Si5, Al-Si10-Mg, and Al-Si12) as potential filler materials for creating robust joints. The ongoing studies aim to understand the role of alloying elements like Si, Cu, and Zn on the formation and behavior of intermetallic compounds (IMCs) at the joint interface [49].

Silicon, for instance, is reported to mitigate the reaction kinetics at the Al/Fe interface, consequently diminishing the volume of IMCs formed, as noted by Spring et al [50]. Copper, conversely, tends to replace some iron atoms within the IMCs, reducing their hardness and making the interface less susceptible to cracking. Zinc, however, exhibits a distinct mechanism. Dharmendra et al [50]found that zinc's greater affinity for aluminum over iron encourages the incorporation of zinc into the IMC phases, particularly the δ-FeZn10 phase, which imparts lower hardness and improved ductility to the joint. This phase notably enhances crack resistance, ultimately bolstering the tensile strength of the joint [49].

Moreover, zinc serves as a protective coating on steel surfaces, providing galvanization that shields against corrosion. This zinc coating not only fortifies the steel but also improves the wettability during the welding process, ensuring comprehensive filler material distribution and joint robustness.

As a facilitator in the joining process, zinc acts as a catalyst, diminishing the melting temperature and optimizing the wetting properties of the metal surfaces. A notable investigation at China's Changchun University showcased the advantages of incorporating zinc into the filler material during the laser welding of aluminum alloy (AA6061) to galvanized high-strength steel (DP590). Utilizing powdered zinc and

aluminum alloy as the filler, the experiment employed 70–110 μm diameter powders, 1.5 mm thick A5052-H34 aluminum alloy sheets, and 0.8 mm thick ST07Z hot-dip galvanized steel sheets with a 10 μm thick zinc coating. The experimental setup positioned the aluminum alloy in an overlap configuration to the galvanized steel, orienting the lap joint at a 60-degree angle relative to the laser beam and feed head, as delineated in the referenced figure [51].

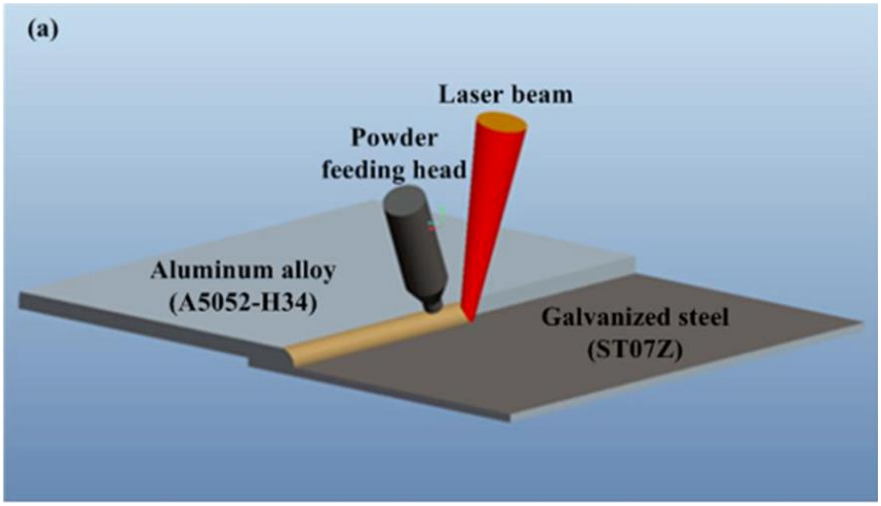

Figure 31: Schematic view of LWB process [51]

The study also included a comparative analysis involving the welding of non-galvanized steel to gauge the impact of the zinc layer. This aspect of the research was conducted to assess the efficacy of the welding process both with and without the addition of filler materials. The findings from these experimental conditions highlighted the beneficial role of zinc in the welding of heterogeneous metal assemblies.

During the tests, the outcomes of laser welding aluminum alloy to galvanized steel were compared for scenarios employing filler powders against those that did not. It was observed that the inclusion of filler powders could augment the energy efficiency of the laser fusion-brazing process, thereby reducing the requisite laser power. The presence of a zinc coating significantly enhanced the wetting dynamics by altering the interaction of the molten aluminum with the base material. This effect substantially lowered the brazing temperature from the melting point of iron (approximately 1535.0°C) to that of aluminum (about 660.4°C). Such a reduction in processing temperature was particularly notable when comparing the results of laser welding aluminum alloy to both galvanized and non-galvanized steel using filler powder.

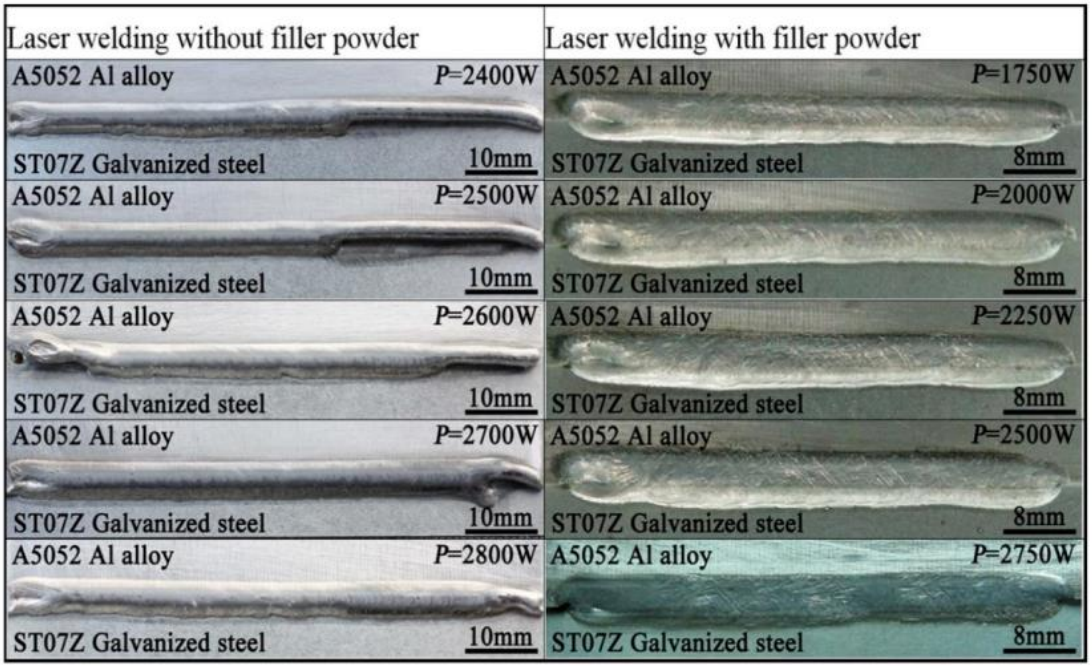

Figure 32: Surface morphologies of the joints produced by laser welding without filler powder and with filler powder [51]

2.5 XRD Technique for Residual Stresses and Phase Detection

The internal stresses that remain in a material or structure after it is produced and processed even in the absence of external forces or temperature changes are referred to as residual stresses. Operational loading, which results in uneven plastic deformation within the material, can also cause these stresses. Residual stresses need to be in an equilibrium state within the material because they do not originate from applied forces or moments.

$$\int \sigma \, dA = 0$$

where dA is any infinitesimal area in material under reference [18]. Residual stresses can be defined as either macro or micro stresses and both may be present in a component at any one time. Residual stresses can be categorized as:

- Type I: These are macro-scale residual stresses that manifest across areas of a component which are greater than the size of its material grains.
- Type II: These are micro-scale residual stresses that fluctuate at the scale of a single grain within the material.
- Type III: These are sub-microscopic residual stresses present inside a grain, typically arising from dislocations and other imperfections at the crystal level.

A variety of manufacturing processes, such as material deformation, heat treatments, and machining or processing that modifies the material's properties or shape, can result in residual stresses. Numerous factors, including unequal plastic deformation, different processing cooling rates, and phase transition-related volume changes, can cause these stresses. They can develop from loads applied during product usage, be induced during manufacturing stages, or exist in the raw material prior to processing.

It's crucial to consider these stresses in the design and manufacturing process to ensure the durability and performance of the products. XRD technique is one of methods to analyze residual stresses without modifying or disturbing the material hence its called Non Destructive Technique (NDT).

2.5.1 XRD Methodology

X-ray Diffraction (XRD) stands as one of the most versatile and widely employed techniques in materials science for analyzing the crystalline structure of materials. This powerful tool can probe the atomic arrangement within a wide array of substances, from metals and polymers to ceramics and biological materials. By directing X-rays toward a sample and capturing the unique pattern of rays diffracted by the crystal lattice, XRD can uncover invaluable information on the material's composition, crystalline phase, orientation, and other structural parameters.

In the field of engineering and materials science, XRD's non-destructive nature makes it an indispensable method for quality control, failure analysis, and the development of new materials. It is especially crucial in the context of residual stress measurement, a field that deals with stresses retained in materials after manufacturing processes such as welding, casting, or forging. These intrinsic stresses can significantly influence a material's mechanical strength, fatigue life, and dimensional stability, making their precise measurement vital for ensuring component reliability and performance.

Beyond stress analysis, XRD is also the technique of choice for phase detection, the identification and quantification of the various crystalline states that exist within a material. Since the properties of a material are profoundly affected by its phase composition, understanding the phases present is key to tailoring materials for specific applications.

The basis of X-ray Diffraction (XRD) is the interaction of X-rays with a material's crystal lattice. Depending on how the atoms are arranged, the electrons in a crystal scatter off X-rays, creating a pattern of both constructive and destructive interference. The material's crystalline structure is shown by the unique diffraction patterns that are produced by this scattering. The fundamental tenet of XRD, Bragg's Law, predicts the angles at which these patterns appear in relation to the interplanar spacings of the crystal. By utilizing the peaks in these patterns, researchers can determine the dimensions of the crystal's unit cell and the locations of its atoms, providing insights into the material's composition and directing its technological uses.

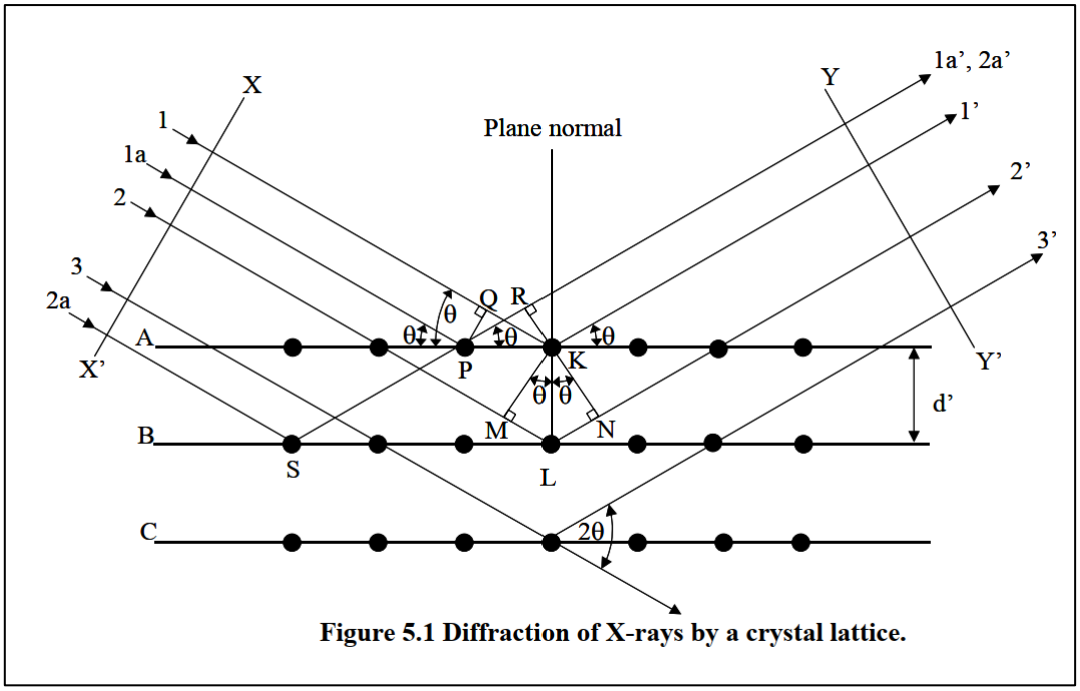

Figure 5.1 Diffraction of X-rays by a crystal lattice.

Figure 33: Diffraction of X ray by a crystalline structure [52]

In 1912 W. L. Bragg (1890-1971) analyzed some results from experiments conducted by the German physicist von Laue (1879-1960) and came up with an equation which forms basis of X-ray diffraction theory.

$$2d \sin\theta = n\lambda \quad \text{(Bragg's Equation)}$$

Process of XRD can be summarized in following way:

- The first step in XRD analysis is the preparation of the sample. This may involve grinding the material to a fine powder to achieve a random orientation of grains, which is particularly important for polycrystalline materials.
- The powder is then mounted on a sample holder or pressed into a pellet. The surface needs to be flat and devoid of any preferred orientation to prevent skewing the diffraction results.
- Once the sample is prepared, it is placed into an XRD instrument. The core components of an XRD setup include an X-ray source, a sample holder, and a detector.
- The X-ray source generates the X-rays, which are directed towards the sample. The sample holder can often be tilted and rotated to achieve various orientations relative to the X-ray beam.

- The detector captures the diffracted X-rays, and its position can be adjusted to scan through different angles, allowing the collection of a complete diffraction pattern.
- A scan is then initiated, during which the detector moves through a range of angles (2θ), while the intensity of the diffracted X-rays is recorded. Modern diffractometers may use a continuous scan mode, where the detector moves in synchrony with the sample rotation.
- The resulting diffraction pattern is a plot of intensity versus 2θ, where each peak corresponds to a set of lattice planes reflecting the X-rays.
- Analysis software is used to match the observed diffraction peaks with known patterns from crystallographic databases to identify the phases present in the sample.
- For residual stress analysis, the peak positions are used to calculate the d-spacing changes, from which the stress is determined using the elastic constants of the material.
- The final step is to report the findings. This typically includes a chart of the diffraction pattern, a table of identified phases, their respective lattice parameters, and the calculated residual stresses if applicable.

2.5.2 Residual Stresses

XRD measures the spacing between crystallographic planes within a material. When a material is under stress, this spacing changes slightly – expansion under tensile stress and contraction under compressive stress. By detecting shifts in the angles at which diffracted peaks occur (according to Bragg's Law), XRD can quantify the strains within the crystal lattice and, hence, the residual stresses.

One common approach in XRD stress analysis is the $\sin^2\psi$ method. This method involves tilting the specimen at various angles (ψ) relative to the incident X-ray beam and measuring the corresponding diffraction angles (2θ). The strain measured at these different orientations allows for the calculation of residual stress using the slope of the linear plot of $\sin^2\psi$ versus the measured strain, applying Hooke’s law for elastic deformation.

Scan of XRD diffraction for one such case is given below:

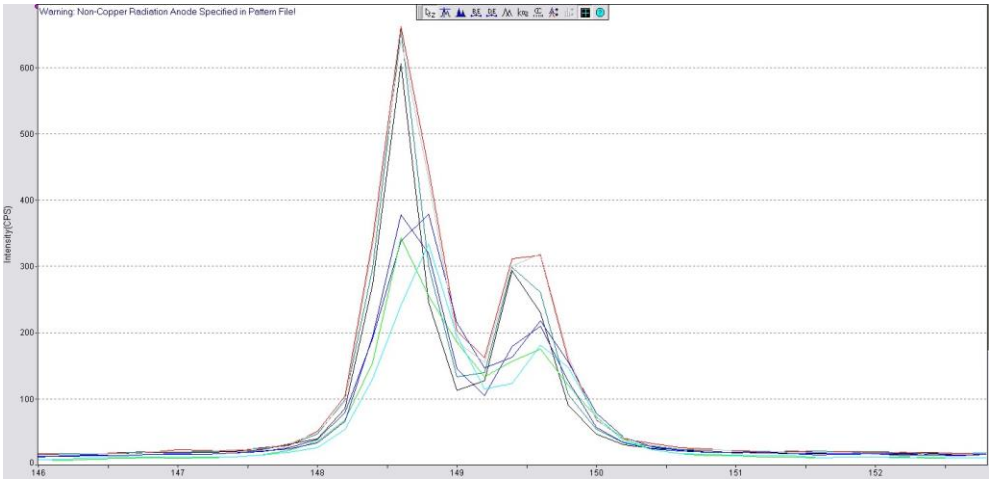

Figure 34: XRD scan for peak shifting at different Psi angles.

Data is elaborated to form a graph between interplanar distance d and sin²ψ which is further used to evaluate stresses.

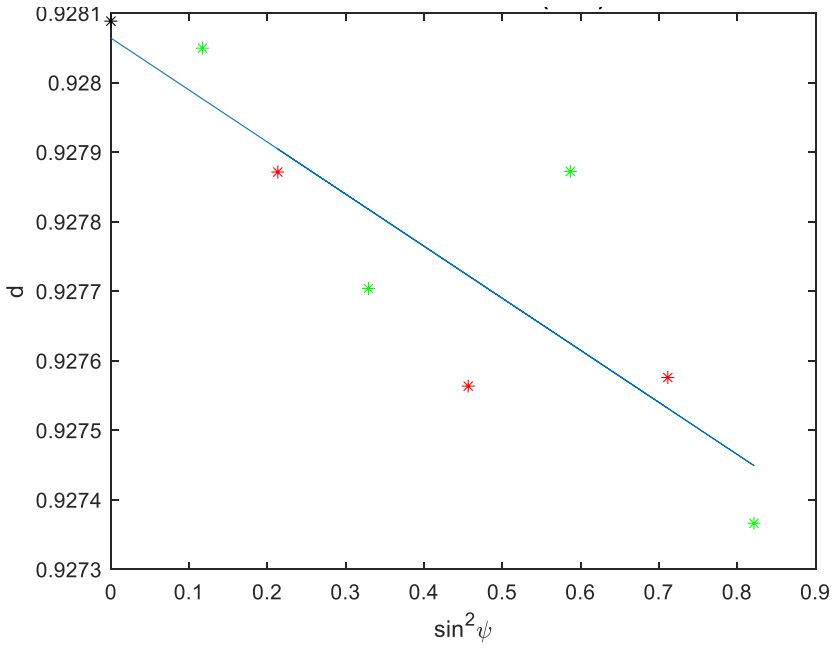

Figure 35: Relationship between d and sin²ψ

2.5.3 Phase Detection by XRD

Phase detection is another critical application of X-ray Diffraction (XRD), which involves identifying the various crystalline phases present within a material. Since the physical properties of a material can drastically change with different phases, accurate phase identification is fundamental for material characterization, quality control, and research and development.

XRD identifies phases by their distinct diffraction patterns, each acting as a unique 'fingerprint'. The positions of the peaks in the diffraction pattern correspond to the distances between planes of atoms in the crystal structure and are specific to each phase present.

When X-rays interact with a polycrystalline sample, each phase will produce its own characteristic diffraction peaks. The combined pattern is a superposition of these individual patterns and can be deconvoluted to identify the constituent phases. XRD not only detects the presence of phases but can also quantify their proportions in a mixture. The intensity of the diffraction peaks is directly related to the volume fraction of each phase within the sample.

While XRD excels at detecting crystalline phases, it can also provide information about the presence of amorphous or non-crystalline phases. These materials do not produce sharp diffraction peaks but rather a diffuse hump in the pattern, which can be used to infer their presence. Complex materials may present overlapping peaks, which can complicate phase identification and require sophisticated analysis and separation techniques.

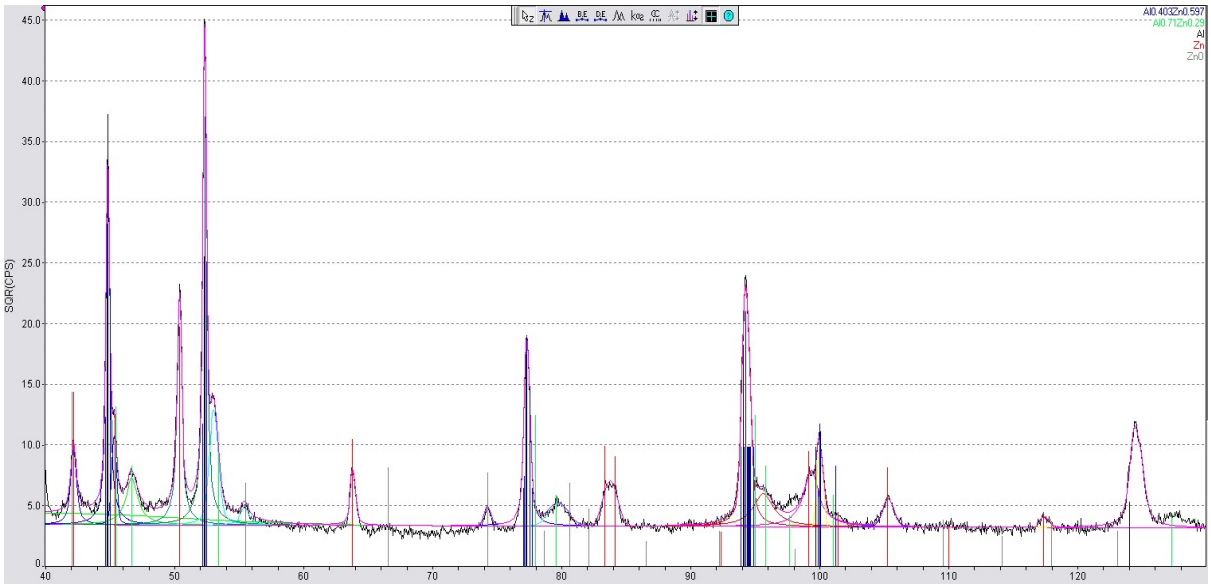

Figure 36: XRD for Phase Detection

3. Experimental Work

This section will be further divided into two parts, materials, and methodology. Materials selection and choice greatly influences the outcome of experiments, and it is therefore necessary to outline the properties of materials. Methodology of experiment and including choice of different parameters would be discussed in the second half of this section.

3.1 Materials

Experimental work mainly involved joining of Aluminum with zinc coated steel along with pure zinc as a brazing alloy. One set of experiments was conducted with flux paste (deoxidizing agent) on aluminum side while the other set was tried without this flux.

3.1.1 Aluminum 6016

Aluminum 6016 is alloy of aluminum 6xxx series with substantial amount of silicon and magnesium with traces of other elements. Detailed chemical composition is provided in Table 1. This American standard name is given by Aluminum Association, equivalent name in Europe in EN AW-6016 with chemical designation AlSi1.2Mg0.4.

Prominent properties include high tensile strength, good elongation, corrosion resistance, high weldability with MIG (Metal Inert Gas) and TIG (Tungsten Inert Gas) and heat treated to achieve T4 temper (Solution treated and natural aging) and T6 temper (heat treated with artificial aging). Primary application includes automotive industry for car body and paneling. Being wrought alloy the Al6016 can be formed into different shapes with manufacturing process such as rolling, forging and extrusion.

Different mechanical and physical properties are reported in Table 2. Sample size used in experiments had width of 1.2 mm.

Material	Si	Fe	Mg	Mn	Cu	Cr	Zn	Ti	Rest
Al-6016	1.0-1.5	0.5	0.25-0.6	0.2	0.2	0.1	0.2	0.15	Al

Table 1: Chemical Composition Al-6016

Material	Temper	Tensile Strength (MPa)	Yield Strength Rp0.2 (MPa)	Elongation at Break (%)	Uniform Elongation (%)	Density (g/cm^3)	Melting Point (°C)	Coefficient of Thermal Expansion
Al-6016	T4	190-240	80-130	≥24	≥20	2.71	570-590	$22.2x10^{-6}$ /°C at 20-100°C

Table 2: Properties of Al-6016

3.1.2 Low Carbon Zinc Coated Steel

Interstitial free steel with low carbon (<0.06) and zinc coated steel has been used for joining with Al-6016. The choice of this was mainly influenced by scope of this material in car body due to high formability as aim of thesis is test practicality of brazed joint for applications in car body. Interstitial free ensures that carbon and nitrogen do not occupy free interstitial sites in lattice structure which results in good deep drawing capability vital for automotive applications. Zinc coating provides an extra layer of protection against corrosion and is exploited for better brazing using zinc as a brazing alloy. Sample size used in experiments had width of 0.7 mm.

3.1.3 Other Materials

Pure zinc (Zn, Lucas MilhauptTM, Cudahy, WI, USA.) was used as a brazing alloy for experiments due to its good reputation in brazing with Aluminum Foam Sandwiches (AFS) as mentioned [45]. Pure zinc has high chemical affinity for aluminum making it a preferred choice.

Aluminum Flux Al-6 containing cesium fluoroaluminate paste was used with one set of experiments which is suitable in temperature range of 420-450°C. Flux effectively dissolves surface layer of aluminum oxide, which is stable, and keep the surface clean and prone to react with zn, which further effects better wettability due to lower surface tension and helps to reduce chances of porosity. Flux used for our experimentation is shown below.

Figure 37: Aluminum Flux AL6

3.2 Methodology

This part of thesis would describe in detail a set of experiments performed in the laboratory about procedure and type of accessories, tool and machines used. It is important to highlight that two sets of 3 x samples each were used for brazing, one with application of flux and one without. To distinguish between both sets, it has been mentioned which step of the process is for any specific set only.

3.2.1 Samples Cutting

Initially aluminum and steel samples are cut from sheet using micro cutting machine (ATA Brilliant 200) equipped with black alumina blade. Figure 38 shows a cutting machine along with alumina blade and samples.

Figure 38: Cutting machine and alumina blade.

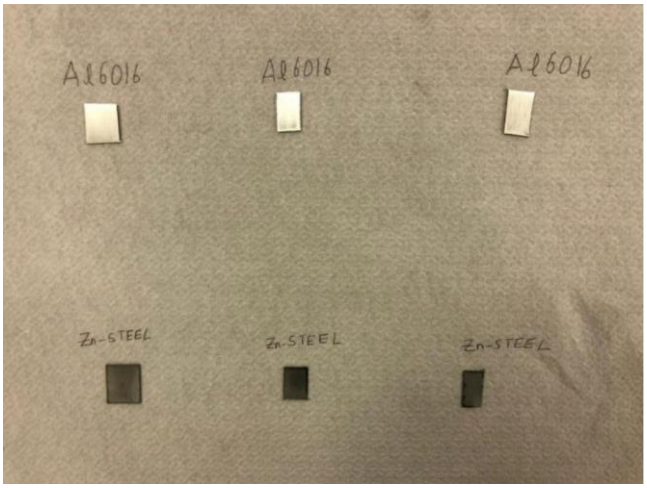

Figure 39: samples after cutting.

3.2.2 XRD Machine Setup for Calculation of Residual Stresses

The first step after samples are cut in shape is evaluation of residual stresses on the surface of the samples using XRD technique. This step is important because after brazing operation residual stresses can be evaluated again for comparison and investigating characteristics of the joint. As surface preparation can alter residual stresses and hence this step is carried out on the opposite side and before any other operations.

For this purpose, XRD machine by Rigaku (Rigaku Geiger-Flex) was used. Machine is θ-2θ system configured in Brentano geometry. The source of X-rays in this setup is through a single tube made of copper, and it prominently features a specific emission line as Cu-Kα1. In terms of its operational capacity, the system functions at a total power output of 1.6 kilowatts, achieved through a combination of a 40-kilovolt voltage supply (achievable through integrated generator) and a current flow of 40 milliamperes.

Figure 40: Rigaku Geigerflex XRD Machine

First both steel and aluminum samples were scanned with a complete scan range of 2θ to identify high and conspicuous peak at higher 2θ to exploit Braggs equation for calculation of residual stresses.

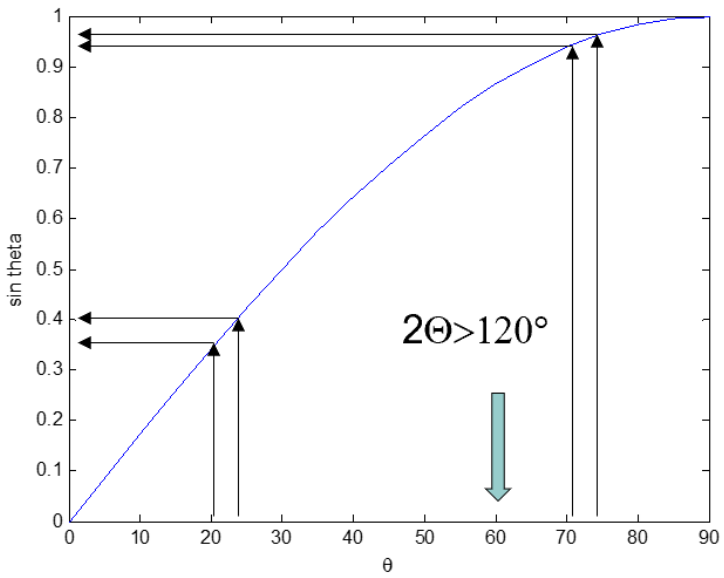

Figure 41: Relationship between sin 2theta and theta

The sample was placed in a holder using polymer clay and positioned at phi zero and then carefully placed in the XRD machine. Extra precaution and strictly abiding by the operating procedure of the XRD machine was ensured for safety reasons. XRD was controlled using dedicated Rigaku software from PC attached for selecting of different

parameters and controlling all functions of the machines for minimum physical interaction with XRD machine.

Figure 42: Sample holder using polymer clay for XRD machine.

After performing the scans, the following information was interpreted for each sample.

1. For aluminum, a vital and considerably high peak was analyzed at the range of 146-153 of 2θ with good counts per second (CPS) / intensity.
2. For zinc coated steel, too many peaks of Fe were found at lower ranges of 2θ which is not great for analyzing stresses. However, a zinc peak at higher 2θ was present shown in figure below and hence it was selected for calculation of stress. 2θ range for this was around 140-145.

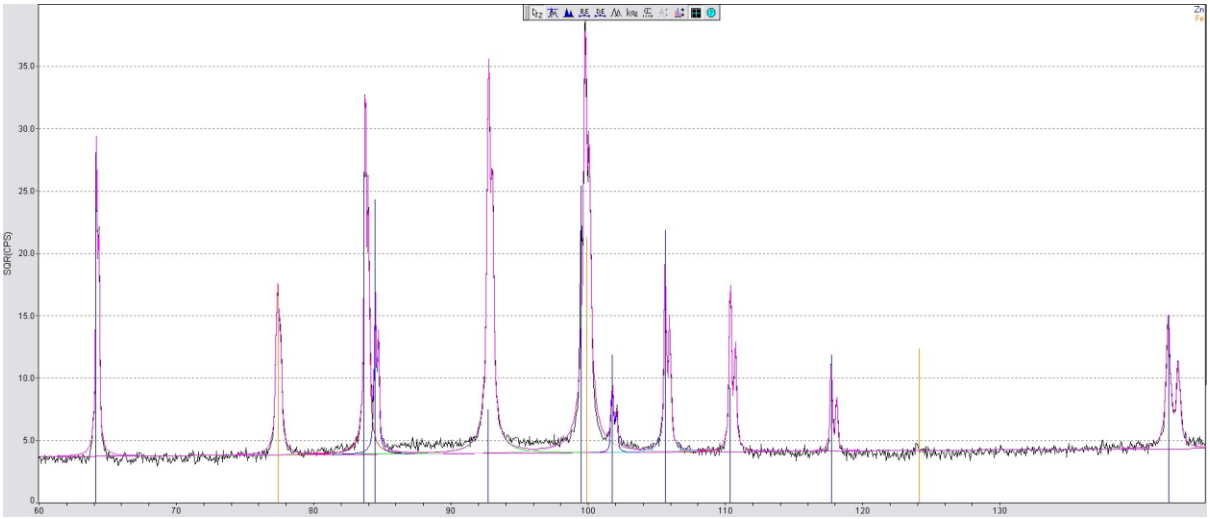

Figure 43: XRD scan of steel for peak selection

3.2.3 Residual Stresses on Exterior side with XRD

General procedure adopted for evaluation of residual stresses with XRD is illustrated as following:

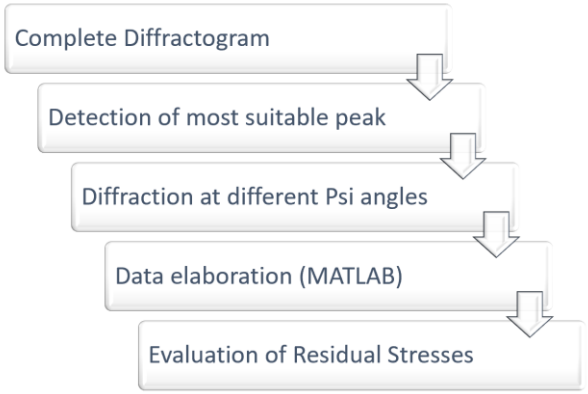

Figure 44: XRD Procedure

After finalizing the 2θ range for both samples, scans were carried out at different psi and phi angles and text files with counts were prepared for further analysis. Evaluation of residual stresses (tensile / compressive & shear) was done using MATLAB. Matlab code was developed for:

- Read the data of counts from text file at all Psi angles.
- Interpolate the data.
- Plot the graph of data and the interpolating curve.
- Calculate the straight line and ellipse interpolating the raw data for the different psi.
- Calculate the stress.
- Evaluate error of the result.

3.2.3.1 Parameters Selection for Samples

2θ range was already identified using complete scan now within that range at different psi angles XRD scan was performed with following parameters:

Serial	Description	Value
1.	No of psi Angles	8
2.	Psi 1	0
3.	Psi 2	20
4.	Psi 3	35
5.	Psi 4	50
6.	Psi 5	65
7.	Psi6	-27.5
8.	Psi7	-42.5

9.	Psi8	-57.5
10.	Initial 2theta	146
11.	Final 2theta	152.8
12.	Angle step	0.2
13.	Modulus of Elasticity	59.4 GPa

Table 3: Parameters for XRD Scan for Al-6016

Similarly, for Zn coated steel a considerable peak of zinc was found at higher 2θ hence for steel following parameters were selected:

Ser	Description	Value
1.	No of psi Angles	8
2.	Psi 1	0
3.	Psi 2	20
4.	Psi 3	35
5.	Psi 4	50
6.	Psi 5	60
7.	Psi6	-27.5
8.	Psi7	-42.5
9.	Psi8	-57.5
10.	Initial 2theta	140.75
11.	Final 2theta	144.15
12.	Angle step	0.1
13.	Modulus of Elasticity	97.5 GPa

Table 4: Parameters selection for XRD Scan for Zn Coated Steel

After the scans MATLAB code was run to find residual stresses in the samples before brazing operation.

3.2.4 Surface Preparation and removal of oxide layer

Surface preparation involves grinding of samples by abrasive papers to remove oxide layer for enhancing reactivity of material during brazing. Abrasive papers have standard diameters of grits which are used for coarse or fine or ultra fine polishing. As a reference paper, the number P320 is finer than P60. Coarse papers are usually employed for fast removal of material and fine are employed for smooth cleaning of samples. Abrasive sandpapers numbering follows CAMI for American standards and FEPA for European standards. The table below describes application of different

papers along with grit diameter [46]. It is important to note that in micro grits the standards differ a lot in their numbering. Sandpaper is also shown in the figure below.

	ISO/FEPA Grit Designation (EU Standards)	CAMI Grit Designation (US Standards)	Particle Diameter (µm)
MACROGRITS			
Extra Coarse (Very fast removal of material, hardwood flooring initial sanding)	P24		764
		24	708
	P30		642
		30	632
		36	530
	P36		538
Coarse (Rapid removal of material)	P40	40	425
		50	348
	P50		336
Medium (sanding bare wood in pre-preparation for finishing, for gentle removal of varnish, also used for skateboard grip tape)		60	265
	P60		269
	P80		201
		80	190
Fine (sanding bare wood in preparation for finishing, not suitable for removing varnish but for removing paint from wood, use for cleaning plaster and water stain from wood)	P100		162
		100	140
	P120		125
		120	115
Very Fine (sanding of bare wood, preparing for varnish or high gloss paint)	P150		100
		150	92
	P180	180	82
	P220	220	68
MICROGRITS			
Very Fine (sanding finishes between coats)	P240		58.5
		240	53.0
	P280		52.2
	P320		46.2
	P360		40.5
Extra fine, start polishing of wood or sanding small errors in coat layers which does not risk coming in separate layers		320	36.0
	P400		35.0
	P500		30.2
		360	28.0
	P600		25.8
Super fine (final sanding of finishes, final sanding of wood)		400	23.0
	P800		21.8
		500	20.0
	P1000		18.3
		600	16.0
	P1200		15.3
Ultra fine (final sanding and polishing of thick finishes and preparing for high gloss polishing)	P1500	800	12.6
	P2000	1000	10.3
	P2500		8.4

Table 5: Sandpaper Grit Standards [47]

Figure 45: P320 Abrasive paper

To remove stable oxide layer from aluminum sample, we used P320 paper and for steel used P4000 was employed as not to remove Zn coating which is good for joining. Using used paper gives the advantage that grits are not conical rather smoother and hence sample is not modified and is only cleaned.

3.2.5 Etching of Aluminum Only (Without Flux Brazed Sets Only)

For sets that were tested without application of flux, Al6016 samples were etched in 12% nitric acid (HNO_3) solution for 15-20 minutes after surface preparation. Etching helps removal of any remaining oxide layer from substrate and also helps in wetting process. Figure below shows this process. After etching aluminum sample is removed from acid beaker and cleaned with water before putting in ethanol beaker along with steel and zinc samples. Extra care and specific operating procedure is adopted in disposing of nitric acid after etching. This step is only used in sets where brazing was carried out without the application of aluminum flux.

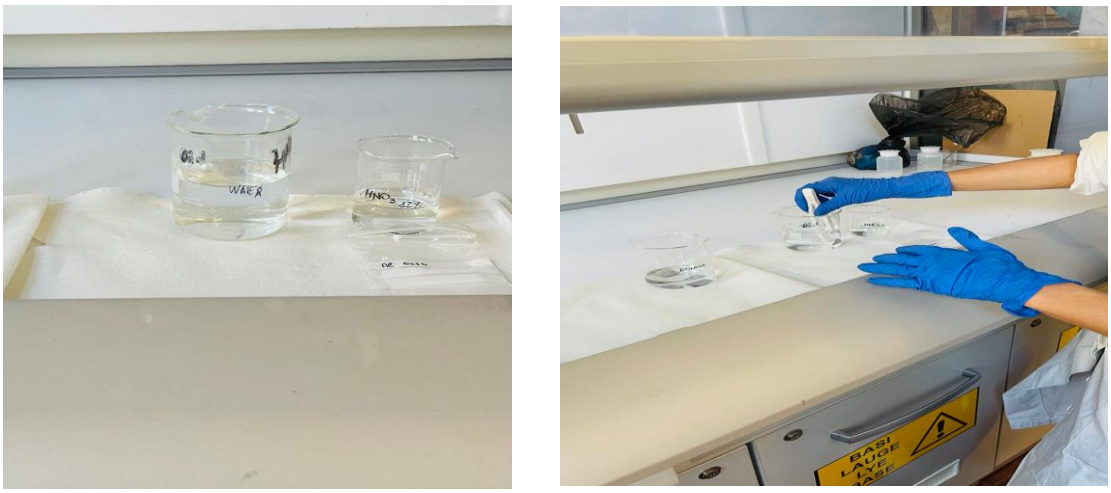

Figure 46: Etching of Al-6016 with 12% HNO3

3.2.6 Ultrasonic cleaning in Ethanol and Drying

After etching of aluminum (in case of without flux brazing sets) and surface preparation, all samples of steel, aluminum and zinc are placed in beaker with ethanol with cleaned surfaces facing upwards. After surface cleaning through abrasive papers some particles and contaminants can remain on surface which are to be removed using ultrasonic cleaning. Ultrasonic cleaning uses high frequency sound waves travelling through liquid where sample surface is merged, contaminants are removed from the surface by the combined mechanical action of ultrasounds and chemical action of the solvent (ethanol). Procedure can be adopted for metal, glass, ceramic, and some hard polymers.

Samples were merged into beaker in ethanol and lid was closed using aluminum foil. Cleaning by ultrasonic was carried out for five minutes at room temperature and then samples were removed from beaker and ethanol was disposed of in specific order. Figure below shows this process.

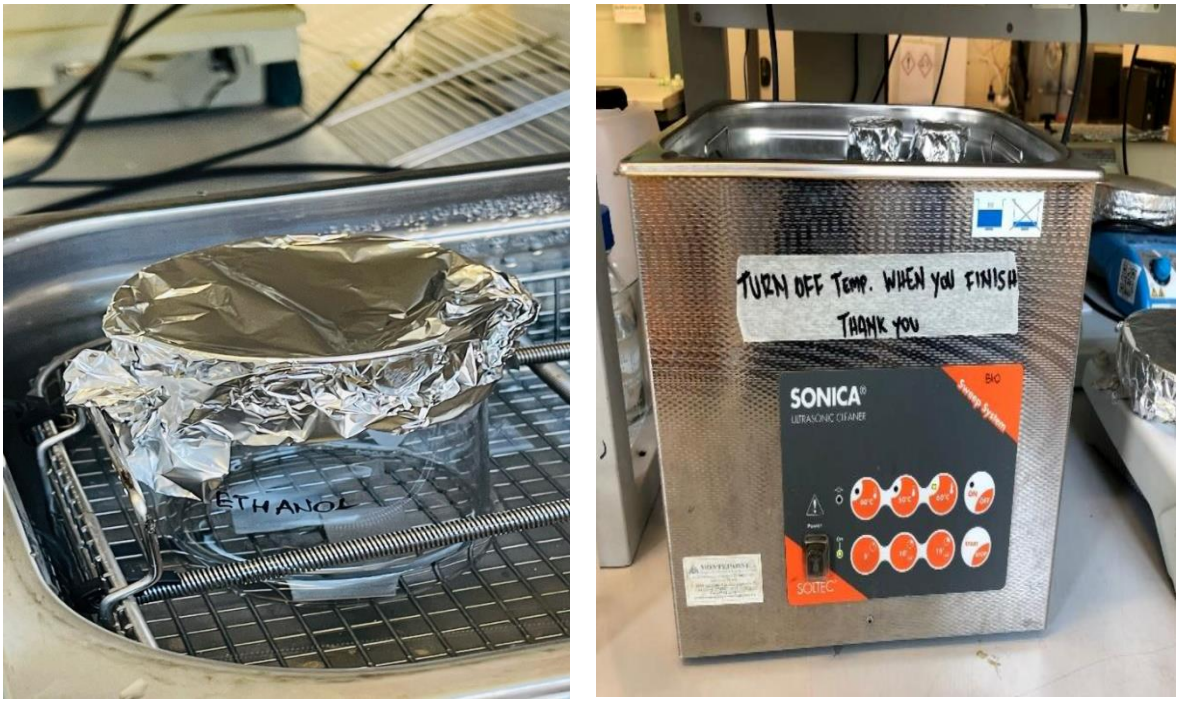

Figure 47: Ultrasonic cleaning in ethanol

After cleaning ultrasonic samples were dried using compressed air to avoid entrapment of any water molecules or liquid particles on surface of substrates. Air gun with compressed air was used on samples to ensure full drying process and then

samples were laid out for stacking. Below figure shows air gun and samples after all process so far.

Figure 48: Compressed air gun for drying

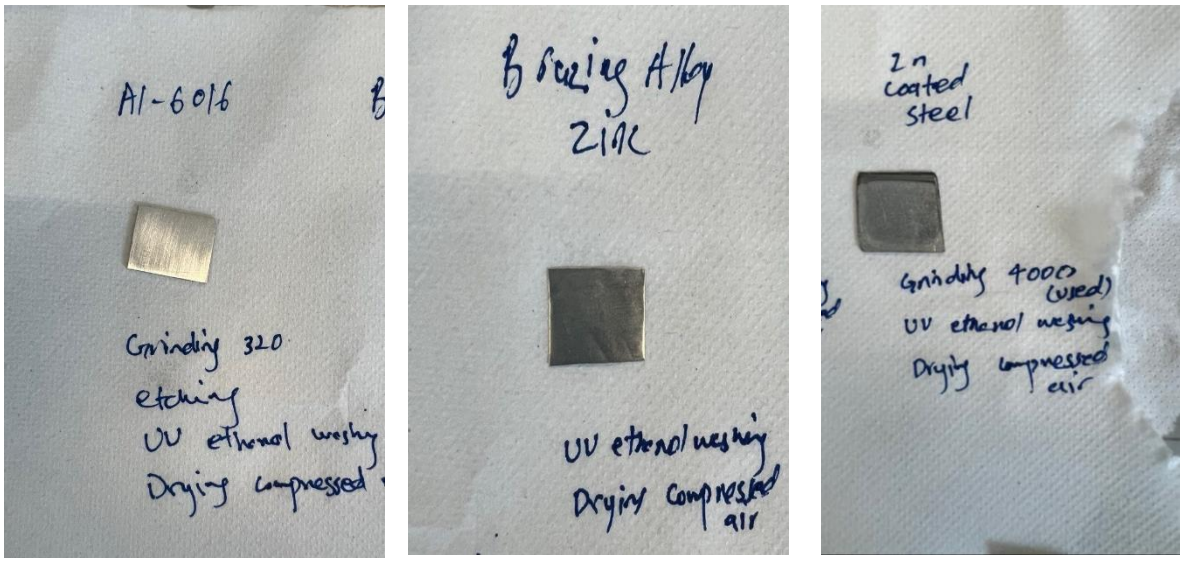

Figure 49: Samples before stacking.

3.2.7 Application of Flux (With Flux Brazed Sets Only)

Aluminum flux Al-6 containing cesium fluoroaluminate paste is applied on aluminum sample using cotton swab under the chemical hood for safety. This step is only done in sets where etching was not carried out and brazing was conducted with flux. Flux helps removal and oxide layer and avoid reoxidation of aluminum and also helps in wetting process of brazing. Below figure depicts the process of applying flux.

Figure 50: Application of flux on aluminum

3.2.8 Stacking of samples for Brazing

Stacking of all three samples (Aluminum, Brazing alloy Zinc, and Steel) in proper arrangement is necessary before putting them in furnace. An important aspect of brazing operation is wetting phenomena where brazing alloy melts and spreads all over substrate surfaces for joining. Through old experiments and also from literature it has already been established that placement of aluminum sample at the bottom of stack helps in wetting process and better results are achieved as compared to placing steel at the bottom of stack.

Flat rectangular iron pieces are used at the bottom and top of the stack to provide stability to sandwich due to its weight. Graphite paper is used on both sides between iron pieces and samples which helps in detaching the samples after the brazing operation. Below figures show stacked arrangement used in our experiments. Sometimes mechanical pressing is also applied to ensure better and uniform stacking in the case of non-planar samples.

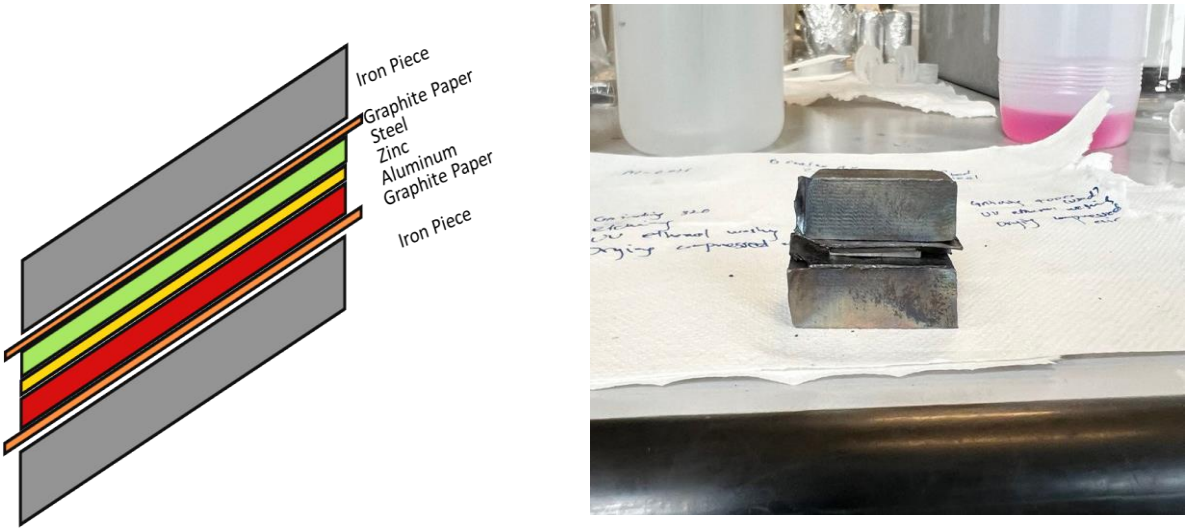

Figure 51: Stacking Orientation of Samples

Figure 52: Pressing of Stack with Mechanical Presser

3.2.9 Furnace Brazing

After sandwich and carefully applying press to keep stack in order, this is placed in the furnace to start the main operation of experiment which is brazing. The furnace used in experiments was tubular furnace (Carbolite, Hope Valley, UK). Stack was carefully placed in the center of the furnace to provide uniform heating, and because the thermal gradient temperature at the sides of furnaces is not exactly as indicated on the program. The furnace is heated with electric induction.

To avoid oxidation of samples at high temperatures Argon atmosphere is ensured in the furnace with attachment of tube to Ar cylinder on one side and in water bath on

the other side. Titanium plugs are also used with locking mechanism of furnace to capture oxygen.

Main parameters used for brazing operations on all sets are as following:

- Initial temperature : 20°C
- Heating rate : 10°C per minute
- Final temperature : 480°C (500°C on program of furnace)
- Dwell : 7 Minutes (Variable in few experiments)
- Cooling rate : 10°C per minute

After cooling of furnace, samples were extracted using special gloves and visual inspection of the success of joint is checked and prepared for further investigation. Images Below represent this process.

Figure 53: Tubular Furnace with attachment to Argon cylinder

3.2.10 Evaluation of Residual Stresses

Before samples are put in resin mounting for further tests, residual stresses are evaluated using XRD on exterior surface of both Al-6016 and Zinc coated steel. Same procedure is adopted as before with same parameters and stresses are evaluated using MATLAB. Peak shifting at different Psi is a good indicator for possible varying of stresses in case of low counts.

3.2.11 Resin Mounting and Traversal Cutting

In the case of successful joining sample is now prepared for further investigation of joint. The first step involved is to mount the sample in resin so that it can later be cut in traverse and reaction layer and joining area can be investigated using optical microscopy, SEM, hardening test, and more tests.

To mount, samples are placed in the rubber die using clips at the bottom of the die holding the sample in vertical position as shown in the figure.

Figure 54: Placement of samples in die for resin mounting

Cold resin mounting was employed which required mixing of Technovit 4071 powder and solution in 1:2 proportion. After the solution is stirred in a cup with powder and is homogenously mixed, it is carefully poured into die under the hood. Care was taken to ensure samples remain in stable vertical position while solution is poured. After this, die is left overnight for hardening of the resin, which normally takes 10-12 hours. After removing from the die, mounted samples are cut in two parts transversely using TR80 Evolution Abrasive Cutter machine. This complete procedure is depicted in the following figure.

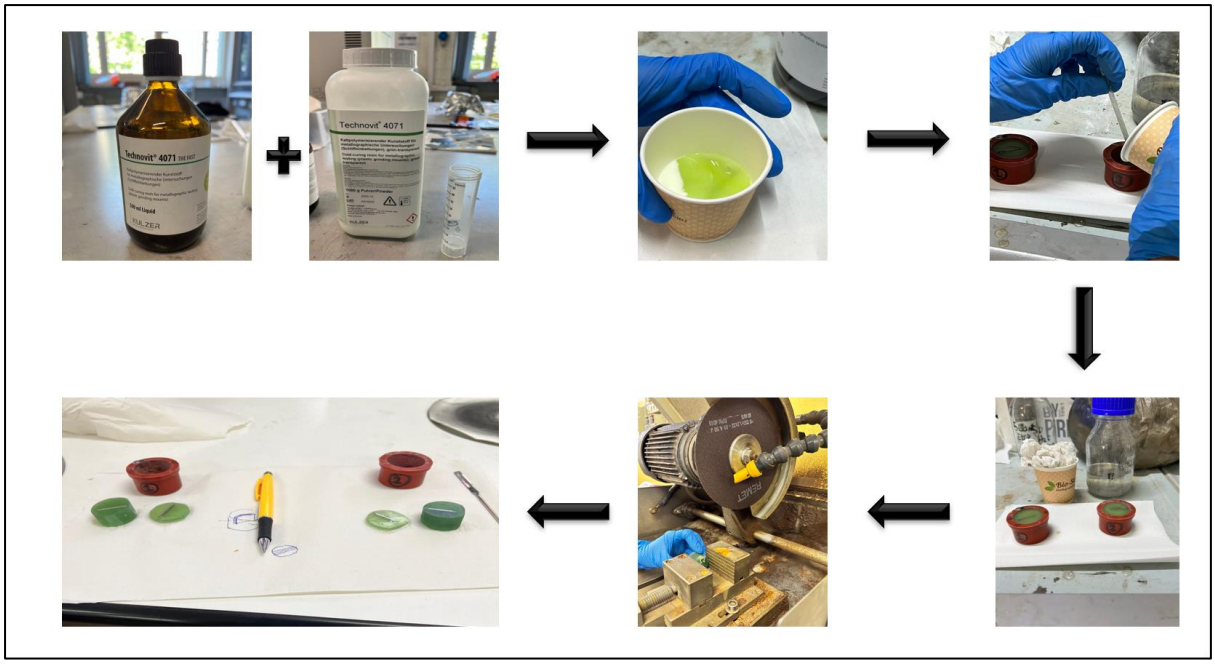

Figure 55: Resin Mounting and Traverse Cutting Process

3.2.12 Polishing Operations

Optical microscopy of the joining area requires mirror like polishing of surface of samples. For this purpose, abrasive papers were used from coarse to ultra fine to remove oxide layer and then provide smooth and shiny surface which can be reflective enough for optical microscopy to analyze reaction layer.

P120 paper was used at the start of polishing which is very coarse to make the surface planar and remove any contamination or excessive from cutting operations. Gradually paper was changed to fine and ultra fine to reduce surface roughness. Order of abrasive paper used was P120, P320, P600, P1200, P2500 and finally P4000. Abrasive paper polishing was used with continue flow of water to cool the sample during grinding. To obtain mirror like finishing diamond paste was used on 1µm setup with lubrication to provide that. Lubrication was necessary during this stage as diamond past if accumulated can scratch the surface easily. The Polishing machine used is depicted in the figure below.

Figure 56: Polishing Machine

As our sample is made of two dissimilar materials and aluminum is soft compared to steel, aluminum could easily get scratch while polishing and this was observed during our experiments. Excessive force to push the samples on abrasive paper is also not recommended which can cause imperfections specially non planarly at micro level which cannot be focused by microscope at higher magnification and also poses difficulties in micro hardness test.

To avoid easy scratching of aluminum as compared to steel another strategy was used. Instead of gradually increasing abrasive paper to P4000 which although provides smoother surfaces but was also giving scratched to aluminum side, so after P1200 paper we directly switched to diamond paste at 1µm. This improved the results of polishing significantly.

3.2.13 Optical Microscopy

After polishing, metallographic observation of the traversal cross section was carried out on optical microscopy at different magnifications. Optical microscope uses visible light to reflect from the surface of the object and produce image through objective lens. The range of optical microscope is limited by wavelength of the visible light which ranges from 400nm (UV) to 700nm (IR).

REICHART MeF3 machine equipped with a digital camera along with eyepiece to display the images on computer screen was used. Capabilities of this microscope were:

- Image modes : Darkfield, Polarized, Brightfield
- Variable luminosity with adjuster
- Objective Lenses : 2x, 5x, 10x, 20x, 50x and 100x
- Eyepiece / camera lens : 10x

So, from 20 to 1000 times magnification was achievable using the optical microscope. Samples were first studied at 20x magnification which gave a generic picture of the joining area and gradually magnification was raised to study and analyze the thickness and continuity of the reaction layer.

Figure 57: Optical Microscope

3.2.14 Micro Hardness Test

Microhardness tests were performed on the cross section of the joint to measure hardness on Vickers scale which can help investigate the presence of intermediate phases or otherwise. Remet HX-1000 machine was used to perform these tests which is equipped with following components:

- Indenter: Diamond pyramid shaped indenter to mark indent on surface.
- Load: Variable range from 10g to 100'g depending on application.
- Optical System: Microscope to view position before and after indentation.

- Control : To set test parameters such as load and dwell time.
- Display : For display of indents with area and performing hardness values.

Figure 58: Microhardness Test Machine

For our experiments we used 25g load with 10 seconds dwell time and hardness was calculated at various points on bulk materials as well as on reaction layers.

3.3 Other Experiments

In addition to the process adopted for samples which joined successfully, some additional investigation was carried out for failed brazing samples in some cases of without flux experiments. Mainly, SEM / EDS and XRD along with Optical microscopy was carried out to check the surface of substrate and investigate failure.

3.3.1 Scanning Electron Microscopy / Energy Dispersive Spectroscopy

Both Al-6016 and zinc coated steel substrates after failed brazing without flux were further investigated with scanning electron microscopy to get detailed results.

To prepare the samples for SEM, there are a few steps involved in sample preparation. An electrical connection must exist between the samples and the microscope since SEM is powered by an electric field. There are additional metal clamping tools available to help keep samples steady inside the microscope. We placed a conductive tape on our sample and on the bottom of the SEM clamp to complete the circuit, which is necessary for the electrons to pass through and complete the circuit. The sample is seen in the accompanying picture being inserted into the vacuum chamber of the scanning electron microscope for analysis.

Figure 59: Sample Placement in vacuum chamber of SEM Machine

To avoid water droplets in the output scan, samples are dry cleaned with compressed air before putting in chamber and applying vacuum. Dedicated software with the machine allowed for varying controls to select area and magnification for higher resolution images than optical microscopy. SEM operates on the same basic principles such as optical microscope however instead of visible light it uses electron beam and an electron field to provide information.

A concentrated beam of high-energy electrons raster across a material under observation, a scanning electron microscope (SEM) produces incredibly detailed images. Using several electromagnetic lenses and apertures, the electron beam that emerges from an electron cannon is precisely focused and directed onto the sample. Secondary electrons, backscattered electrons, and distinctive X-rays are produced by interactions between the electrons and the atoms in the sample. These emissions are then picked up by a variety of detectors. The X-ray detectors show the sample's elemental composition, the secondary electron detector provides detailed topographical information, and the backscattered electron detector provides insights into compositional differences based on atomic number contrast. The basic SEM configuration is illustrated below.

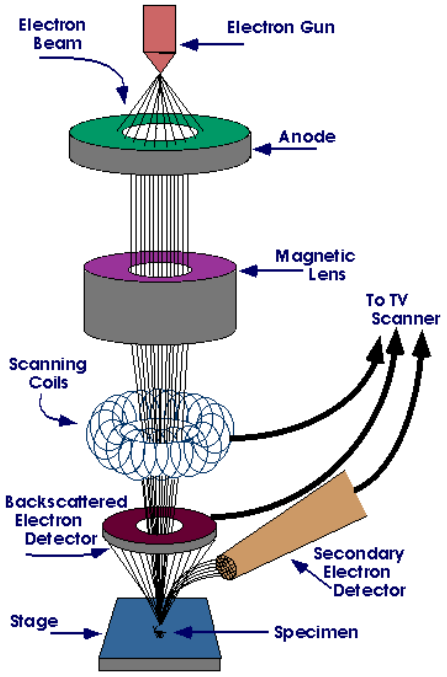

Figure 60: Schematics of SEM working [47]

As JOEL machine is equipped with Xray spectrometer, it can provide elemental composition of the spot along with higher magnification. So, it can simultaneously create chemical microanalysis to provide elemental composition in conjuncture with SEM analysis.

The high-energy electron beam from the scanning electron microscope (SEM) after interaction with the sample can dislodge inner-shell electrons from the atoms. This triggers electrons to transition from higher to lower energy levels to fill these vacancies, which causes the elements present to release characteristic X-rays. These released X-rays are detected by a semiconductor detector in the EDS system, which then transforms them into voltage signals. The elements contained in the sample may be identified since the X-rays' energy are typical of the elements from which they came. The multichannel analyzer that is connected to the detector sorts the incoming X-ray photons according to their energy and generates a spectrum that shows the X-ray emissions' intensity as a function of energy. various elements have various peaks in the spectrum, and the area beneath each peak indicates how much of that element is present in the sample. This makes it possible to analyze the elemental makeup of the sample both qualitatively and quantitatively.

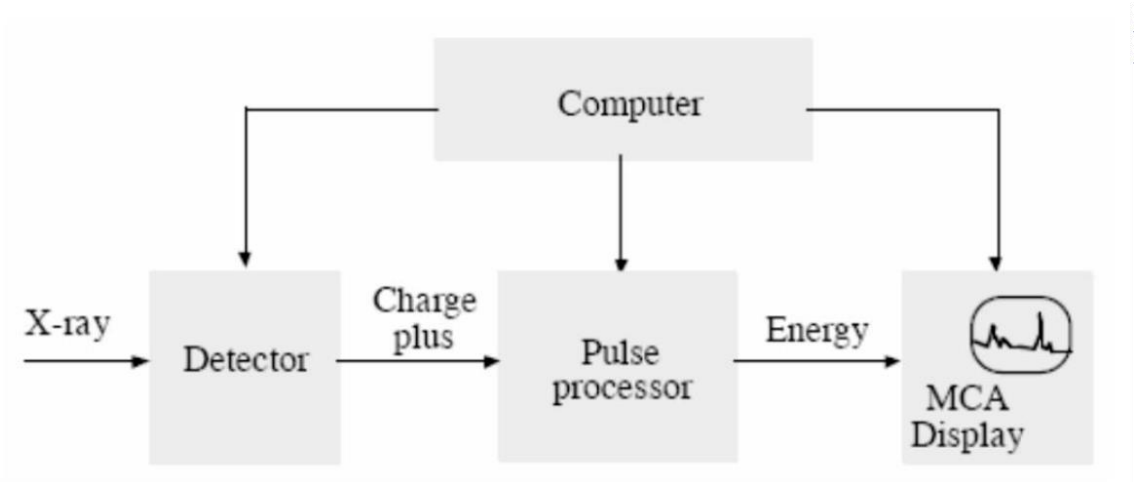

Figure 61: Xray spectral by EDS

3.32 Phase constituents by XRD

Previously XRD scan was used to carry out scans in very specified 2θ range where isolated and significant peak at higher angle was present. However, XRD scan can also be used on failed samples substrate surfaces (after failed brazing) at complete range to identify peaks for possible formation of intermediate phases formed during brazing operation.

Diffraction is the result of interactions between a monochromatic X-ray beam and the crystal lattice on a metal substrate. Bragg's Law states that constructive interference happens at specific angles, resulting in the formation of diffraction peaks that are indicative of the material's lattice parameters and crystal structure. A recording and analysis are made of the resulting diffraction pattern, which consists of peaks at different angles and intensities. The peaks' locations match the crystal's interplanar spacings, and their intensities are connected to the atomic locations inside the unit cell as well as the existence of different crystallographic planes. The experimental diffraction pattern is compared to standard references to determine the phases that are present in the substrate.

4. Results and Discussions

In this part of the thesis, results obtained from our experiments and testing carried out on samples with XRD, optical microscopy, micro hardness and SEM / EDS are elaborated. It is Important to understand that not all samples went through same set

of testing hence table below describes the outcome of brazing experiments on 6 x samples and specific testing done on each sample.

Samples	Pre-Brazing Tests / Steps	Brazing Conditions	Result of the Brazing	Post Brazing Tests	Remarks
Samples With Flux (Set 1)					
Sample 1	Residual stress calculations on exterior side of samples	• Surface Preparation • Ultrasonic cleaning in ethanol • Drying with compressed air • Applying flux on aluminum substrate • Stacking with Al at bottom • Brazing at 480°C with 7 minutes dwell time	Success	• Optical Microscopy • Post brazing residual stress calculations. • Micro hardness test	
Sample 2			Success		
Sample 3			Success		
Samples Without Flux (Set 2)					
Sample 4	Residual stress calculations on exterior side of samples	• Surface Preparation • Etching of AL-6016 in HNO_3 solution • Ultrasonic cleaning in ethanol • Drying with compressed air • Stacking with Al at bottom • Brazing at 480°C with 7,8 and 9 minutes dwell time respectively	Failed	• Optical Microscopy on traversal cross section • SEM and EDS analysis of substrate • XRD scan for phase detection	
Sample 5			Success	• Optical Microscopy • Post brazing residual stress calculations! • Micro hardness test	
Sample 6			Success		Steel clips used to ensure reasonable binding during brazing

Table 6: Summary of Experiments

Results and discussion on samples is now discussed in detail.

4.1 Optical Microscopy

This section would illustrate in detail the results of optical microscopy done on samples at traversal cross section at the joining area. Along with failed sample no 4 to check the presence of reaction layer.

4.1.1 Sample 1-3 (Set 1: Samples with Flux)

Set 1 samples were done by applying aluminum flux AL-6 on aluminum side and brazed at 480°C for 7 minutes. Visual inspection showed that joining was confirmed. After resin mounting and polishing, an optical scan was done, and results are detailed below.

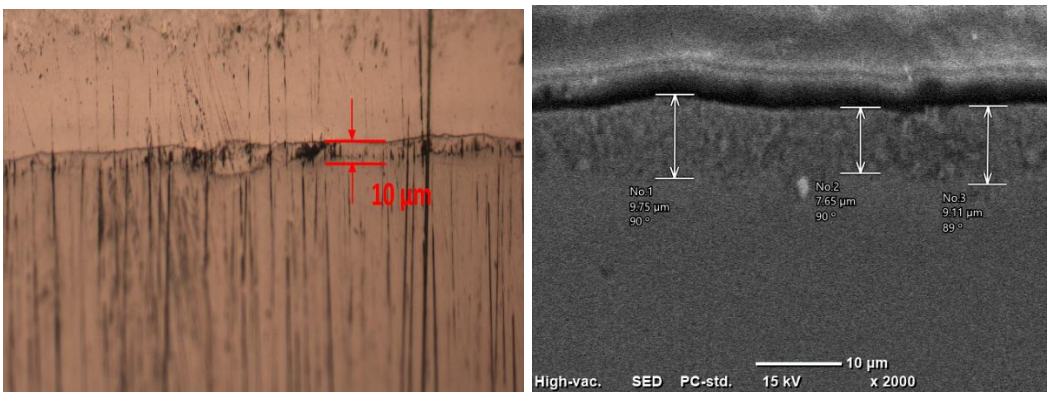

Figure 62: Zinc coating thickness on steel opposite to reaction side

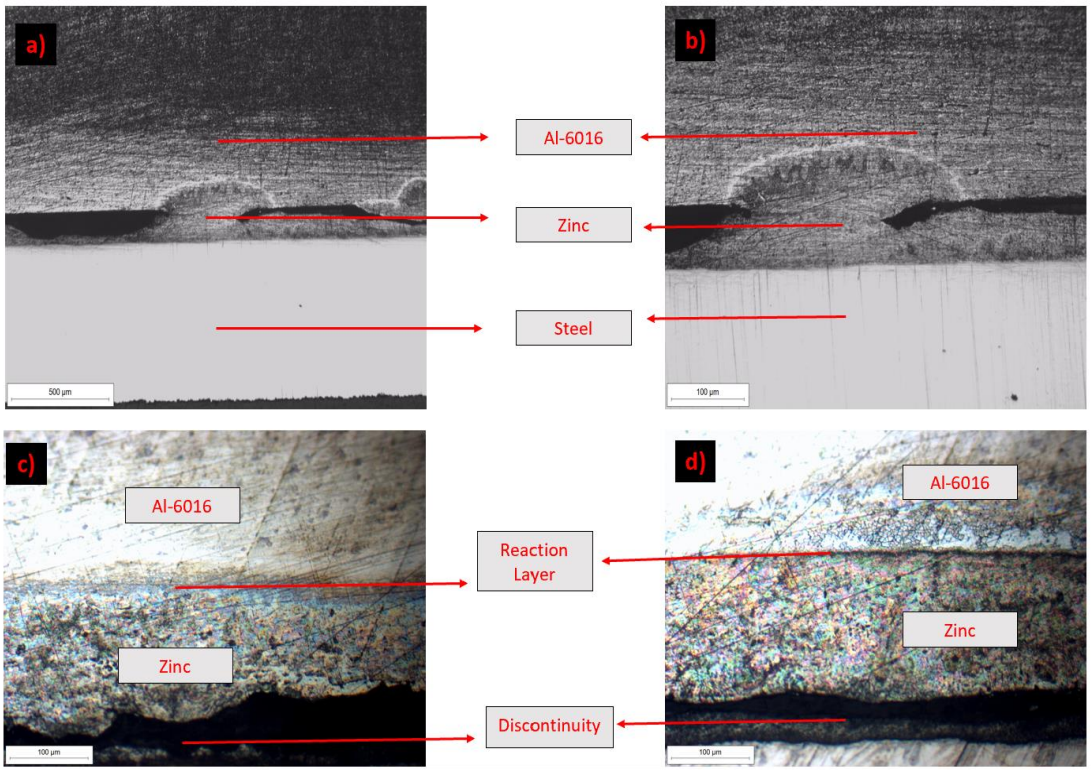

Figure 63: Optical microscope image of traverse section of set 1 samples a) & b) showing joining area while c) & d) showing discontinuity on steel side.

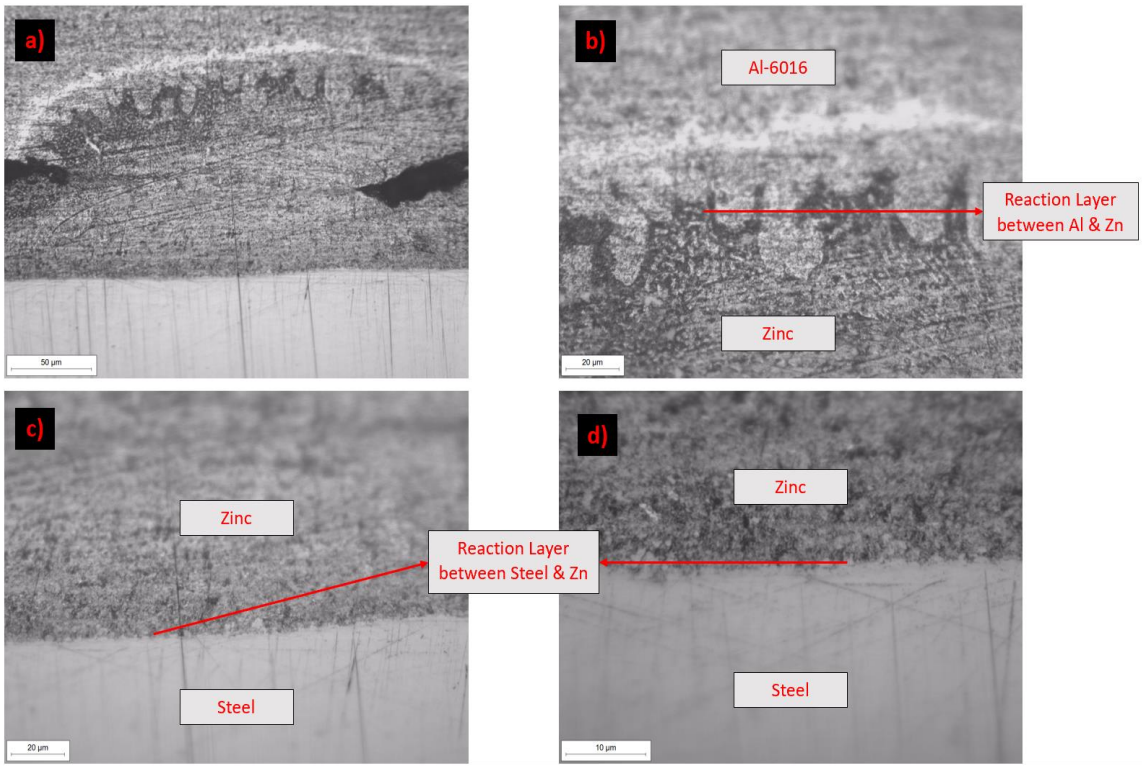

Figure 64: Optical microscope image of traverse section of set 1 at higher magnification.

Zinc coating of around 10 µm was observed on steel side towards non reaction side. Layer width varies due to melting and solidification after brazing operation. As seen on the transvers section by microscope, appreciable joining at some points of complete zone were observed. Furthermore, aluminum surface sheet was able to react with zinc because of high affinity of zinc towards aluminum, as it can be seen a continuous reaction layer towards aluminum side, with some discontinuities (figure 63 a and b). In the case of zinc coated steel, it can be observed very few joining lines, while rest were discontinuities between zinc coated steel and zinc brazing layer (figure 63 c and d). It must be pointed out that in macro view of produced samples, a certain amount of material localized on outside perimeter of sample between two sheets. This material is probably the liquid material formed during brazing, that modified by the flux addition, and changed its chemical and fluid properties, moving from the center to the external perimeter (shown in figures below).

Zinc in presence of flux (containing cesium fluoroaluminate) when melted and at higher temperatures, moved outward towards perimeter due to increased fluidity and low viscosity. This caused liquid material to have non homogenous spread over substrates

with lower thickness in the center, coupled with not alignment of sheets at microscale resulted in joining at some points while discontinuity on others as seen in optical microscope images of transverse section.

Figure 65: Localization of brazing material on perimeter

4.1.2 Sample 5 (successful joint without flux from set 2)

Sample 5 experiment did not use aluminum flux rather etching of aluminum after surface preparation was done to avoid reoxidation of aluminum. Brazing conditions were like set 1 however dwell time was increased to 8 minutes. Visual inspection after brazing showed possible success in joining which led to resin mounting and polishing of traversal cross section of sample which was then observed under optical microscope. Results are as follows.

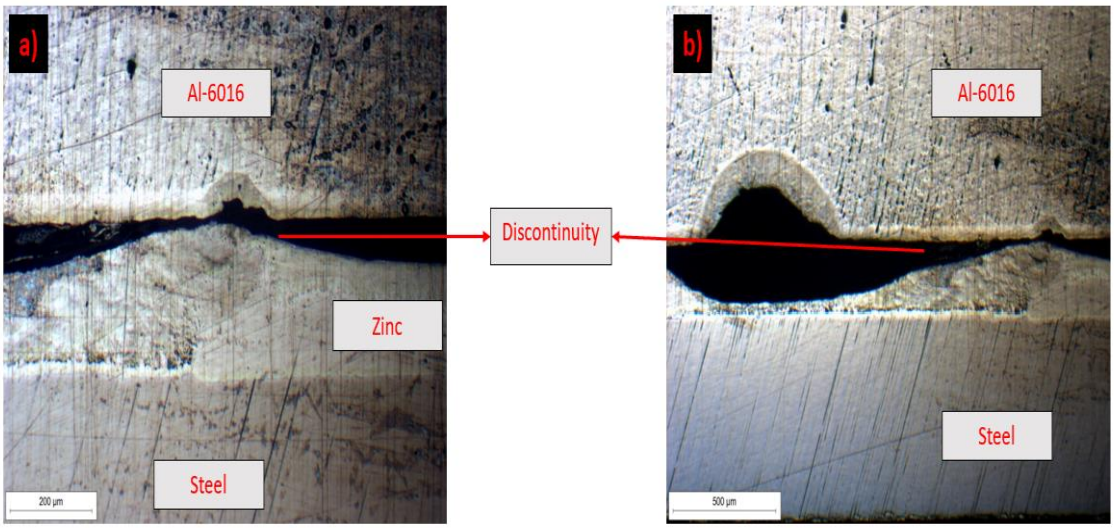

Figure 66: Optical microscope scan of traversal section showing discontinuity.

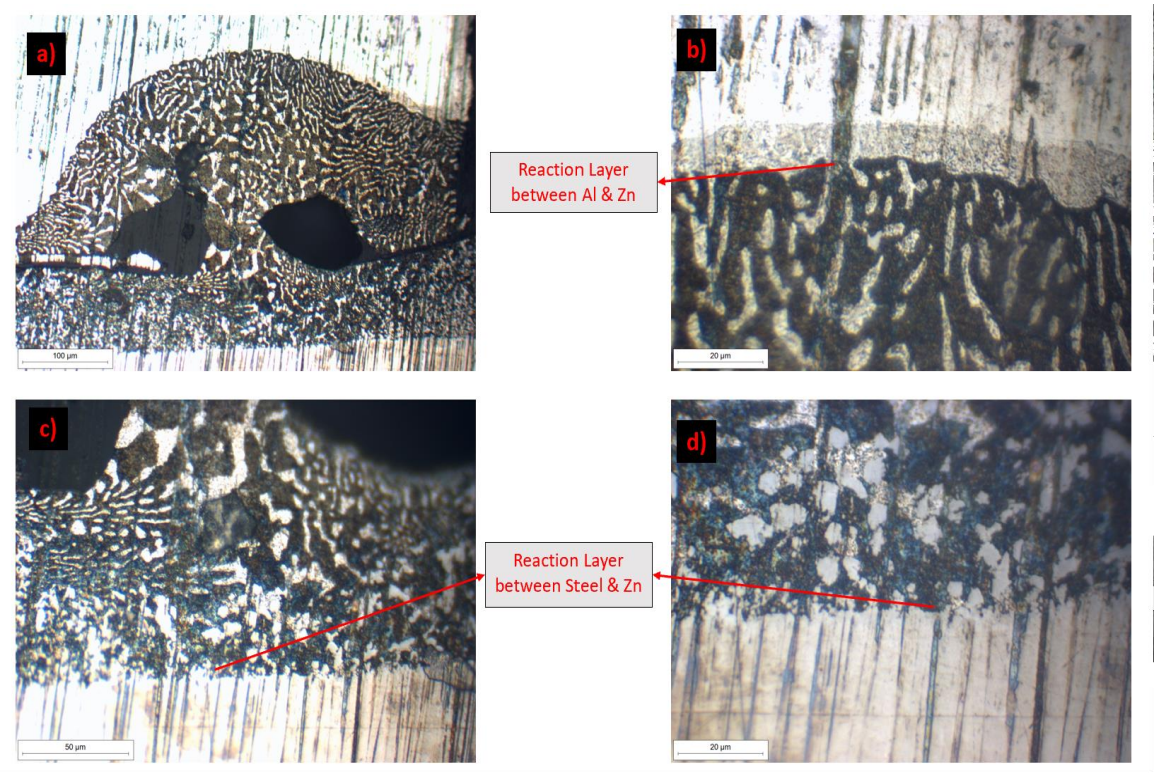

Figure 67: Optical microscope scan of traversal section showing joining at different magnifications.

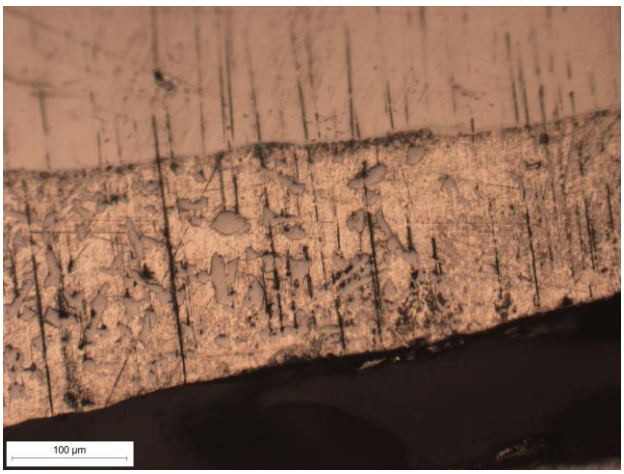

Figure 68: Brazing alloy zinc phases

Visual inspection of sample observed joining, however in optical microscope it was seen joining was not continuous and only a few points. This sample without application of flux showed significant reaction layer continuity on zinc coated steel side while discontinuity was observed towards aluminum side. This observation was opposite to what we observed in set 1 samples where flux was used. A possible explanation could be zinc coating on steel reacted with brazing alloy while absence of flux caused on aluminum side to remain less affected towards brazing alloy.

Reactivity of aluminum in absence of flux is reduced towards liquid zinc because of Aluminum passivation. Porosity is seen in (figure 67 a and c) because of shrinkage of molten material in liquid to solid transformation.

In figure 68, it was observed that zinc formed two phases upon solidification.

4.1.3 Sample 4 (Failed sample without flux)

Sample 4 was experimented without flux and brazed at 480°C (500° set) with dwell time for 7 minutes could not joined and stack was separated when removed from the furnace. The traversal cross section of both aluminum and steel was cut and polished in resin mounting as shown in the figure. Afterwards cross sections were observed under an optical microscope to investigate reaction outcomes.

Figure 69: Resin mounting and polishing of traverse cross section of failed sample

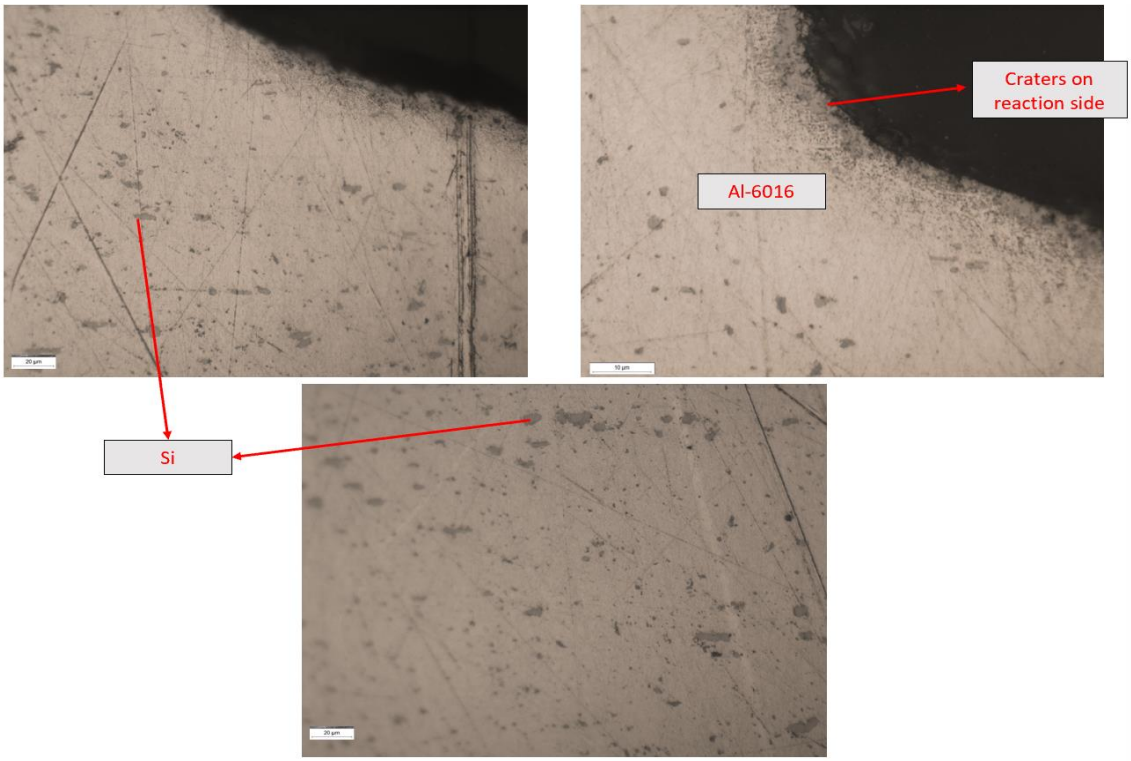

Figure 70: Al-6016 traverse cross section scan after failed joining (top side reaction layer)

Microscope images showed some craters like pitting on reaction side of Aluminum sample. Liquid zinc reacted with aluminum and upon solidification left craters on aluminum side, the amount of liquid was low and joining could not be succeeded.

After polishing silicon particles were observed on aluminum side that are present in base material Al-6016. These silicon rich particles were harder than α aluminum phase and they could not be scratched so easily as metallic aluminum.

A similar observation of steel was also performed, and images are shown below.

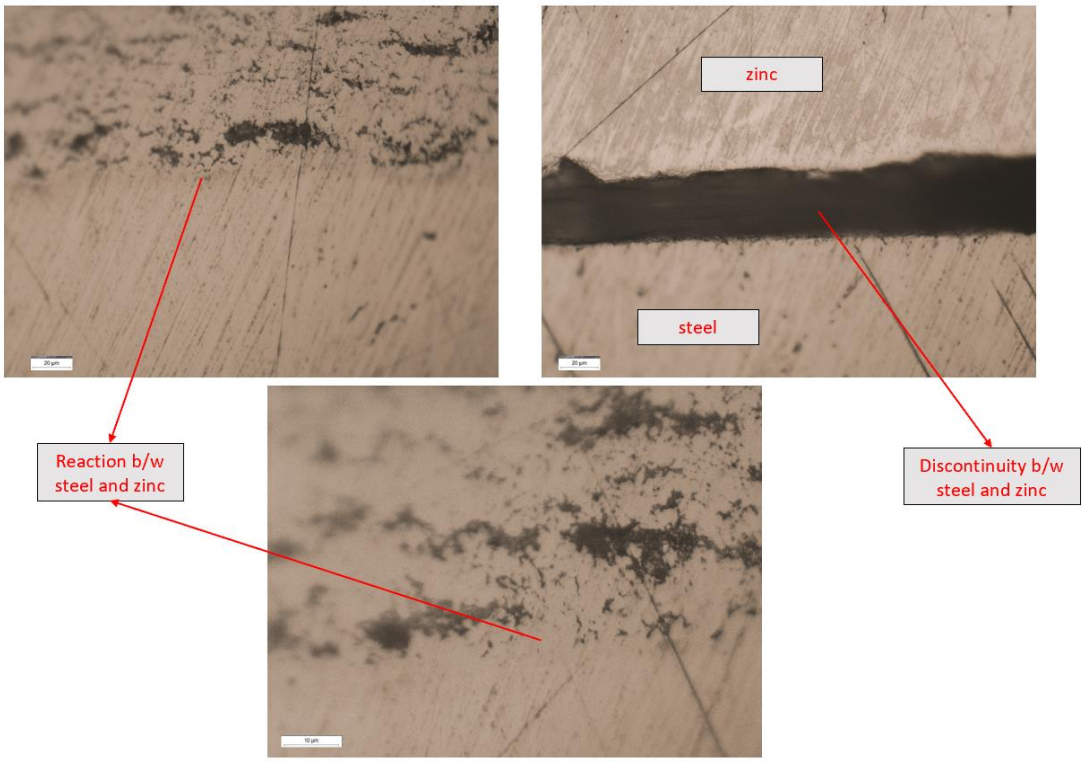

Figure 71: Zn coated steel traverse cross section scan after failed joining.

Similar results were observed in the case of successful joining without flux as there was continuous layer of reaction between steel and brazing alloy while some discontinuities were also observed.

It can be proposed that zinc coating on steel plays a vital role in case of brazing without flux. This coating melts with zinc brazing alloy and on solidification, some porosity or etched area is seen on reaction layer along with some discontinuities with complete removal of zinc coating on steel side.

4.2 SEM and EDS Analysis

SEM analysis provides higher resolution at greater magnification along with chemical composition given by EDS provides a clearer understanding of substrate and reaction layer. SEM & EDS were performed on successful samples on joining area to ascertain type and weight of different elements at local areas. Similar analysis was also conducted on failed sample without flux, in particular observation was carried out on substrates of Al and Steel on reaction side.

4.2.1 Joining Area Analysis

Results of SEM & EDS analysis of both samples, one with flux and without flux is discussed separately.

4.2.1.1 Sample 1 (With Flux)

After observation by optical microscope, the joining area was observed under SEM-EDS for better resolution and local elemental characterization.

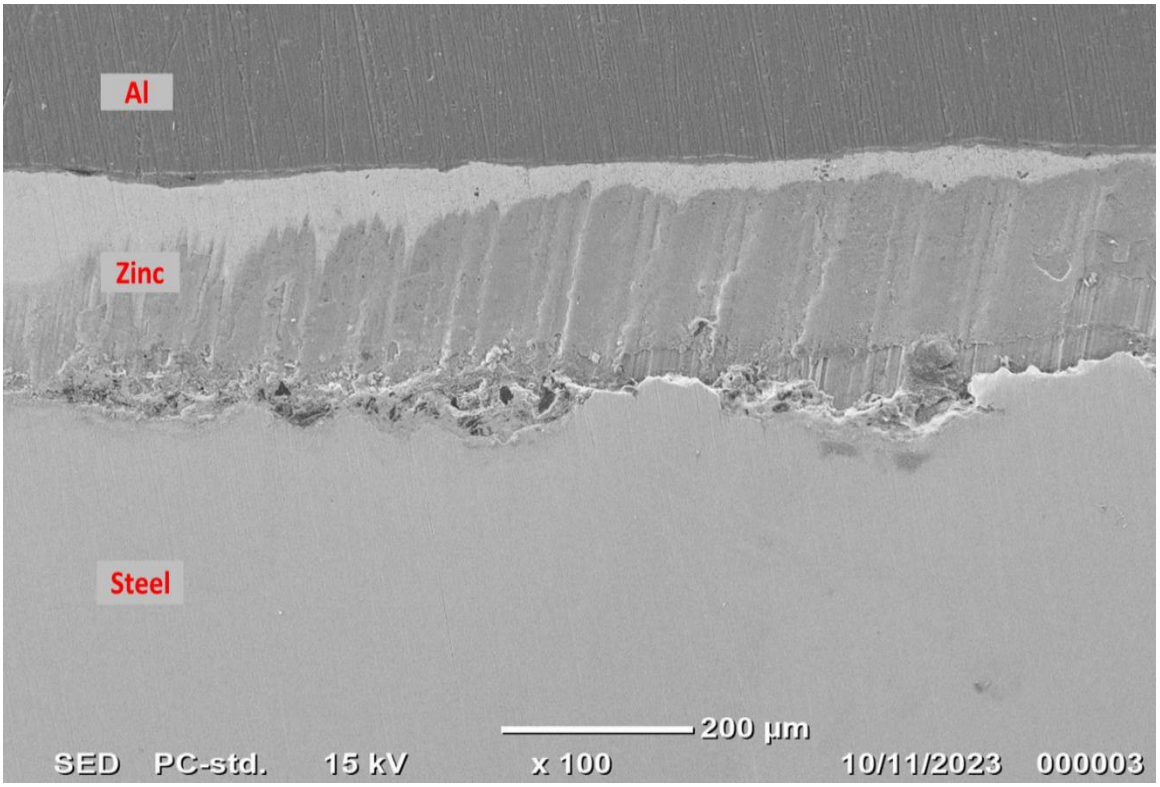

Figure 72: Scanning Electron Microscopy-Energy Dispersive Spectroscopy (SEM-EDS) analysis of joining area of traversal cross section of sample with flux.

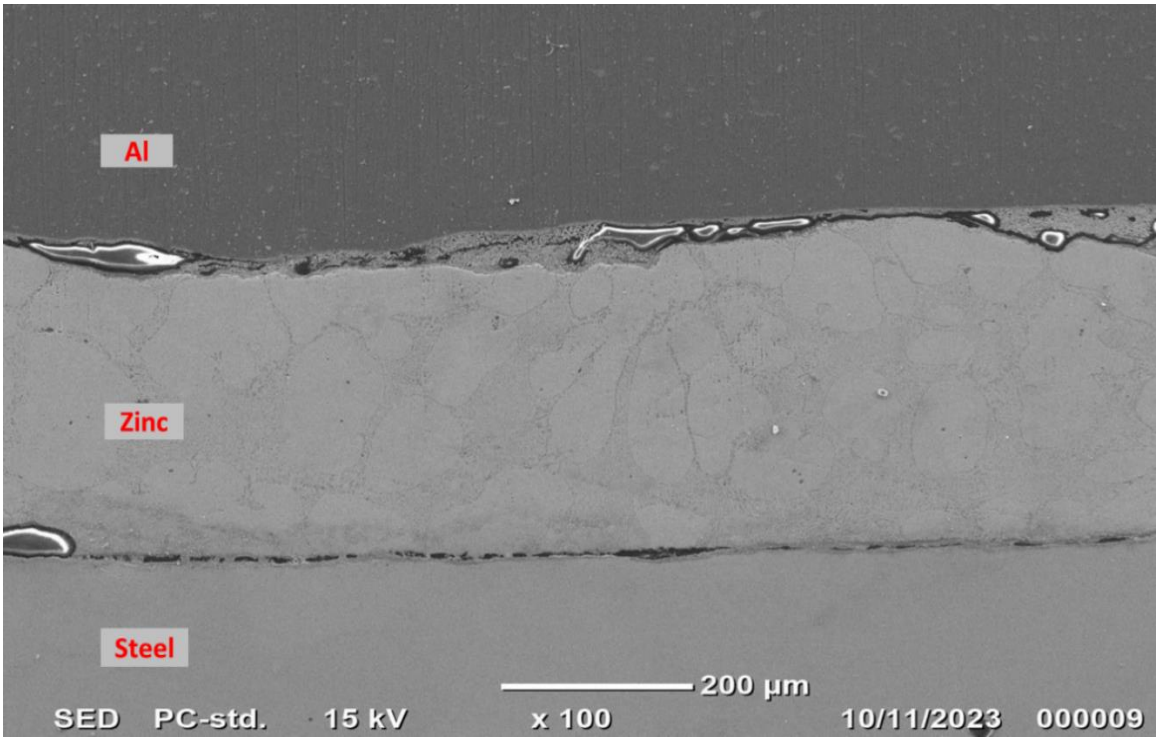

Figure 73: SEM-EDS analysis of joining area of traversal cross section of sample with flux.

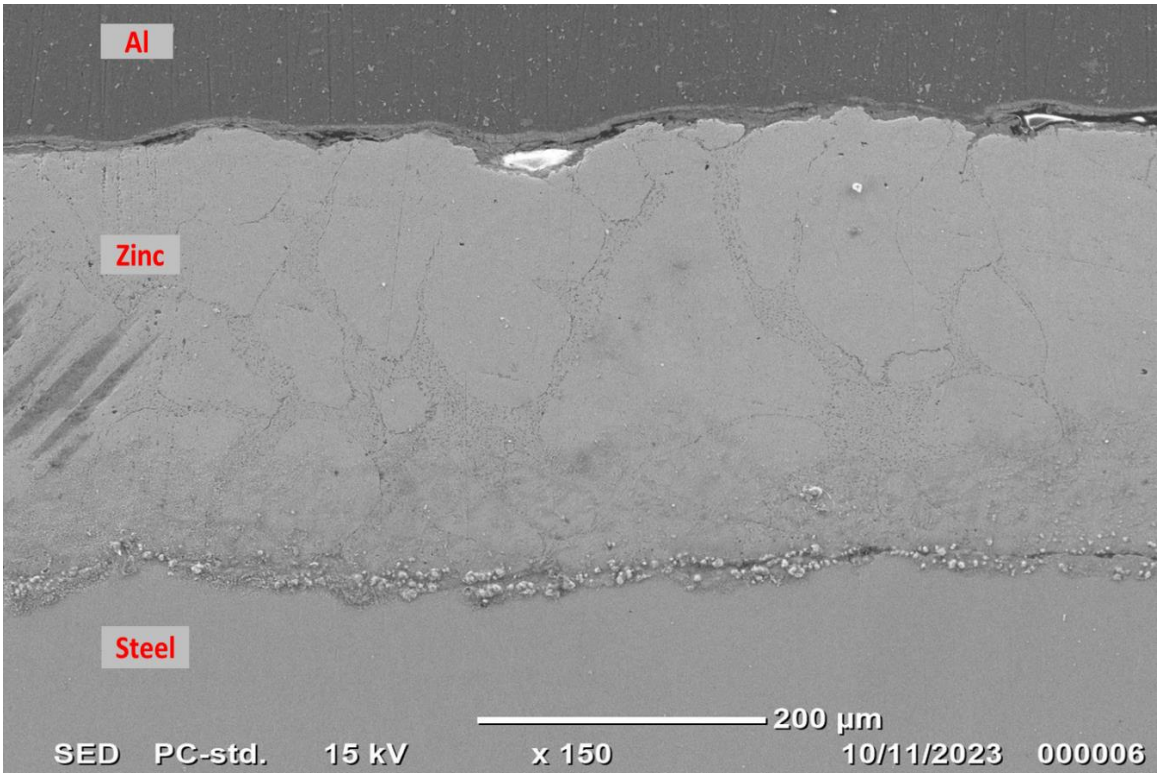

Figure 74: SEM-EDS analysis of joining area of traversal cross section of sample with flux showing continuity of reaction layer.

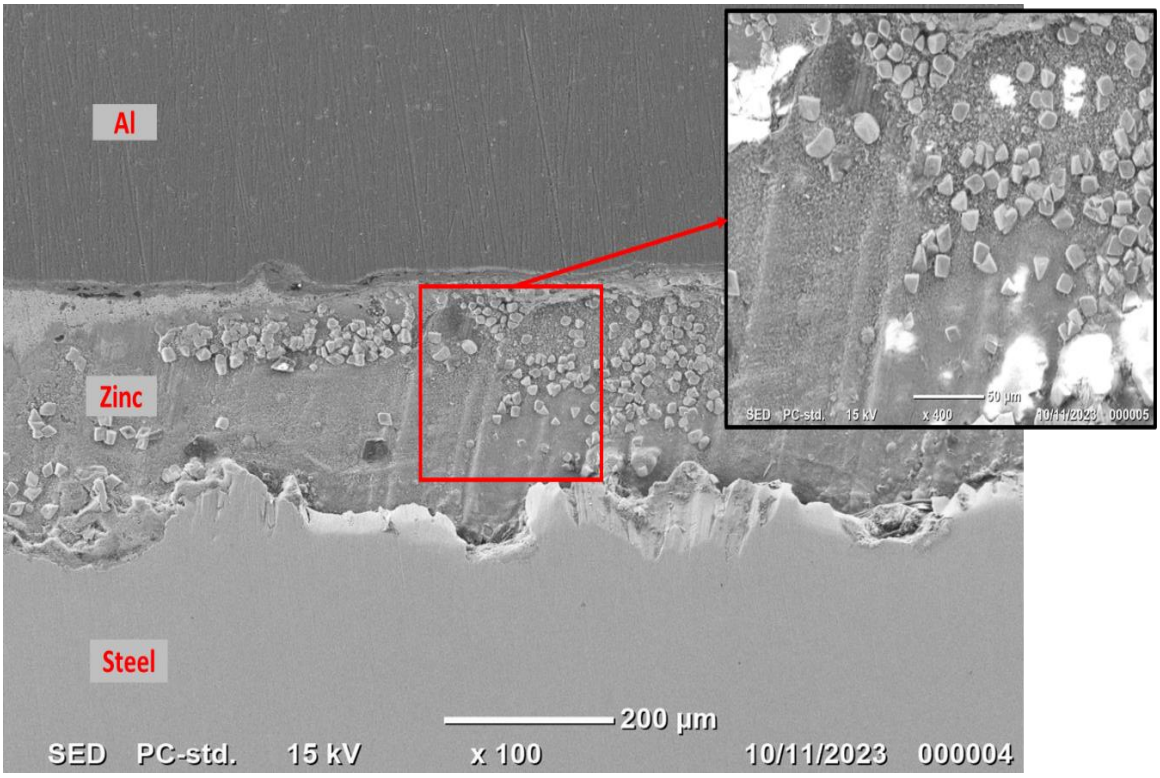

Figure 75: SEM-EDS analysis of joining area of traversal cross section of sample with flux.

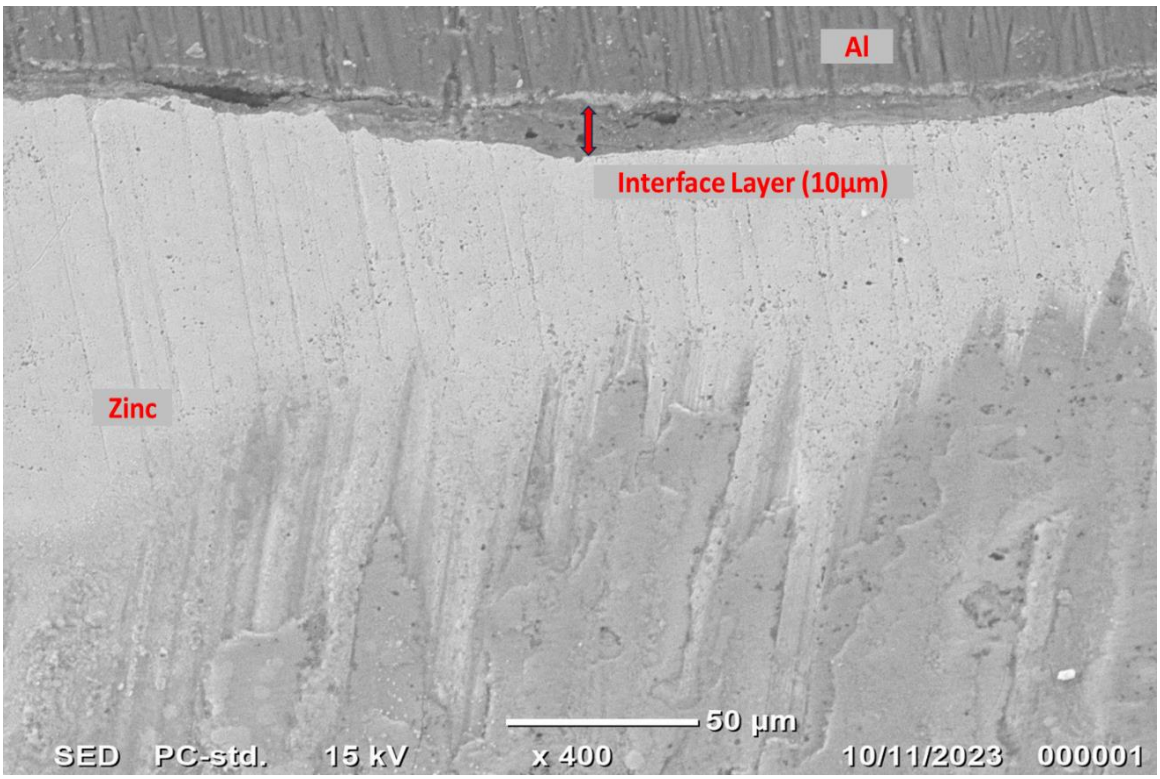

Figure 76: SEM-EDS analysis of joining area of traversal cross section of sample with flux showing interface layer between Al and Zn.

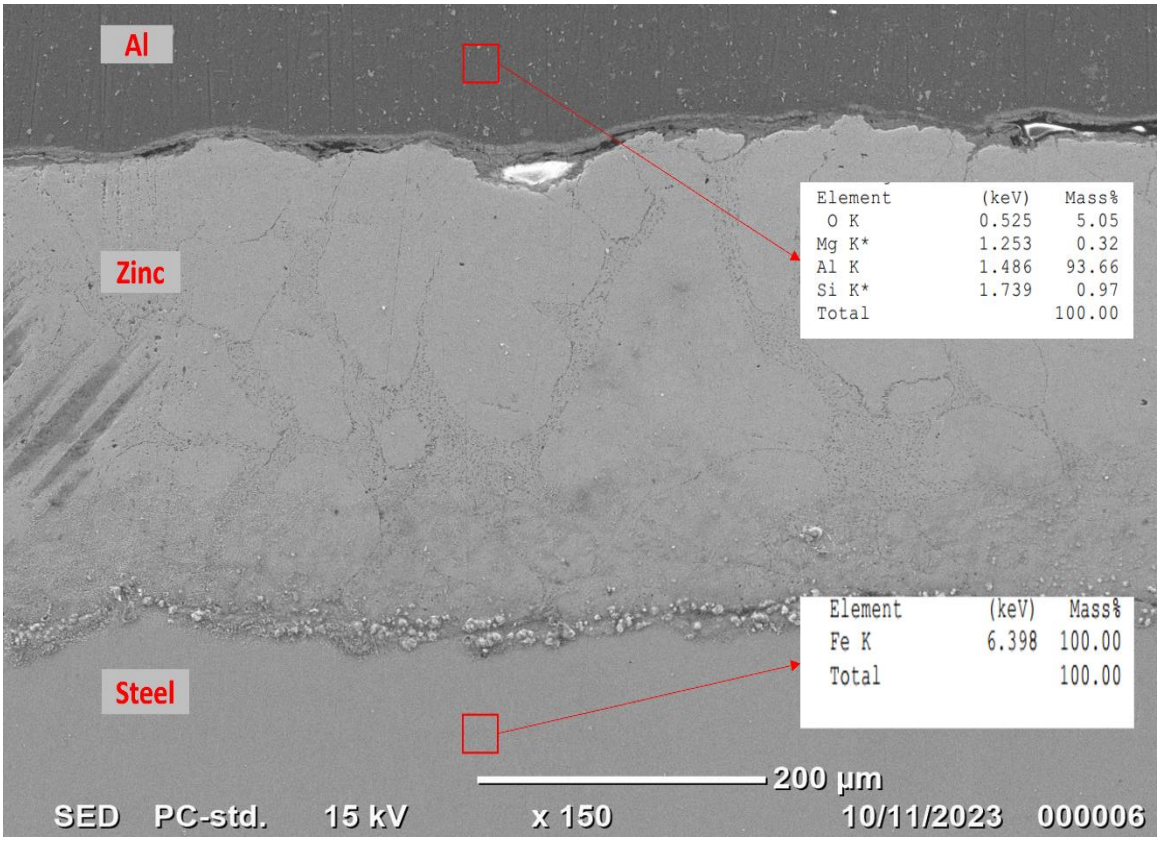

Figure 77: SEM-EDS analysis of joining area of traversal cross section of sample with flux showing local chemical composition of base materials.

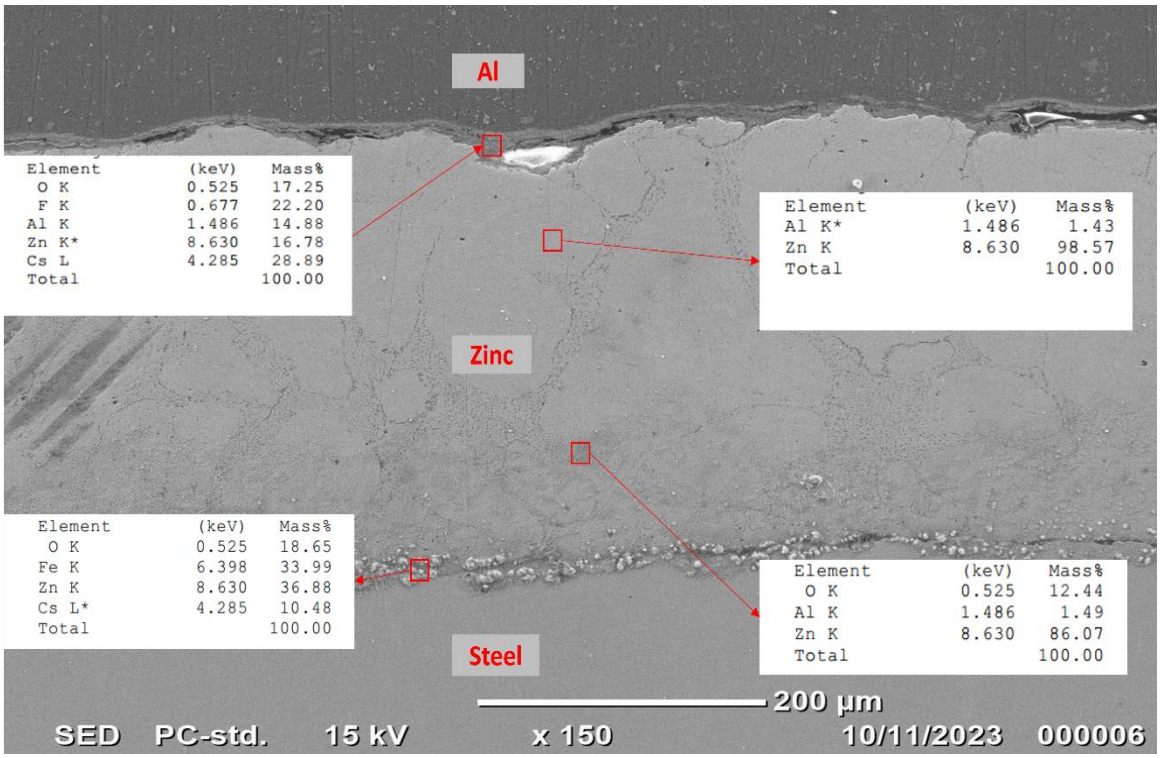

Figure 78: SEM-EDS analysis of joining area of traversal cross section of sample with flux showing local chemical composition on interfaces and in joining area.

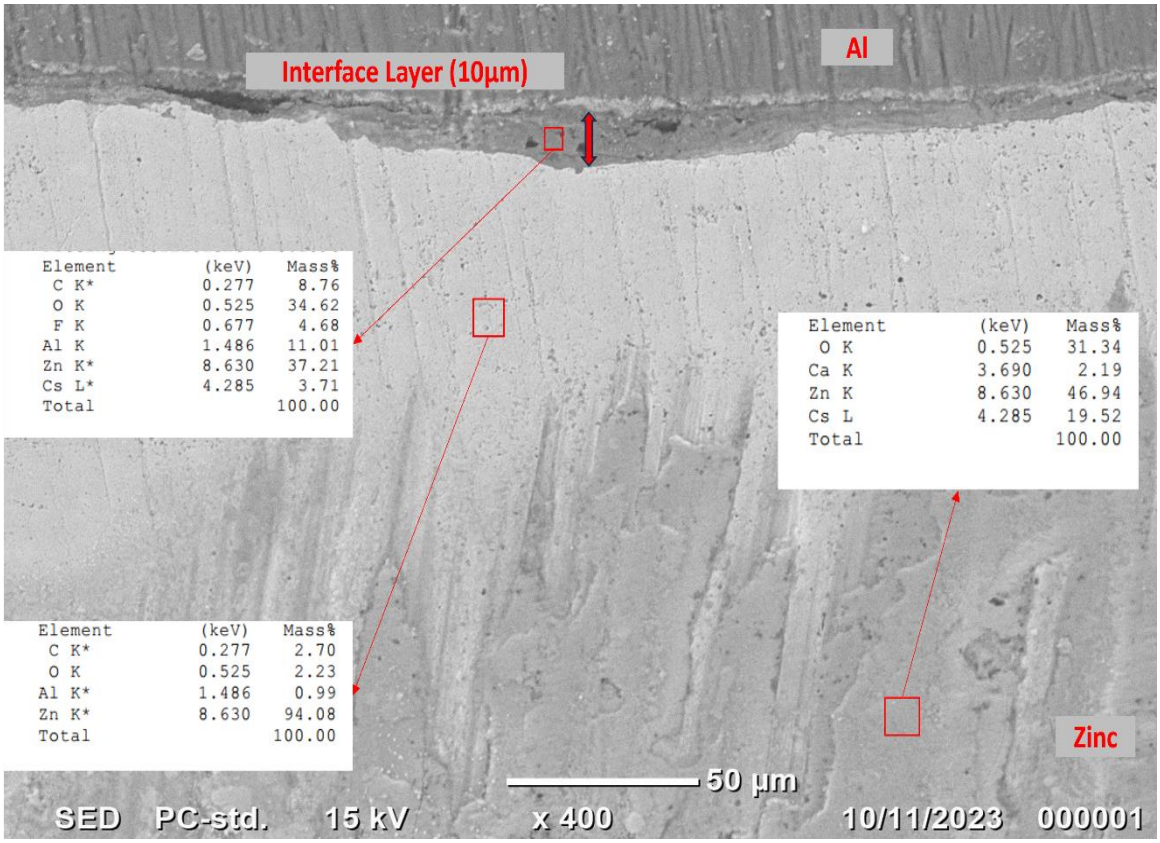

Figure 79: SEM-EDS analysis of joining area of traversal cross section of sample with flux showing local composition of joining area with two different phases.

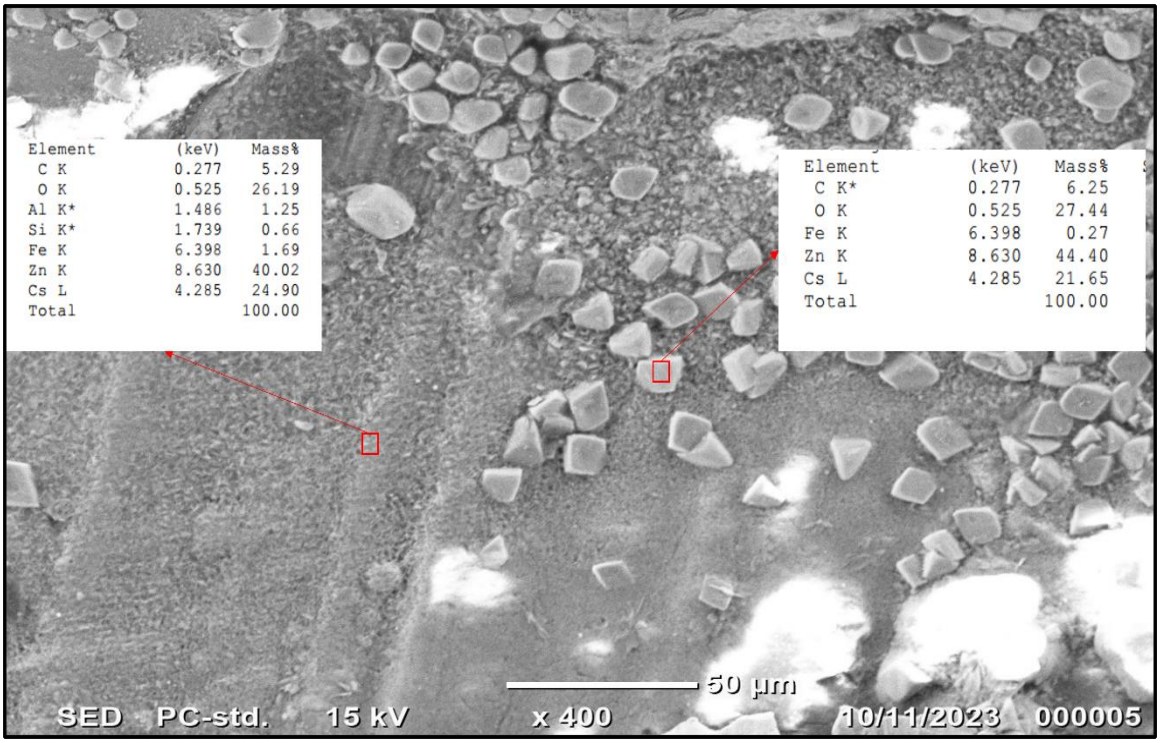

Figure 80: SEM-EDS analysis of joining area of traversal cross section of sample with flux showing crystalline morphology in joining area.

Figure 81: SEM-EDS analysis of joining area of traversal cross section of sample with flux showing local chemical composition on interface layer between Steel and Zn.

Following observations are noted in above shown images:

- The interfaces between the steel and aluminum plates are reported in figure. from 72 to 81. Distinct layers of Aluminum, zinc and steel are visible, the interfaces between these layers are continuous, with small scale voids indicating porosity in few areas. The Zinc layer shows different structures with different morphologies which could indicate locally different solidification rates and the presence of other phases.
- Furthermore, in some zones of the joining layer (Figure 79) it can be seen a darker grey layer (with a crystalline grain like structures) that shows a high percentage of oxygen as well as high presence of Cs, which are present at high percentage in the flux. This interface layer between aluminum with zinc has variable thickness and can reach up to 10 µm in certain areas. The EDX analysis conducted on some zones of the darker grey layer shows the presence of Cs and F (important elements in the flux) together with O, Al and Zn (Fig. 78).
- Figures 74 and 77 show the interface layer between steel and zinc which appears with a dendrite morphology and an average thickness of 280 µm. The

EDX analysis, conducted on the plates, shows respectively the presence of Fe for the steel and Al and Si for the aluminum alloy.

- The zinc layer sometime shows a heterogeneous appearance (Figure 80) with the presence of small crystals (around 10 µm). This could be due to the influence of oxygen that promotes the formation of oxide compounds containing Zn and Cs due to solubility limits between the materials involved.
- The presence of oxygen with varying percentages shows the argon atmosphere was sufficient to protect and decrease the oxygen content, and some oxidation of zinc and aluminum is present. Furthermore, a certain presence of oxygen may be attributed to spontaneous oxidation of the metallographic samples after surfaces polishing for optical and SEM observations, as well as surface contaminants or residuals of surface oxides.
- Cesium from flux was also detected on steel interface with zinc in (Figure 81), which may indicate that flux, when reacted with liquid zinc increased wettability and fluidity of molten material and cesium elements also diffused towards steel side plate, positioned on the top of the brazing joint.
- on interface layer between aluminum and zinc some peaks of Fe were also observed (Figure 78 and 79) which indicates reaction of liquid zinc with aluminum and Zn- coated steel, and Fe, due to higher weight, diffused towards aluminum positioned at the bottom of the stack.
- The sometime detected presence of small percentage of carbon is due to resin mounting and surface contamination.

4.2.1.2 Sample 2 (Without Flux)

On sample joined without flux, a similar process was carried out and after optical microscopy, joining area was observed under SEM-EDS.

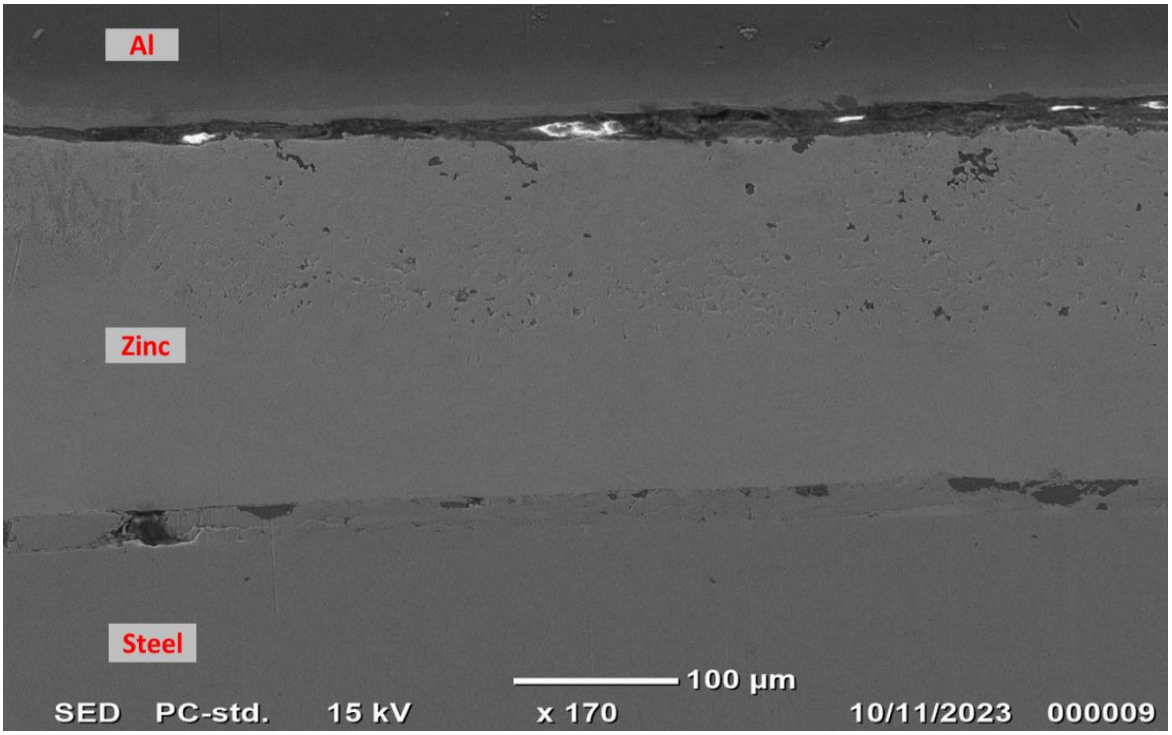

Figure 82: SEM-EDS analysis of joining area of traversal cross section of sample without flux showing continuity of reaction layer.

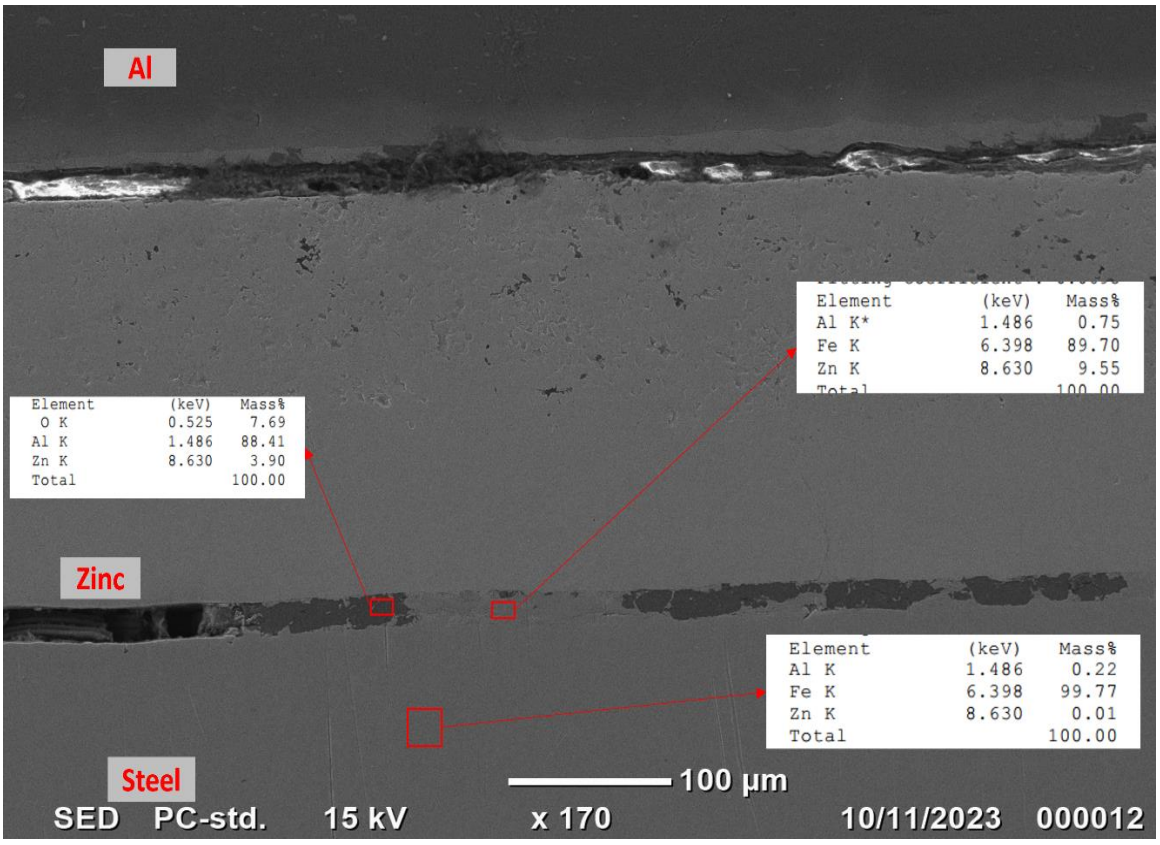

Figure 83: SEM-EDS analysis of joining area of traversal cross section of sample without flux showing local chemical composition on interface between Steel and Zn.

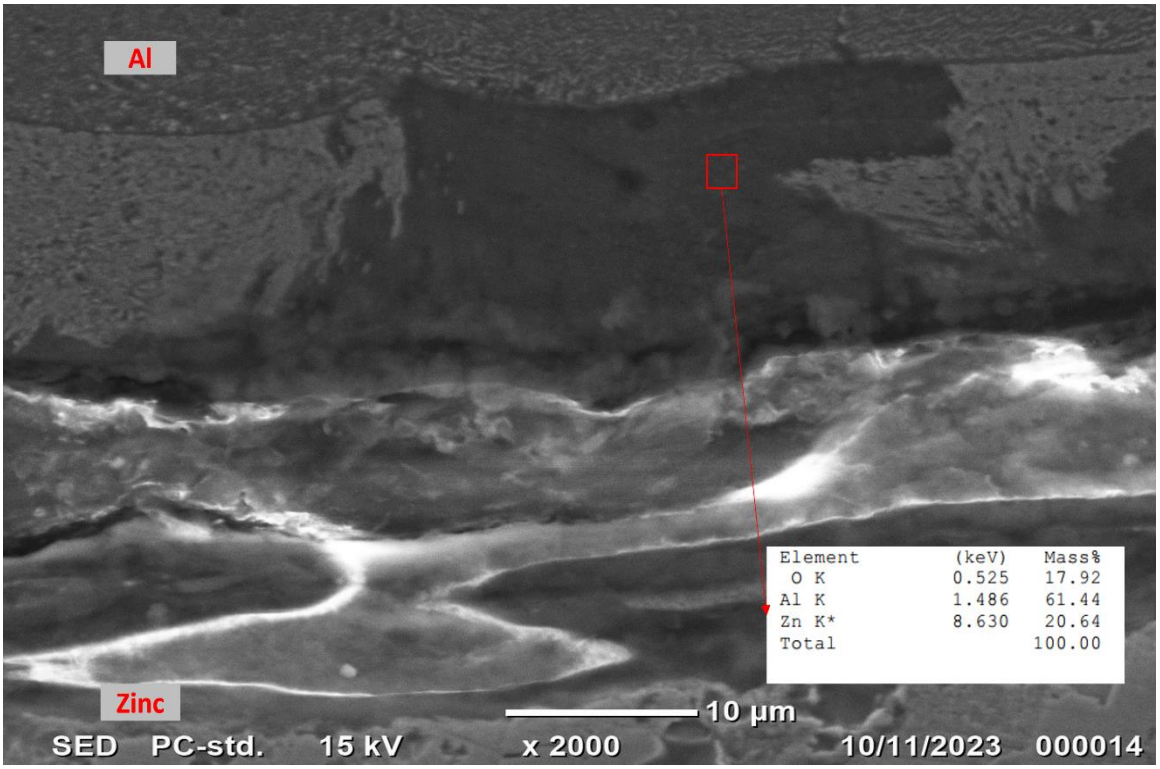

Figure 84: SEM-EDS analysis of joining area of traversal cross section of sample without flux showing local chemical composition on interface between Al and Zn.

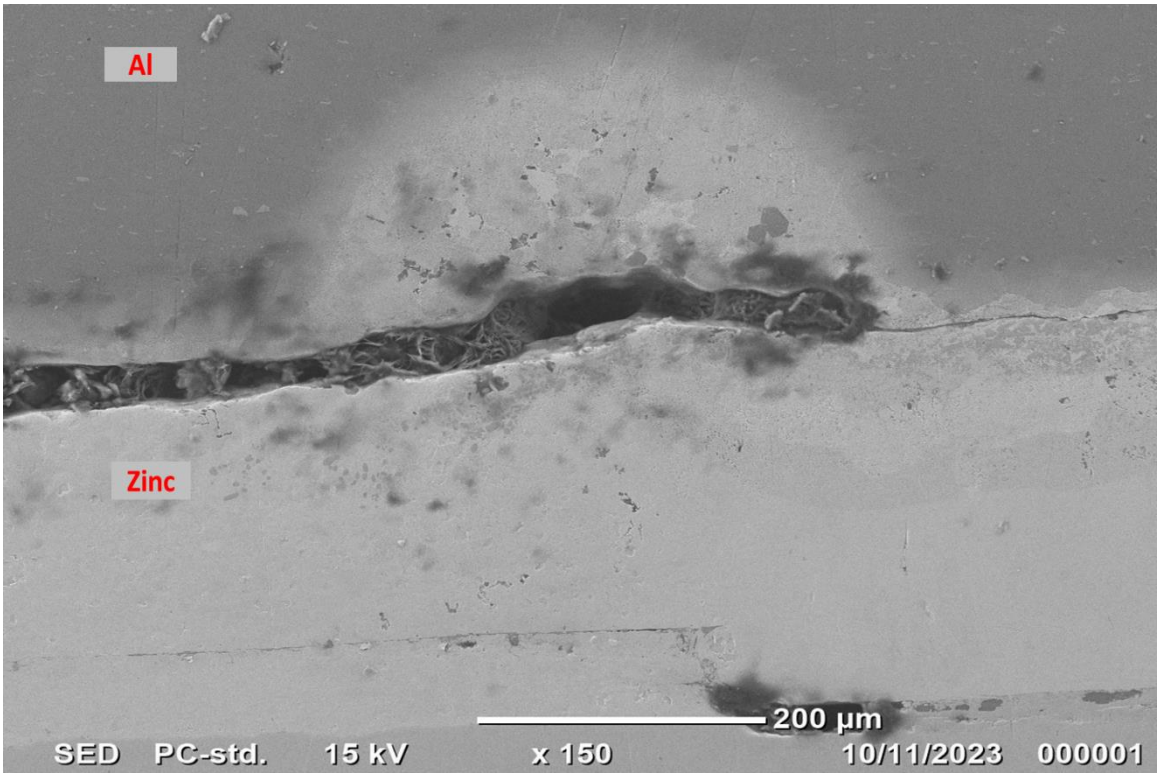

Figure 85: SEM-EDS analysis of joining area of traversal cross section of sample without flux.

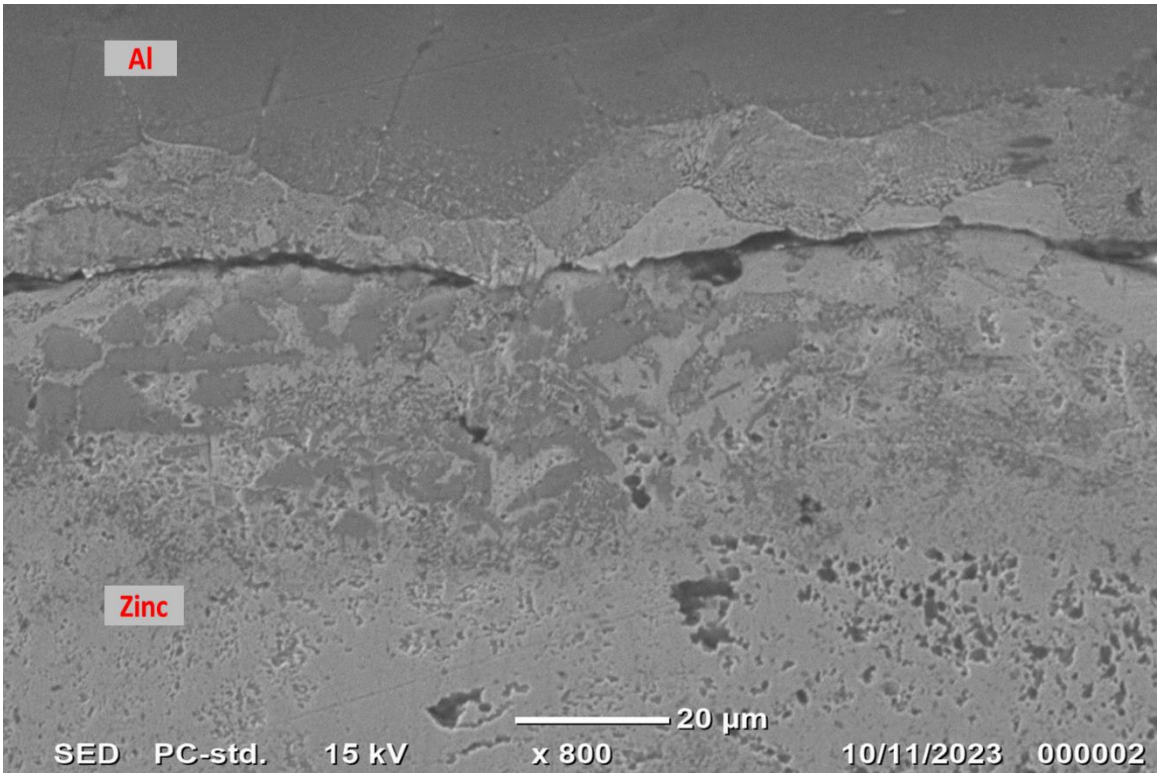

Figure 86: SEM-EDS analysis of joining area of traversal cross section of sample without flux at higher magnification of Al and Zn interface.

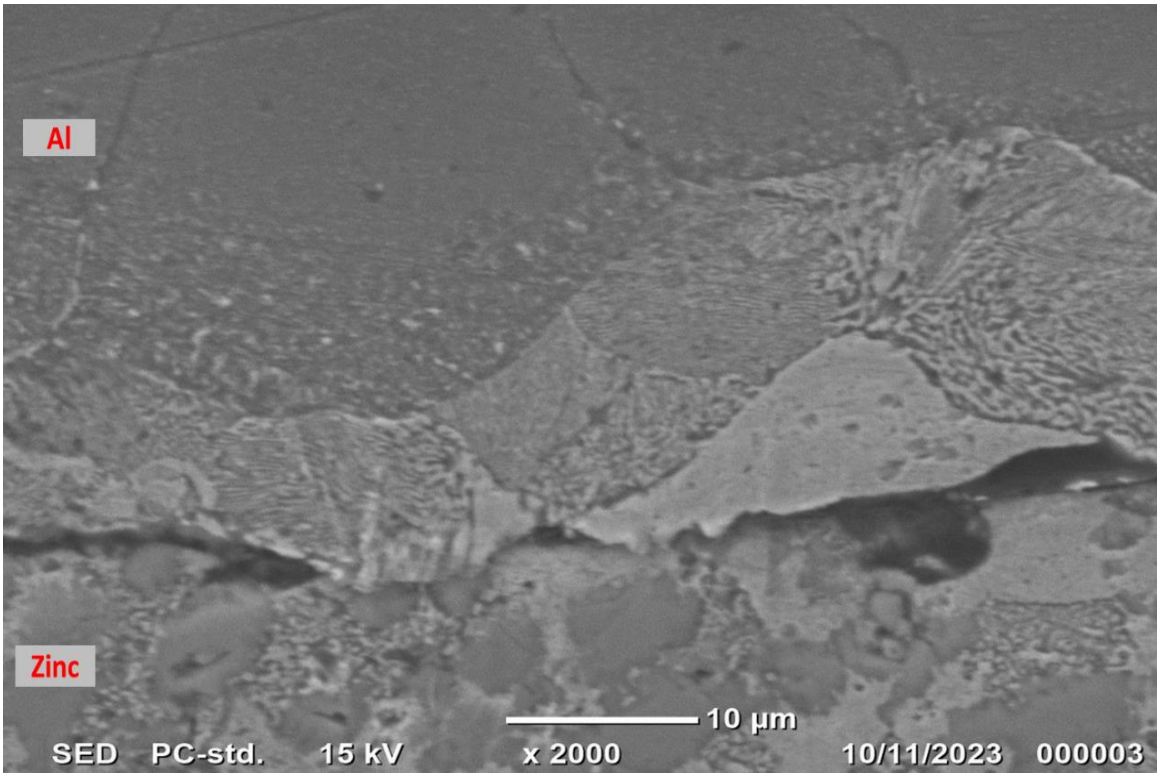

Figure 87: SEM-EDS analysis of joining area of traversal cross section of sample without flux at higher magnification of Al and Zn interface.

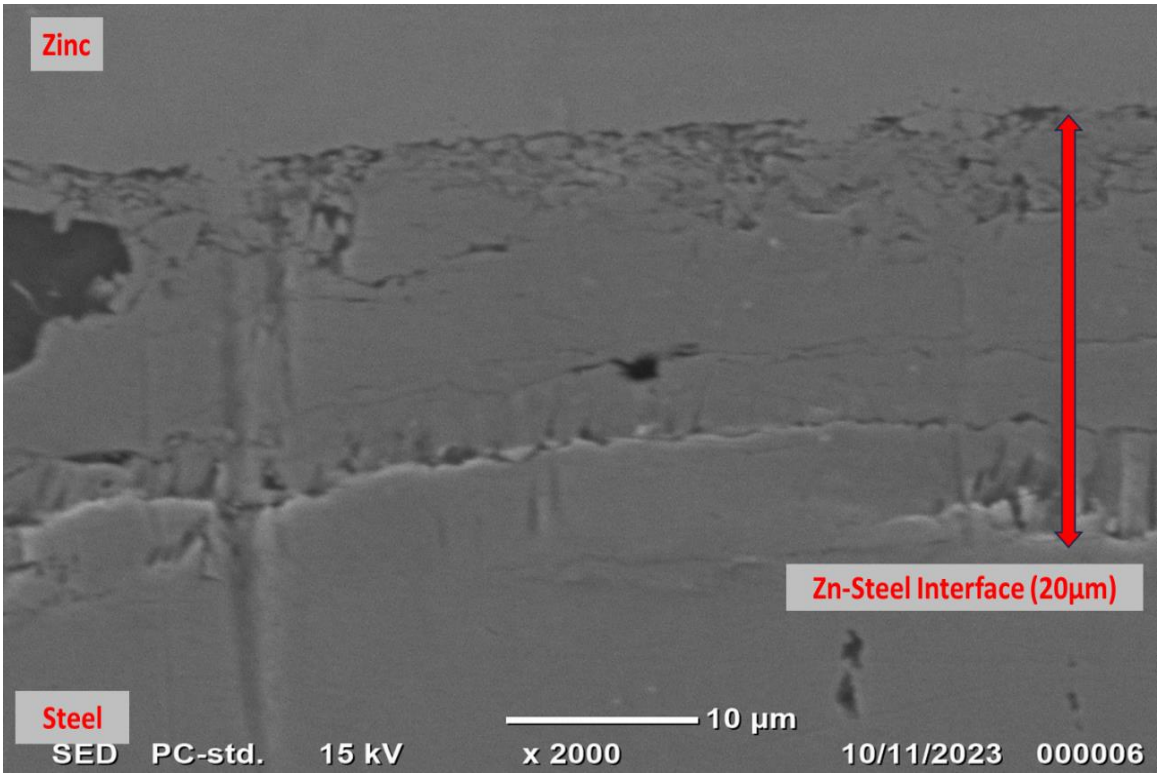

Figure 88: SEM-EDS analysis of joining area of traversal cross section of sample without flux showing interface layer thickness between Steel and Zn.

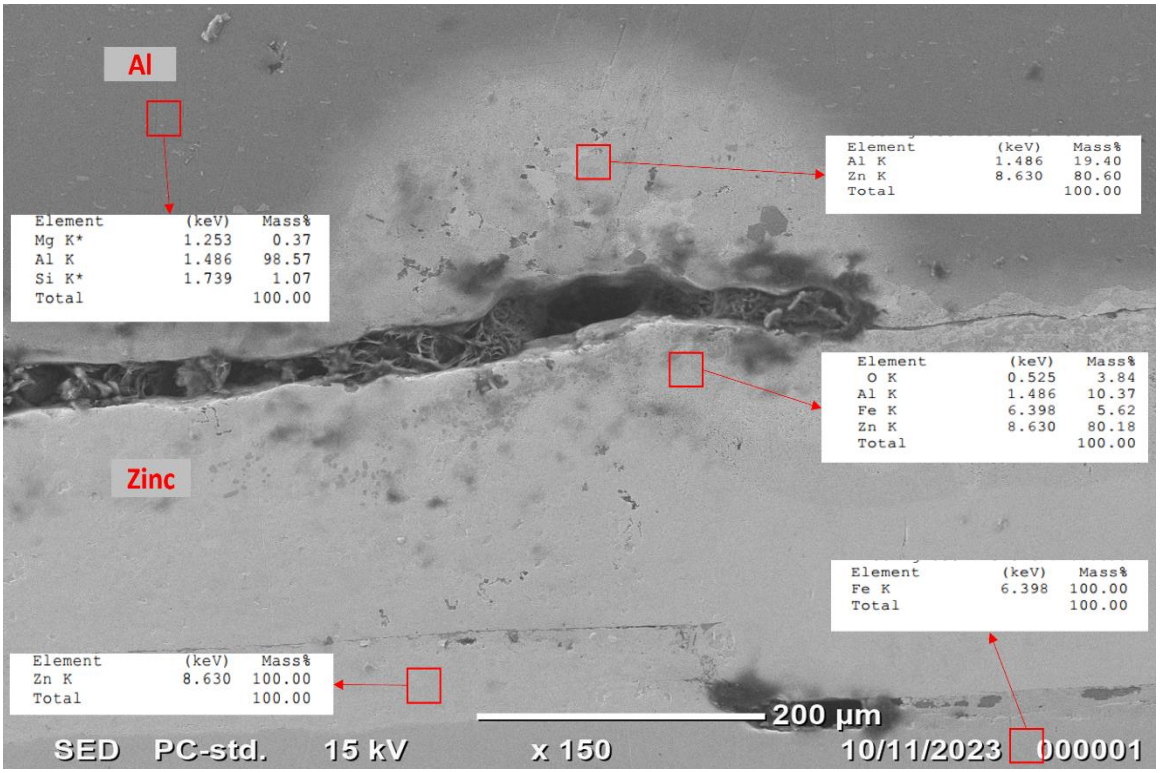

Figure 89: SEM-EDS analysis of joining area of traversal cross section of sample without flux showing local chemical composition at different areas around Al-Zn interface.

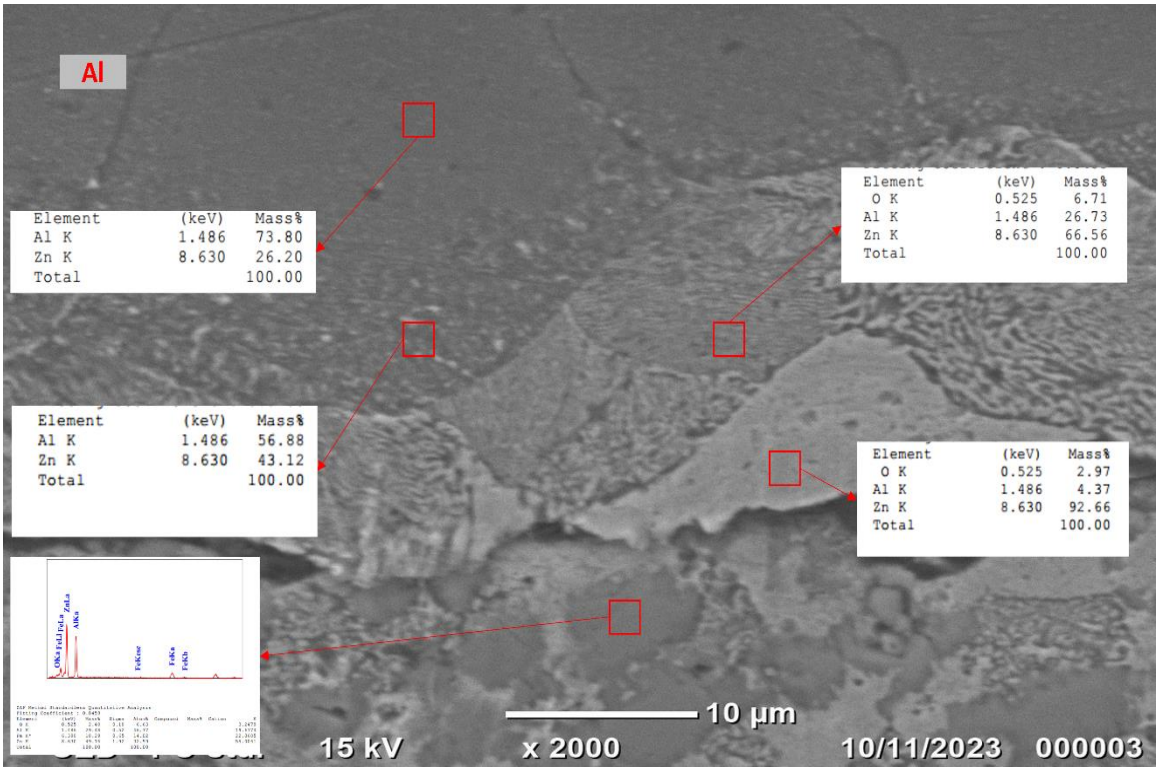

Figure 90: SEM-EDS analysis of joining area of traversal cross section of sample without flux showing local chemical composition in Al-Zn interface.

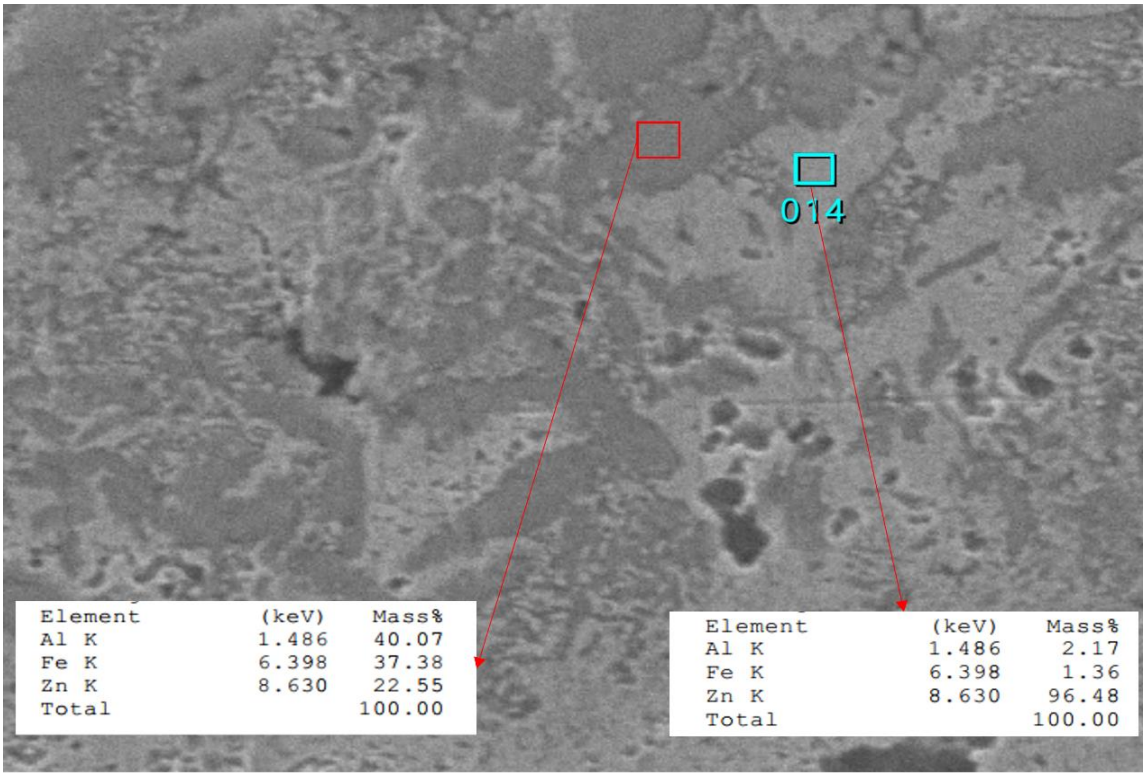

Figure 91: SEM-EDS analysis of joining area of traversal cross section of sample without flux showing local chemical composition Al-Zn interface.

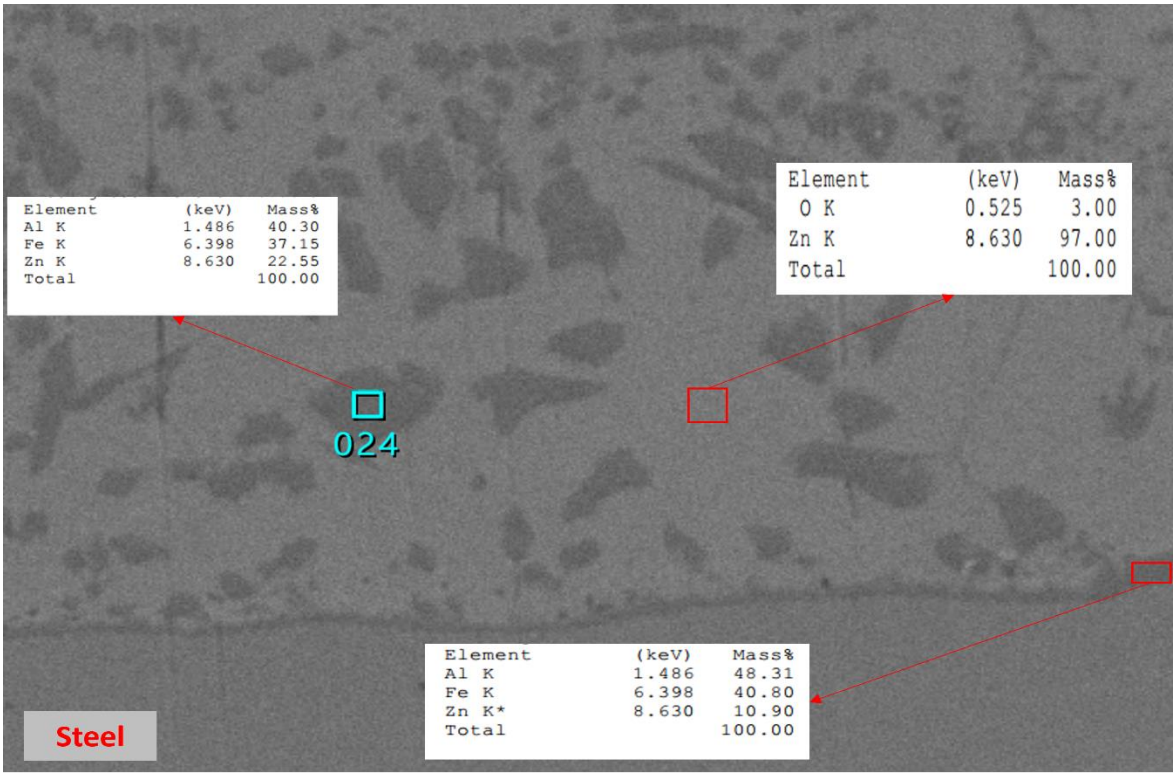

Figure 92: SEM-EDS analysis of joining area of traversal cross section of sample without flux showing local chemical composition of joining area.

Some observations can be made based on SEM-EDS images shown above for sample without flux:

- Figure 82 shows distinct layers of Aluminum, zinc and steel, Interface between steel and zinc is continuous while toward aluminum and zinc some discontinuities are observed. This observation is in line with the optical microscopy observations.
- In Figure 83, Two different phases are present on interface between steel and zinc. While one phase is Al rich phase with zinc with small traces of oxygen (88% Al and 4% Zn) other is Fe rich phase with zinc (90% Fe and 10% Zn). This indicates liquid zinc reacted with both aluminum and Fe and diffusion of zinc into bulk materials was successful. Especially, liquid zinc partially melted aluminum and on solidification, aluminum was observed on both interfaces.
- Figure 84 provides elemental composition on a small area on interface between aluminum and zinc. Aluminum rich phase with zinc is seen while oxygen presence is also observed in a very low amount.
- Figure 85 shows a prominent region with a similar color texture as of zinc, which indicates liquid zinc diffused deep into aluminum sheet and caused partial

melting of aluminum. Same is confirmed by Figure 89 which shows Zn rich phase with Al (80% Zn and 20% Al) is present towards aluminum sheet and up to depth of 180 µm.

- Interface layer thickness between steel and zinc varies along the joining layer and up to 20 µm thickness can be seen at some points as shown in Figure 88.
- In Figure 86 and 87, interface layer between aluminum and zinc is observed at higher magnification which shows eutectic transformation. Some inter-dendritic microstructures are observed locally while other regions show the presence of two different phases.
- These phases are mainly zinc rich phases with varying proportions of aluminum as seen in Figure 90.
- In another local region of the joining area, zinc layer showed two prominent regions of different phases. One was mainly pure zinc with a small percentage of oxygen while other phases showed all three major elements (Fe, Al & Zn) with significant mass percentages.
- Some Fe is also seen on aluminum side which indicates liquid zinc reacted well with Fe and Al, and different phases were formed upon solidification.
- SEM-EDS analysis also points to the fact that reaction layers can be seen with some voids and discontinuities, however elemental composition shows non homogenous distribution along the interfaces with different phases which may be some intermetallic.

4.2.2 Failed Sample Analysis

On failed sample without flux, another analysis was conducted to observe at higher magnification using SEM along with chemical composition with help of EDS scan. These scans were carried out on Al and steel top surfaces where reaction should have occurred and not on the traversal cross section.

First aluminum surface was analyzed, and results are shown below.

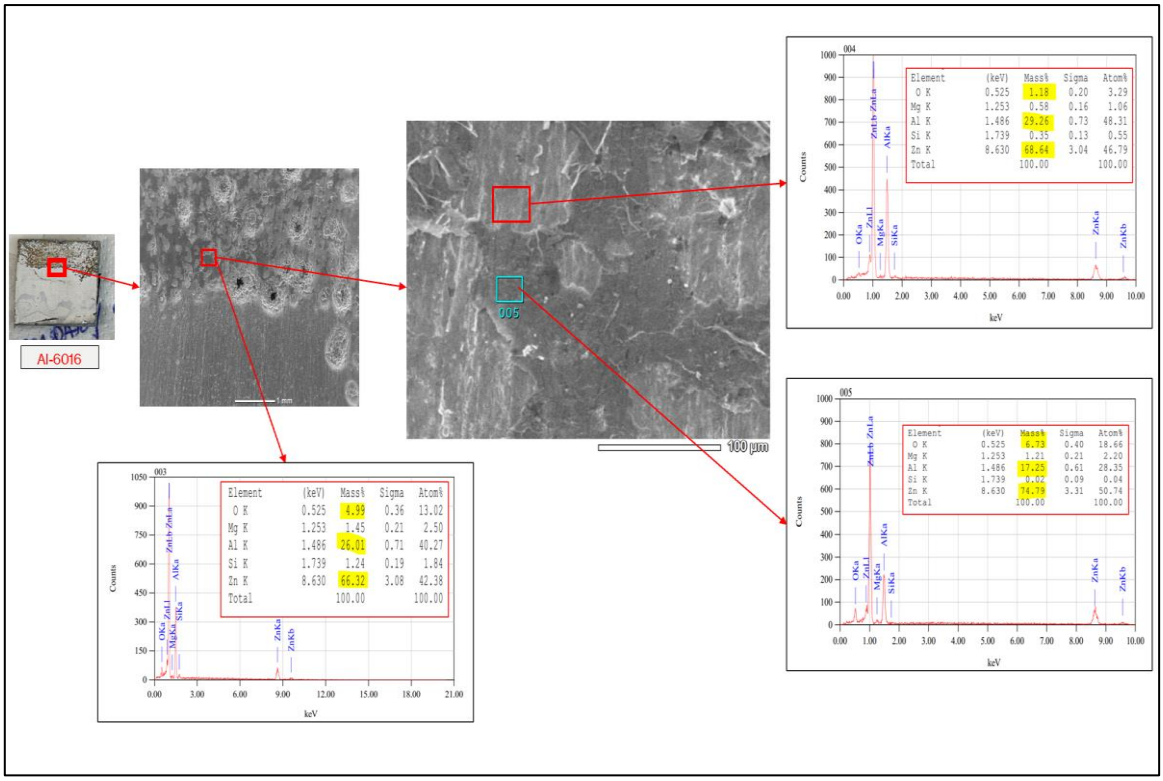

Figure 93: SEM EDS scan of Aluminum substrate (1)

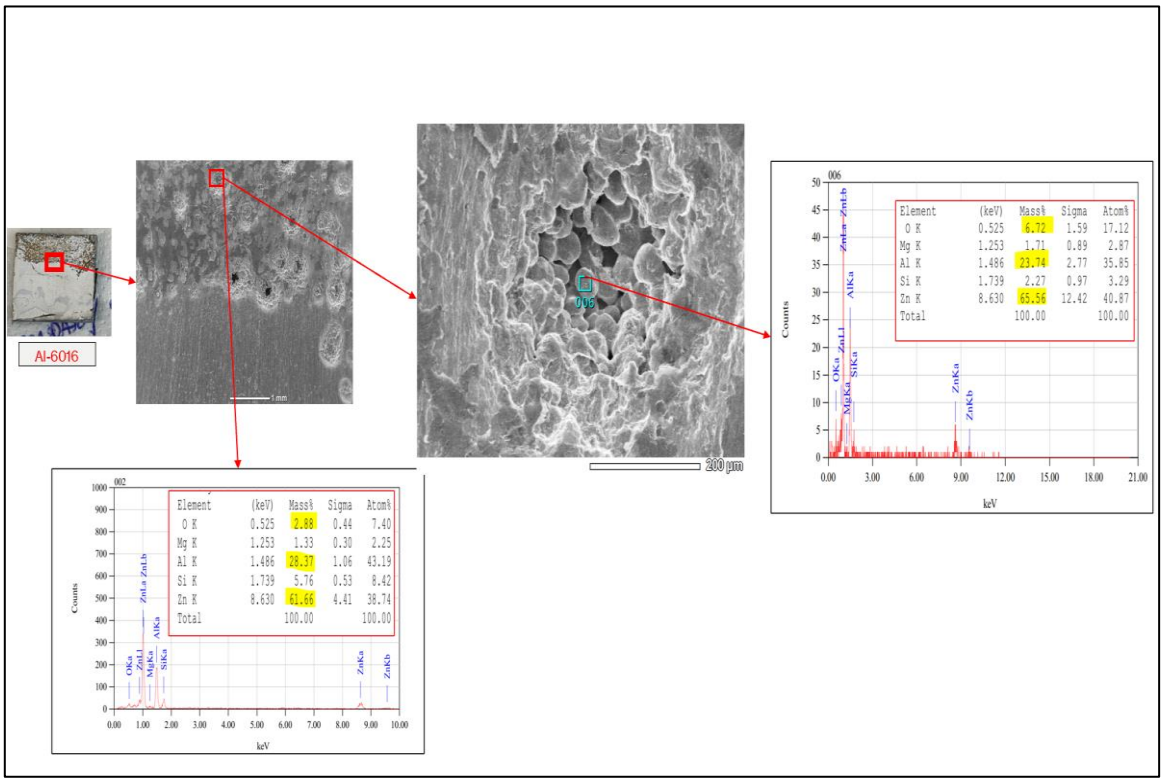

Figure 94: SEM EDS scan of Aluminum substrate (2)

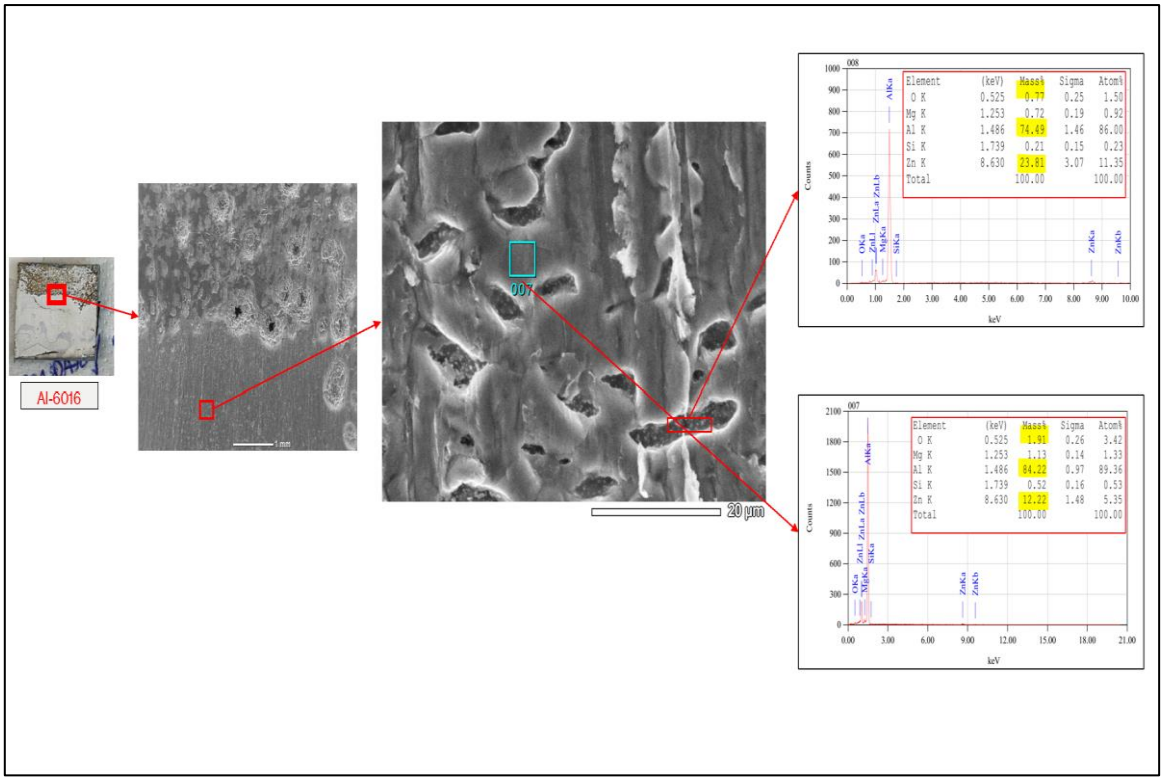

Figure 95: SEM EDS scan of Aluminum substrate (3)

- Zinc presence on surface predicts that liquid zinc reacted with aluminum and some aluminum rich phases are formed. The limited presence of oxygen can be attributed to some oxidation of aluminum which can partially hinders reactivity.
- In the last figure 95, rich aluminum phase with zinc is seen with varying solubility. SEM observation seems to further augment our optical microscope analysis that in absence of flux liquid zinc reacted with aluminum but not uniformly and homogeneously. Some phases are detected with varying composition of zinc.

Scans of steel top surface are as follows.

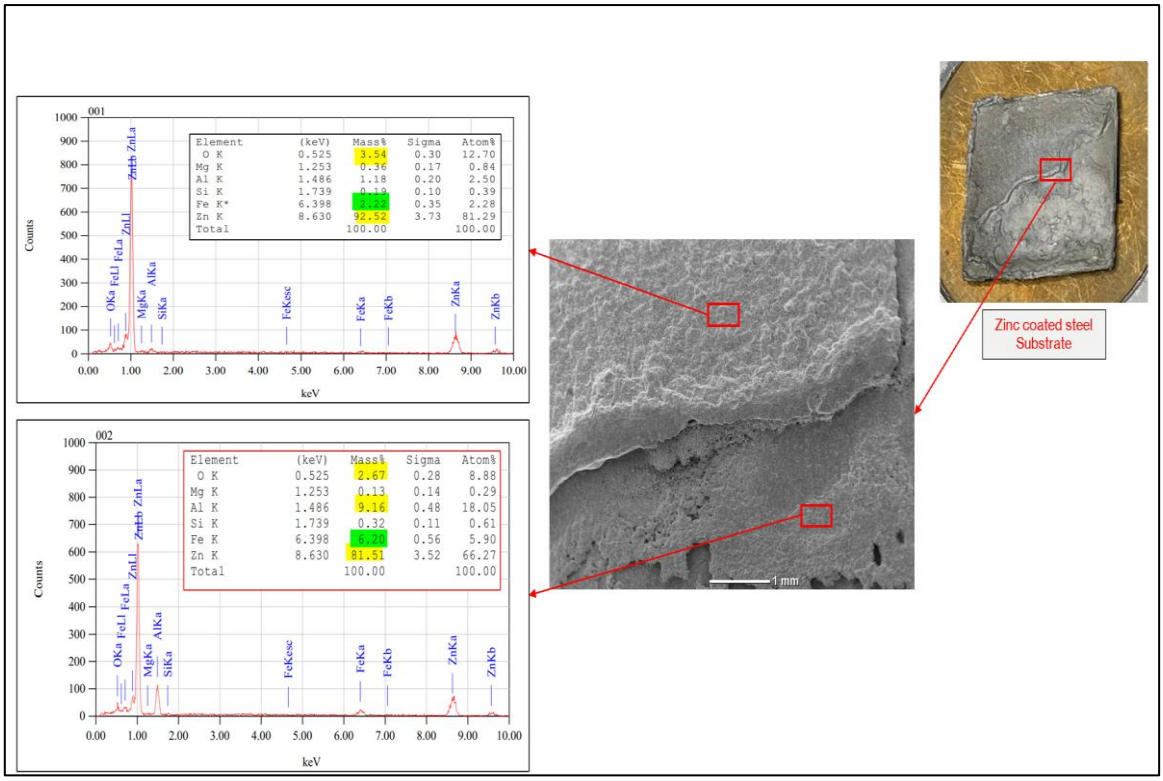

Figure 96: SEM EDS scan of zinc coated steel substrate (1)

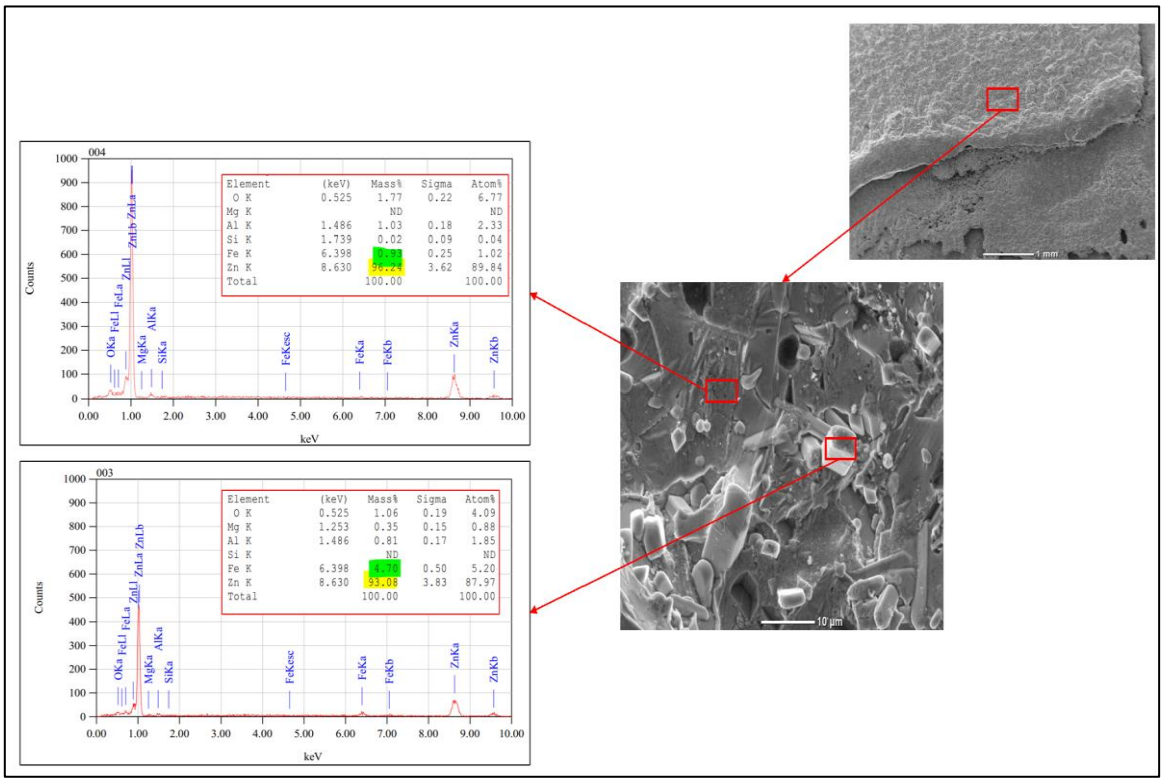

Figure 97: SEM EDS scan of zinc coated steel substate (2)

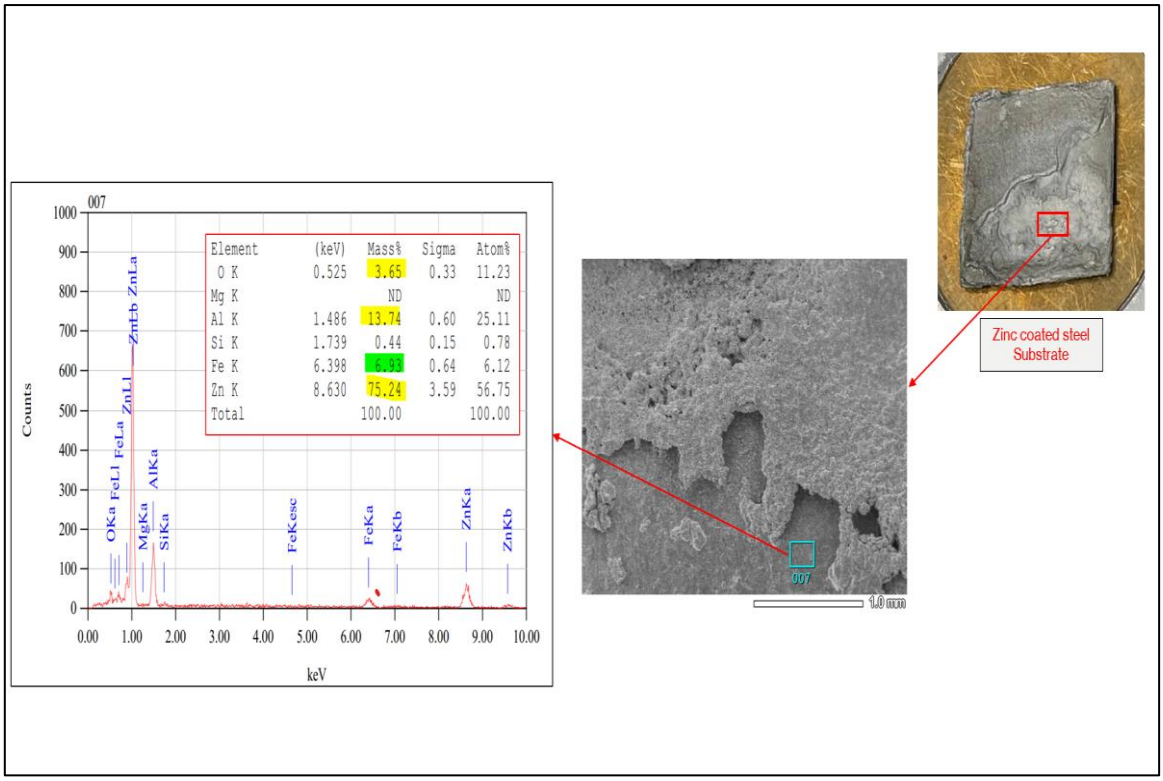

Figure 98: SEM EDS scan of zinc coated steel substrate (3)

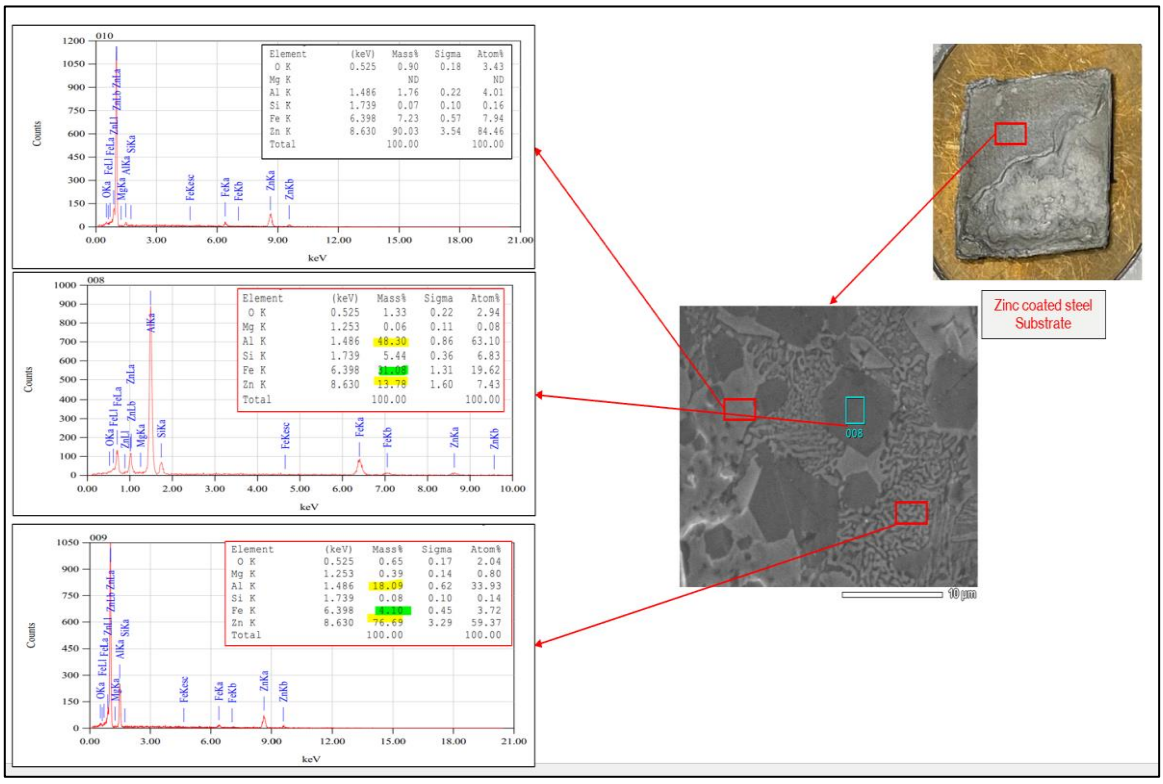

Figure 99: SEM EDS scan of zinc coated steel substrate (4)

- In Fig 96, two regions of interest are seen. On the top side liquid zinc reacted with zinc coating on steel and formed a phase while on bottom part it shows presence of zinc phase with aluminum.
- In Fig 97, some crystal of intermetallic compound with zinc and Fe is seen while the remaining region is mainly zinc.
- Fig 98 shows a good mass percentage of all three main elements, as liquid zinc reacted with both Al and Fe and formed a compound phase, however its not homogeneous all over the surface.
- In Fig 99, eutectoid transformation is observed with different phases and chemical composition.

4.3 XRD Analysis of Residual Stresses

This section would discuss results of XRD technique to evaluate residual stresses and their implication. As discussed during the last chapter, after selection of 2θ range for both aluminum and steel scans were performed at different psi angles and data was elaborated using MATLAB code to measure residual stresses. A similar process was carried out after brazing on exterior sides of aluminum and steel to note the alterations in stresses. Details of process and results are mentioned below separately for both steel and aluminum.

4.3.1 Residual Stresses in Al-6016

Aluminum scan gave a significant high peak with good intensity (counts per second) in the 2θ range of 146 – 152.8. Each sample was rotated at Phi zero and Phi 90 to evaluate stresses in complete plane. Some scans of XRD are shown below.

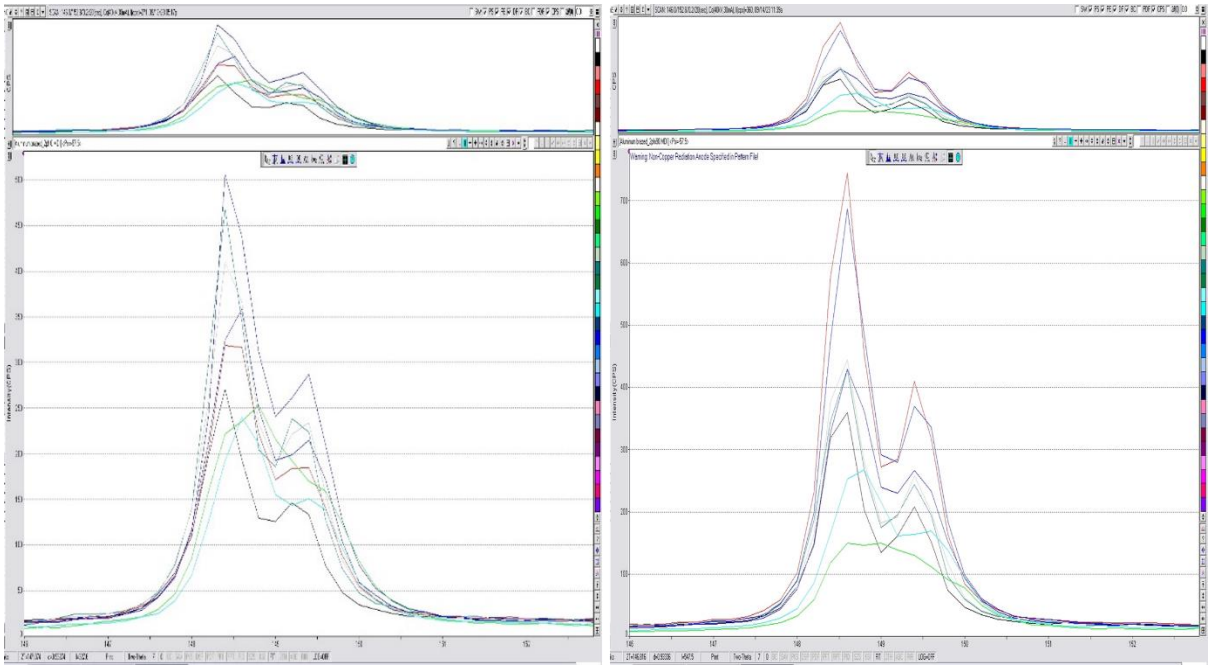

Figure 100: XRD scan of Aluminum sample 2 at phi-0 and phi-90

Different curves are depicting count intensities at different psi angles. Shift of peaks indicate presence of residual stresses due to change of interplanar distance d.

Post brazing residual stresses were calculated in both cases, one with flux and one without flux. MATLAB was able to interpret and interpolate the data using pseudo-Voight and Pearson functions and resultantly straight line and ellipse approximation was produced between d and sin φ^2.

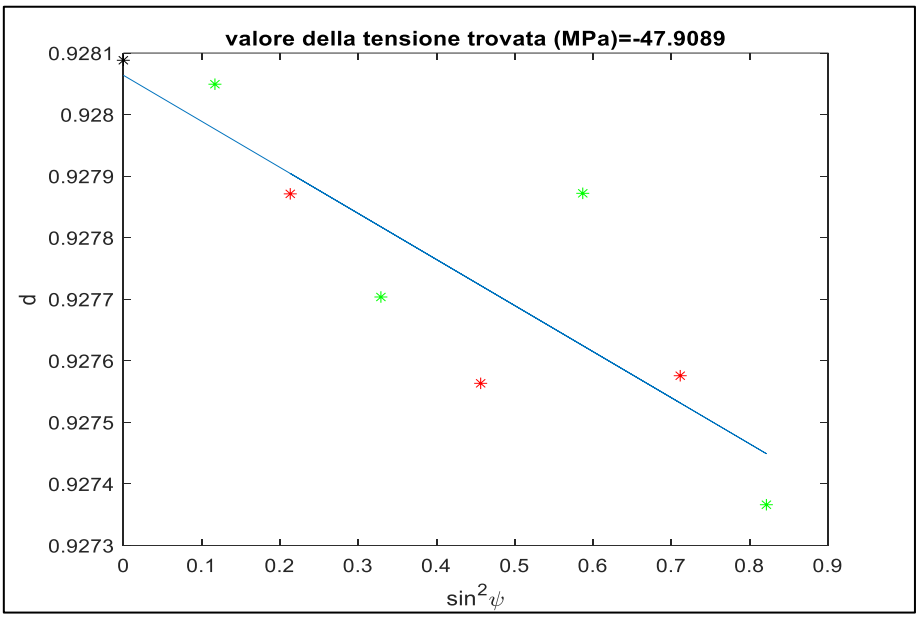

Figure 101: Relationship between d and sin φ^2 for Aluminum (Straight Line Approximation)

Green and red dots are representing the experimental data in positive and negative values of psi respectively while straight line is approximation of that data to provide values of residual stresses.

Similarly, using Pearson approximation an ellipse was formed where measure of minor axis provided information on shear residual stress. Experimental data along with elliptic approximation is shown below.

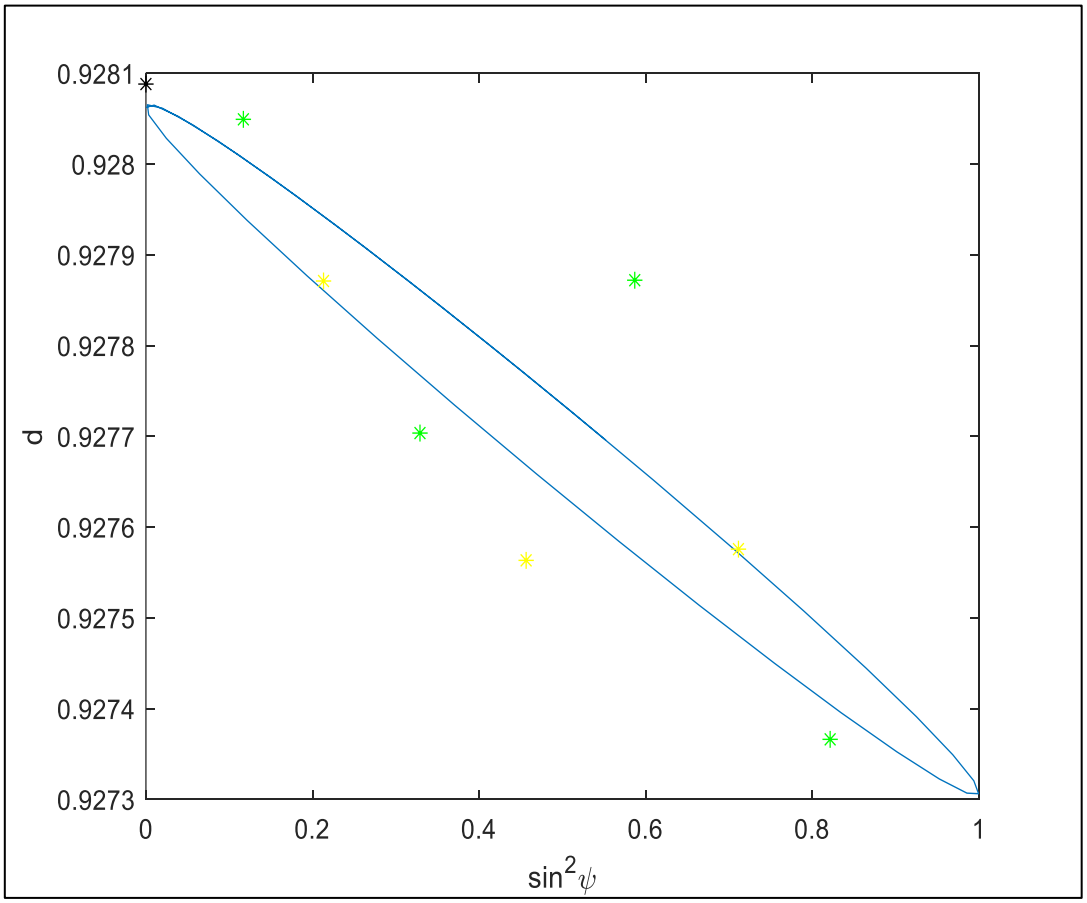

Figure 102: Relationship between d and sin φ² for Aluminum (Elliptic Approximation)

Error values originated from original or theoretical values and experimental data was also calculated and residual stresses so calculated must be read with error in consideration and can be used as best approximation.

Finally, results of all samples pre and post brazing with calculated values of normal stresses (σ) and shear stresses (Ʈ) are reported below.

Sample	σ Line (MPa)	Error σ Line (MPa)	σ Elliptic (MPa)	Shear Stress Elliptic (MPa)	Error σ Elliptic (MPa)	Error Shear Stress Elliptic (MPa)
aluminum_1phi0	-48.8703	9.8759	-48.2204	-5.4906	7.961	2.664
aluminum_1phi90	-53.437	7.7858	-53.4347	-0.0195	8.5356	2.8562
aluminum_2phi0	-43.0644	4.6332	-43.2537	1.5566	4.634	1.5505
aluminum_2phi90	-45.8005	7.417	-45.8519	0.4339	8.1106	2.714
aluminum_3phi0	-43.5673	6.8758	-43.6547	0.7388	7.473	2.5007
aluminum_3phi90	-49.1983	7.3177	-49.2058	0.0629	8.022	2.6844
Aluminum_3_Brazed_flux	-25.302	6.0407	-25.5615	2.1923	5.9391	1.9874
Aluminum_Brazed_Noflux	-47.9089	11.5277	-48.2894	3.2144	11.8854	3.9772

Table 7: Residual Stresses in Al-6016

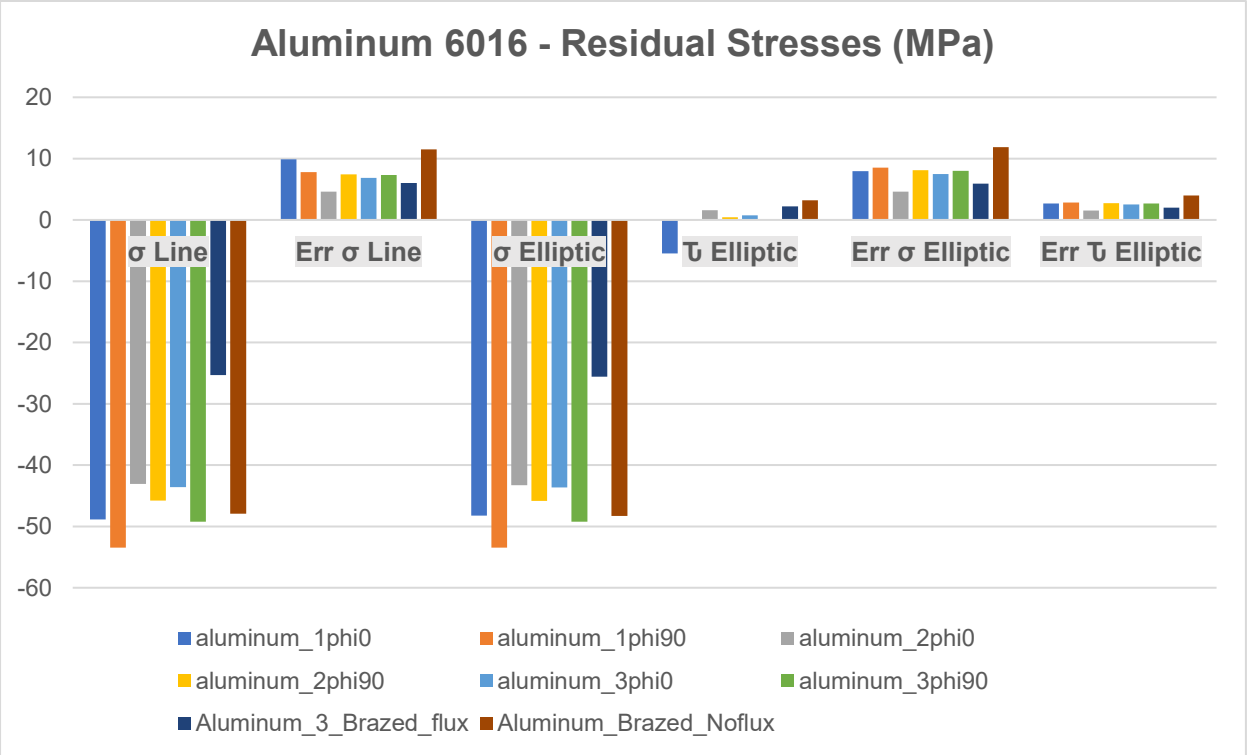

Figure 103: Residual Stresses Al-6016

After analyzing the data and chart values some deductions can be made such as:

- Considerable compressive residual stresses (45-55 MPa) were present in Al-6016 which could have resulted how it was manufactured as rolling and machining can significantly introduce residual stresses.
- Shear stress is not present significantly and comparing to error in shear values compared to original values basically make it void.
- Pre brazing samples residual stresses ranged between -43 MPa to -52 MPa within tight band so we can assume all samples had similar residual stresses and rightly so because they were cut from same sheet.
- Reduction of stress in case of brazed with flux sample can be explained possibly by the different thermal coefficient of expansion of steel and aluminum. After heating to 500°C both Al and steel were expanded and during cooling down aluminum tried to shrink more than steel due to higher coefficient of thermal expansion but because of good joint to steel could not do so and resulted in lowering of compressive residual stresses compared to pre brazing sample.
- No change in case of brazed without flux could be explained in similar way that although sample seems to be joined visually however joint is not so sound and there is no exchange of stresses between Al and steel plates. Heat treatment seems to not modify the original material.

4.3.2 Residual Stresses in zinc coated steel.

In the case of steel as discussed before, complete range scan of sample did not give a significant high peak of Fe which was also isolated in 2θ range. Therefore, a zinc peak at higher range of 2θ was selected and scans at different angles of psi were performed. Results of scans for samples are illustrated below.

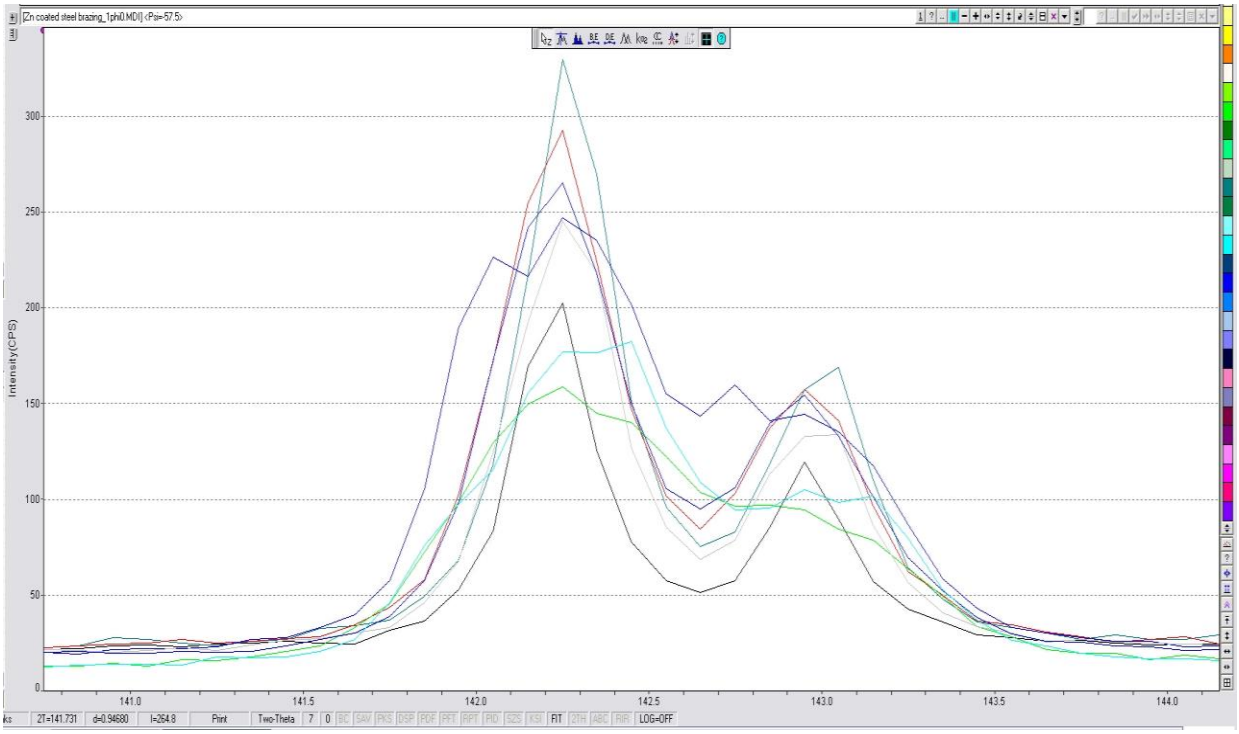

Figure 104: XRD scan of zinc coated steel sample 1 with zinc peak

One observation before elaboration of data by MATLAB can be seen that intensity (cycles per second) in case of zinc peak in steel sample is not as significant as in case of aluminum. And there is also not significant peak shifting with changing values of psi which gives indication to values of residual stresses, but we will continue with analysis with MATLAB code.

Line and elliptic approximation of sample after brazing without flux is as follows.

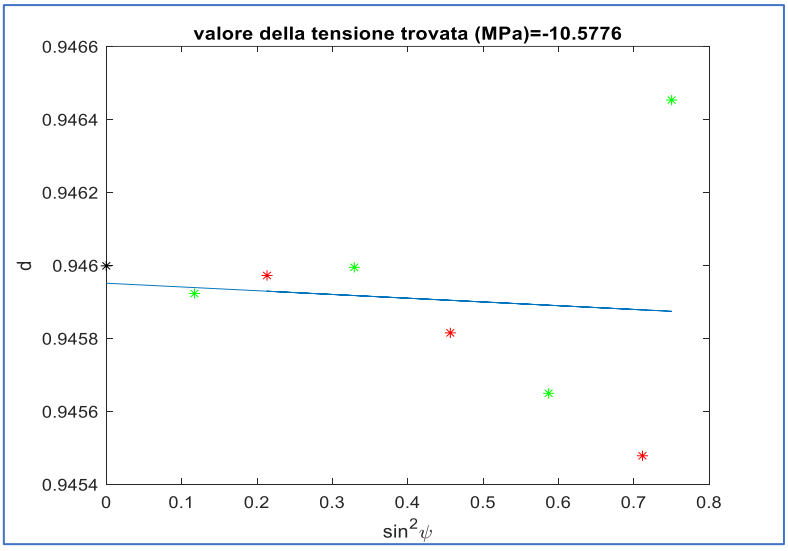

Figure 105:Relationship between d and sin φ2for zinc coated steel (Line approximation)

It is evident from line and experimental data that significant error is present between theoretical values and experimental values.

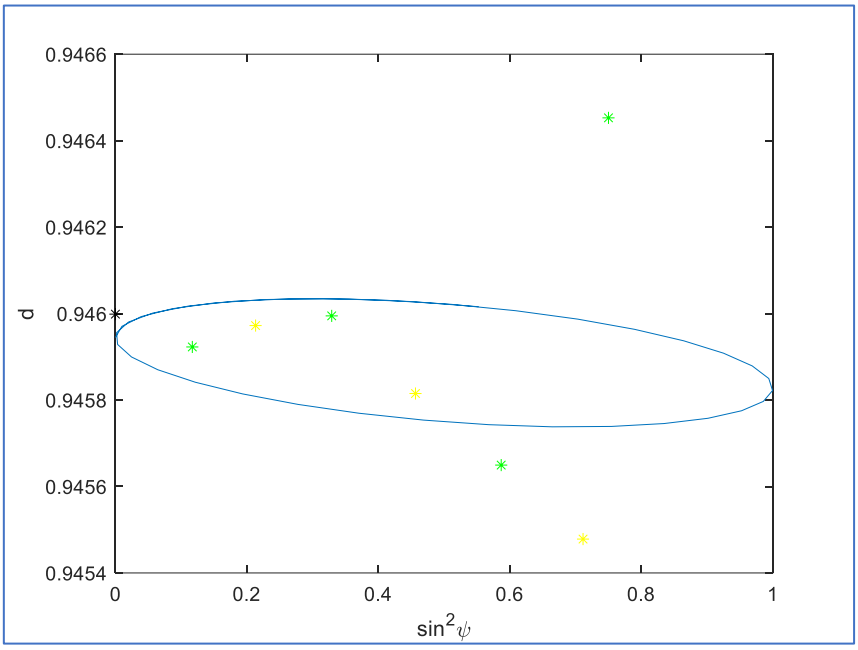

Figure 106: Relationship between d and sin φ² for zinc coated steel (elliptic approximation)

The result of stress values and chart for comparison is illustrated below.

Sample	σ Line (MPa)	Error σ Line (MPa)	σ Elliptic (MPa)	Shear Stress Elliptic (MPa)	Error σ Elliptic (MPa)	Error Shear Stress Elliptic (MPa)
Steel_1phi0	-4.5817	11.1469	-4.9947	3.9403	10.8557	3.4127
Steel_1phi90	-25.733	19.6383	-26.5843	8.1204	18.1619	5.7095
Steel_2phi0	-20.738	16.0354	-20.7752	0.3556	17.5682	5.5228
Steel_3phi0	-35.6289	8.9327	-35.8521	2.1292	9.3103	2.9268
Temp_effect_steel_2	-25.6758	18.7575	-25.8926	2.0682	20.3474	6.3965
Steel_3_Brazed_Flux	-25.3124	72.1402	-30.6069	50.5032	33.021	10.3807
Steel_Brazed_NoFlux	-10.5776	48.3836	-12.0525	14.0705	43.1322	13.5593

Table 8: Residual stresses in zinc coated steel.

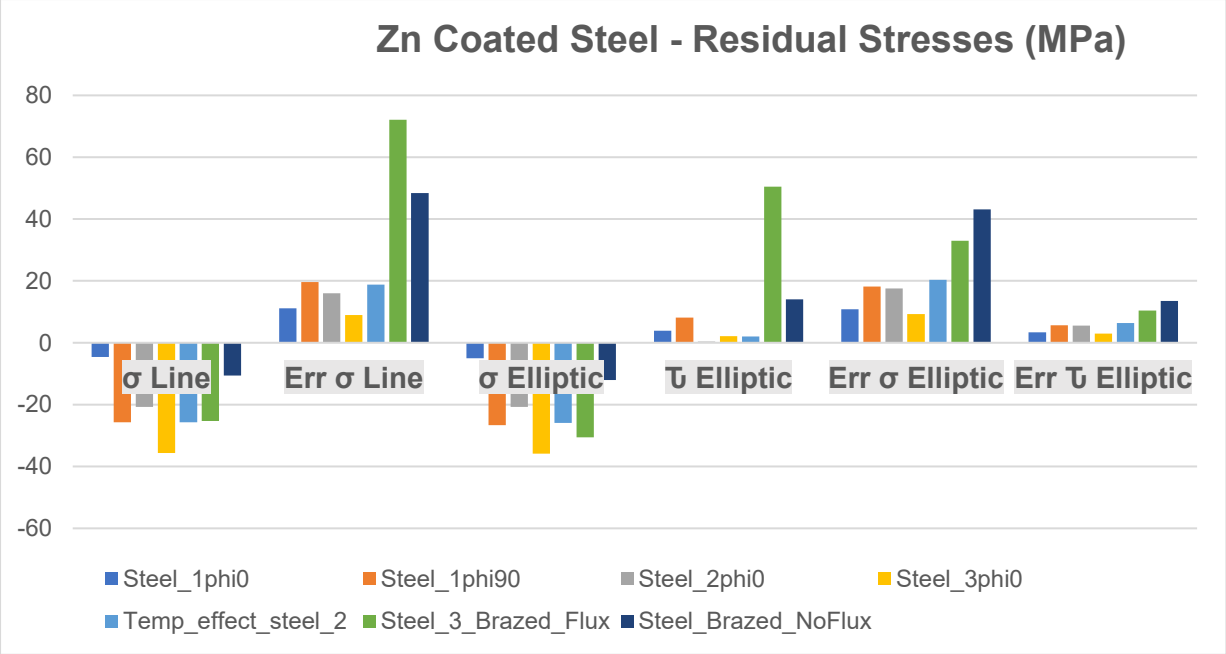

Figure 107: Residual stresses in zinc coated steel

Seeing residual stress values and error percentages, some conclusions can be drawn.

- Samples represent similar values of compressive residual stress in tight band around -20 MPa.
- However, noting that yield strength of IF 260 steel is around 270-300 MPa these small values with considerable error values does not represent any significant residual stress.

4.4 Phase Detections by XRD (Failed Samples)

It was observed during SEM and EDS scan of aluminum and steel substrates (from failed sample without flux and 7 minutes dwell time) showed presence of different elements which indicated possible presence of intermetallic compounds and phases. XRD scan of reaction side substrate of aluminum and steel was carried out and all possible peaks were seen on the scan. We have previously seen that intensities show presence of atoms position in crystalline structure and when compared with standards these peaks position can help to find possibilities of different phases. Below XRD scan of both aluminum and steel is explained separately.

4.4.1 Phase Detection by XRD for Zn Coated Steel

Scans by XRD were elaborated by MDI Jade software which can identify peaks automatically. However, if the fitting of peaks does not match good, peaks were added manually and fitted to ensure maximum accuracy. After peaks were identified, material jade inbuilt chemical library was searched through with possible phases among known elements present in sample like Fe, Zn, and Al. All possible combinations of Fe, Zn and Al were checked and matched with our peaks and with little margin of error if peaks matched showed presence of that phase / intermetallic compound. This margin of error is understandable due to the difference between standard reference peaks had different conditions such as X-Ray emission material and its wavelength, material manufacturing methods and so on.

After analyzing the steel reaction side from material jade software as discussed above, results are shown below.

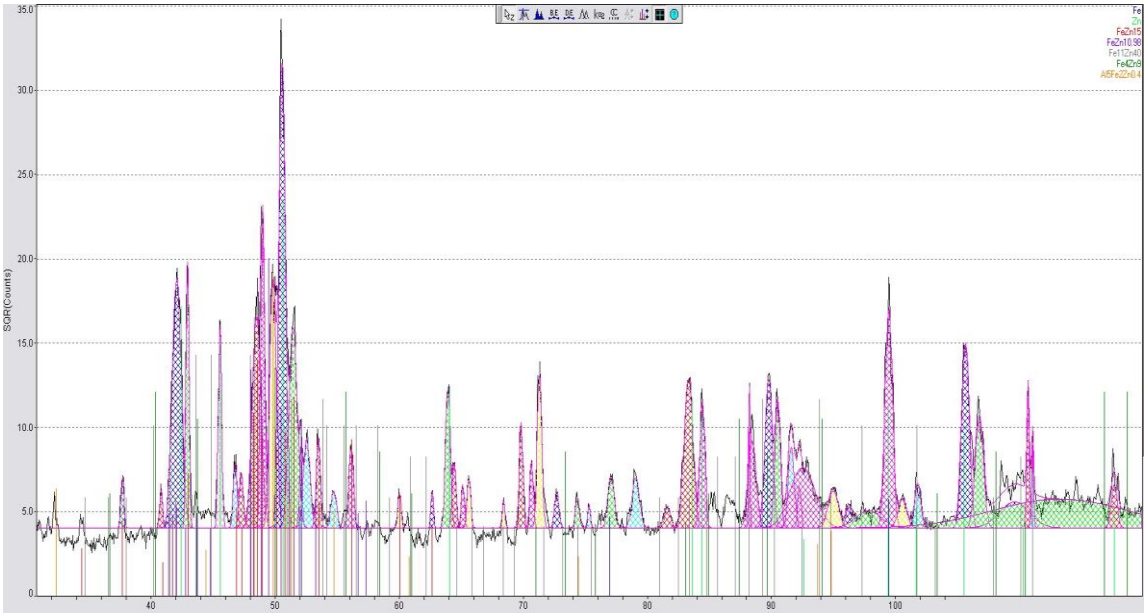

Figure 108: XRD scan of Zn coated steel reaction side after failed brazing

We can see that there are a lot of small and big peaks from XRD scan as compared to before brazing as shown in figure below where only Fe and Zn peaks were observed. These peaks directly give indication for presence of additional IMC and phases are now present after reaction.

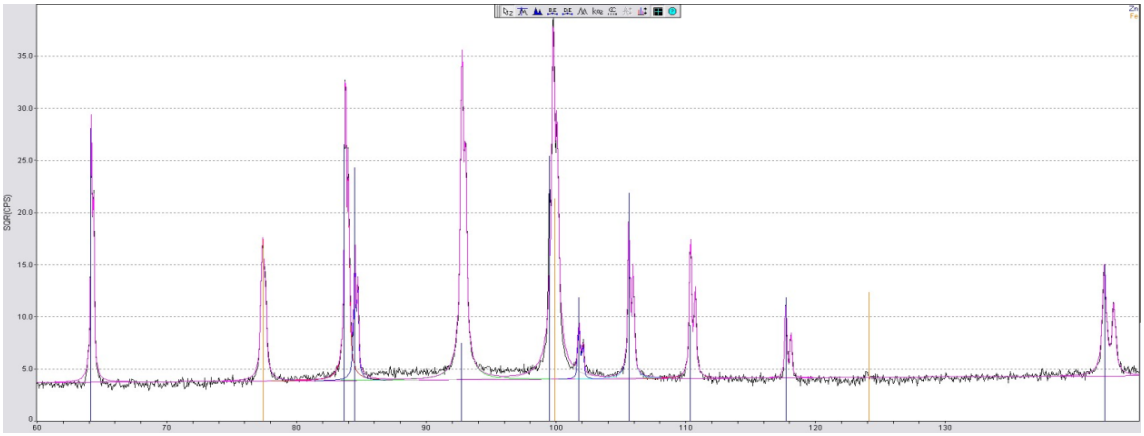

Figure 109: XRD scan of zinc coated steel before brazing.

Pure Zinc is present in high proportion while pure Fe is also present but not as high. Fe formed intermetallic compounds with zinc (FeZn15, FeZn10.98, Fe11Zn40, Fe4Zn9) with different compositions and as supported by EDS scan as well (figure 97). There can also be noted that some other compounds with aluminum (Al5Fe2Zn0.4) are also detected on the surface. These compounds indicate that reaction occurred between liquid zinc and Fe and with Al too; however, either IMC were not strong enough to hold the joint or reaction could not occur homogenously all over the surface.

4.4.2 Phase Detection by XRD for Aluminum

A similar procedure was adopted for aluminum reaction side after it failed to join in brazing operation without flux. After fitting of peaks and consulting chemical library for matching possible combinations of AL, Zn, Fe, and Si, result of the scan is illustrated below.

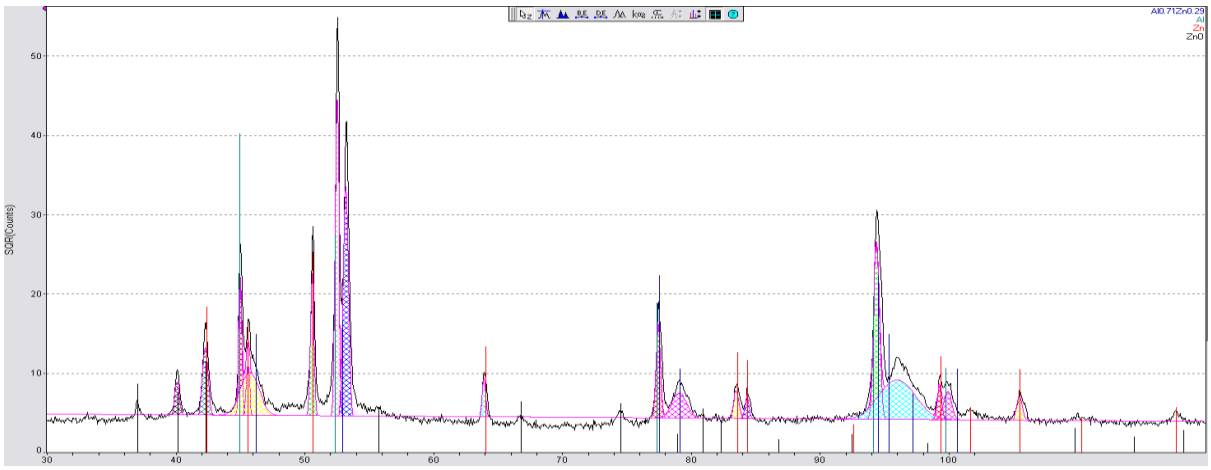

Figure 110: XRD scan of Aluminum reaction side after failed brazing

Some observations can be made after matching peaks with intermetallic phases and pure elements, such as:

- A considerable amount of pure Aluminum is seen which shows not so good reactivity of aluminum with liquid zinc, especially with the lower dwell time used in failed joint. in absence of flux as deduced after optical observations.
- The presence of phase of Aluminum with zinc (Al0.71Zn0.29) shows reaction occurred however it was not uniformly distributed and not strong enough for joining.
- The presence of ZnO although not in huge percentage may also have hindered reactivity between zinc and aluminum.

4.5 Micro Hardness test

Both samples with successful brazed joints after polishing and microscope scans were also tested under micro hardness test. The aim of this test was to reveal trend of hardness and its variation in different zones of reaction due to formation of intermetallic phases. As mentioned before, a load of 25g for 10 sec dwell time was used and resulted values of hardness on HV scale were obtained automatically as software can match the area of indentation with applied load and gives out hardness values. Below results of both samples are discussed separately.

4.5.1 Micro Hardness Test (Sample with Flux)

Results are displayed below when sample with flux was tested under micro hardness test.

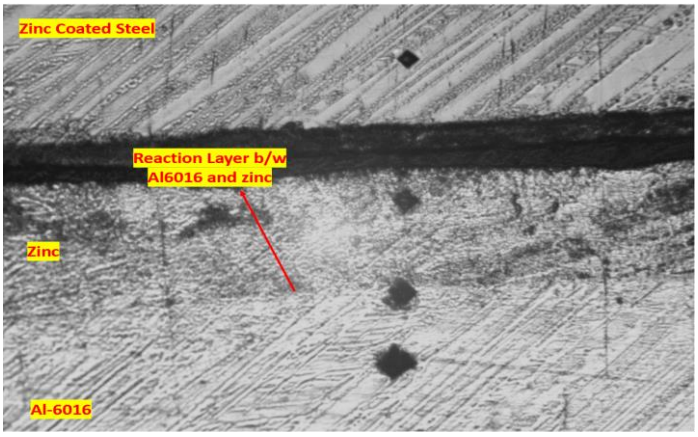

Figure 111: Micro hardness test on sample with flux

Several values were calculated on each section of joint and mean was evaluated and is displayed on the table below.

Region	Area of Indent (µm x µm)	Hardness Value (HV)	Remarks
Steel Side	23	86.1	From base material towards reaction layer side
	23.5	80.6	
	23.5	79.6	
	24	76.1	
	20	107	
	20	109.4	
Zinc Region	20.5	104.3	Higher values seen closer to Steel Side while lower values on Al side
	22	93.6	
	22	92.3	
	23	85.6	
	26.5	64.2	
Aluminum Side	29	54.5	From reaction layer towards base Al side
	24	71.9	
	39	29.1	
	40	28.3	
	41	27.5	
	55	15.2	

Table 9: Micro hardness values for Sample with Flux

Variation of HV value on reaction layers and in brazing alloy region can be explained by the fact that some phases of aluminum and Fe with zinc are present especially at interface layers between base materials. Higher value of reaction layer shows higher hardness values compared to base materials.

4.5.2 Microhardness Test (Sample without Flux)

In the case of sample without flux, similar hardness tests were carried out.

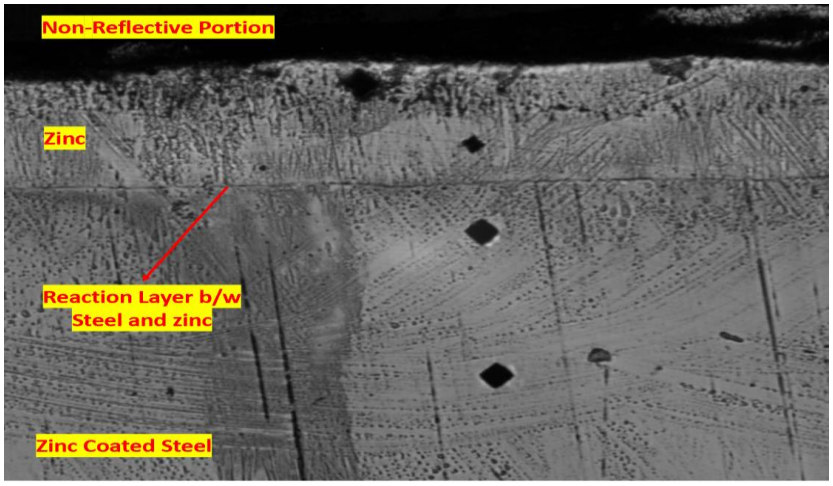

Figure 112: Micro hardness test with sample without flux

Region	Area of Indent (µm x µm)	Hardness Value (HV)	Remarks
Steel Side	25	69.7	From base material towards reaction layer of steel with zinc
	24	74.2	
	22	94.9	
Zinc Region		167.9	A high value of 167.9 was found on steel side in reaction layer
	23	87	
		69.9	
		56.7	
Aluminum Side	37	32.1	From reaction layer towards base Al side
	40	24.4	
	41	22.1	
	42	20.4	

Table 10: Micro hardness test with sample without flux

Similar results were seen in the case of samples without flux with high values of hardness measured on reaction layers with brazing alloy. General trend of hardness is shown in the graph below, higher value of hardness in interface layers is associated with presence of different phases formed due to reaction of liquid zinc with Al and steel.

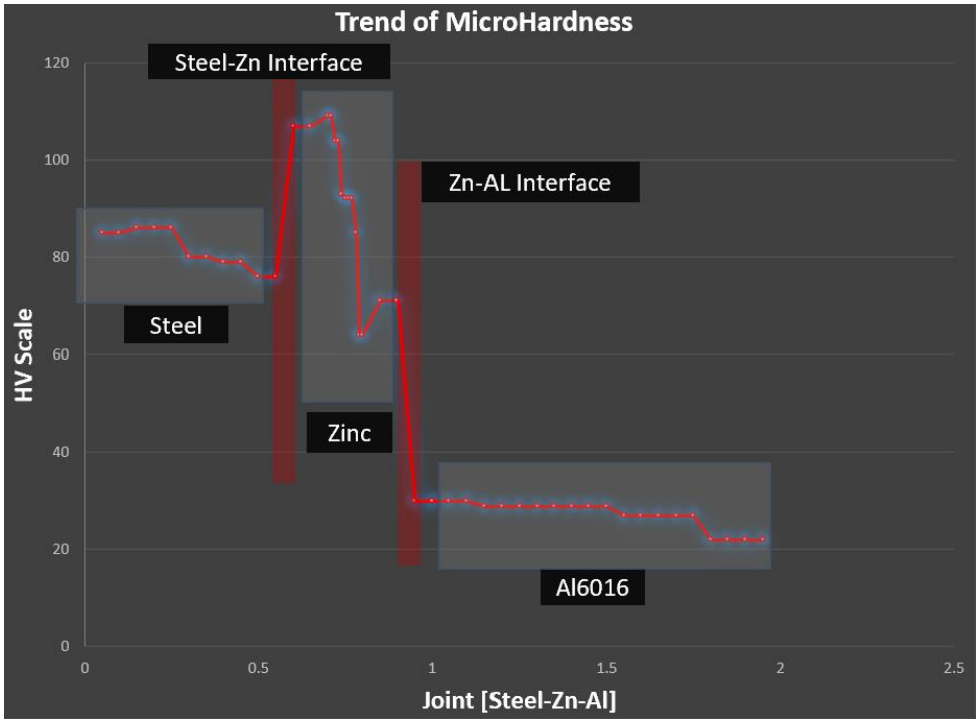

Figure 113: Trend of Microhardness in joining cross section.

Conclusion

Research proposed at the start focused on problems of automotive industry where aluminum alloys are increasingly being used for their strength and weight reduction while steel is still an important choice for some parts of car. To increase fuel efficiency and reduce carbon emissions, weight reduction is necessary which demands studying different techniques which can join aluminum and steel with good joint strength and characteristics.

To contribute to this research, thesis begins with a comprehensive literature review that covers the range of joining technologies (Fusion welding, solid state welding, mechanical joining, and brazing) that are currently being used and explored in joining dissimilar metals especially aluminum and steel. Thesis primarily focuses on brazing technology which uses a brazing alloy to fuse different metals together. Zinc was found as an essential filler material in case of Aluminum and zinc coated steel joining with its own benefits and drawbacks. It works exceptionally well with aluminum, offering a superior wetting surface that strengthens joints. Moreover, it has an high affinity with the zinc layer of zinc coated steel making possible the brazing of these dissimilar materials. On the other hand, Zinc can be volatile, prone to corrosion and can vaporize at high temperature producing toxic fumes and causing possible voids or cracks in the joint.

Major part of this research was extensive experimental work to perform brazing operation on Al-6016 and zinc coated steel using pure zinc as brazing alloy and then analyzing joint characteristics. Experimentation consisted of brazing two sets of joints, one using Al-6 (containing cesium fluoroaluminte) flux on aluminum side while other set was brazed without any flux application. Flux, although beneficial in reducing oxide formations and increasing wetting of the aluminum alloy, it also has adverse effects and can lead to corrosion, thermal decomposition at higher temperatures, residuals on surface, and can be hazardous to environment. These drawbacks called for an investigation into brazing process without use of flux.

After the brazing, samples from both sets were cut transversely and were studied under optical microscopy, Scanning Electron Microscopy and Energy Dispersive Spectroscopy (SEM-EDS), X-Ray Diffractometry (XRD) techniques, Microhardness tests. Conclusion of the experiments is summarized below:

- Liquid zinc reacted both with steel and aluminum at high temperature, joining was achieved in both sets of experiments. However, joining layer investigation revealed non homogeneity of phases and chemical compositions locally, which could indicate different rates of solidification and non-homogeneity of molten material all over the reaction surface.
- Flux applied on aluminum side helped to make continuous interface layer between Aluminum and zinc and thickness of up to 10 µm is observed at some points. Macro inspection of the sample showed local concentration of melted material on periphery of sheets, which could indicate flux when reacted with zinc at high temperature altered its chemical and fluid properties and high liquidity resulted in outward flow of molten material from center to the sides. Zinc coated steel also showed some continuous layers with zinc in some areas only.
- Without flux sample showed continuous interface layer between zinc coated steel and zinc and measured up to 20 µm thickness at some points, although some voids or discontinuities were also observed. Liquid zinc reacted with aluminum causing partially melting, different zinc rich phases with varying composition of aluminum is seen on interface layer between aluminum and zinc.
- SEM-EDS analysis suggested presence of different phases on interface layers in both sets. At some points closer to Al-Zn interface, some percentage of Fe element was seen while aluminum was seen on some parts of interface layer between steel and zinc, this shows that liquid zinc reacted well with both base materials and was able to diffuse into both materials. Some inter-dendritic phases between zinc and aluminum were observed at some areas of Al-Zinc interface in case of no flux. In the case without flux, Zinc layer showed presence of different phases locally some containing all parent elements like Fe, Zn and Al.
- Some discontinuities seen can be attributed to non-alignment of sample sheets which could have resulted in molten material of variable width at different points of surface.
- XRD analysis of residual stresses after the brazing process showed decrease of compressive stresses in aluminum when flux was used, which strongly

indicates presence of good joint between aluminum and steel. Both having different thermal expansion coefficient, aluminum tried to shrink faster but because of joint could not do so, and hence a decrease in compressive residual stresses.

- XRD technique to detect phase constituents on reaction side of both aluminum and steel sheets for one of failed sample (without flux) showed major portion of sheets remain unreacted while some areas showed presence of different phases indicating partial reaction occurred. Dwell time was increased from 7 minutes to 8 minutes which resulted in successful joining.
- The micro-hardness tests conducted on the samples provide a clear picture of the mechanical properties across different zones of the brazed joint. The variation in hardness values, especially at the interface and within the brazing alloy, identifies the formation of different phases due to the reaction between molten zinc, aluminum, and steel.
- Optimal dwell time is 7 minutes with flux while 8 or 9 minutes without flux.
- Flux was more effective in achieving continuous reaction between aluminum and zinc. However, it produces significant residuals in the joining area, and discontinuities have been detected in correspondence of the joining zones with high concentrations of flux constituents. While without flux, zinc coating on steel provided better joining with continuous interface layer between zinc and steel.

The detailed analysis of the interfaces formed through brazing, the exploration of the effects of using flux, and the comprehensive mechanical testing provide valuable information for automotive applications. Thesis lays a foundation for further studies in the area, particularly in optimizing brazing parameters for improved joint strength and durability. The detailed examination of intermetallic compounds, other phase and the evaluation of residual stresses are areas that can be explored further to enhance the understanding of material behavior in dissimilar metal joints.

Bibliography

[1] Mayur Mhapankar. (n.d.). h*ttps://www.aranca.com/assets/uploads/resources/special-reports/Weight-Reduction-Technologies-in-the-Automotive-Industry.pdf*.

[2] Taub, A. I., Krajewski, P. E., Luo, A. A., & Owens, J. N. (2007). The evolution of technology for materials processing over the last 50 years: The automotive example. *JOM*, *59*(2), 48–57. https://doi.org/10.1007/s11837-007-0022-7

[3] Taub, A., De Moor, E., Luo, A., Matlock, D. K., Speer, J. G., & Vaidya, U. (2019). Materials for Automotive Lightweighting. *Annual Review of Materials Research*, *49*(1), 327–359. https://doi.org/10.1146/annurev-matsci-070218-010134

[4] Singh H. (2012). Mass reduction for light-duty vehicles for model years 2017–2025. *DOT HS 811 666, US Dep. Transp.*

[5] Martinsen, K., Hu, S. J., & Carlson, B. E. (2015). Joining of dissimilar materials. *CIRP Annals*, *64*(2), 679–699. https://doi.org/10.1016/j.cirp.2015.05.006

[6] Berger, L. , Lesemann, M. , Sahr, C. , Hart, S. , &, & Taylor, R. (2009). SuperLIGHT-CAR-the multi-material car body. *7th European LS-DYNA Conference (Pp. 1-10).*

[7] F.C. Campbell. (2011). *Joining: Understanding the Basics*. ASM International.

[8] American Welding Society (AWS). (1991). *BRAZING HANDBOOK*. 5th ed Miami(FL): American Welding Society; 2007.

[9] ISO/TC 44. Brazing filler metals (ISO 17672:2016) [Internet]. 3rd ed British Standards Institution; 2016.

[10] R.W. Messler. (2004). *Joining of Materials and Structures: From Pragmatic Process to Enabling Technology*. Butterworth-Heinemann, New York. 790 pages.

[11] Atabaki, M. M., Nikodinovski, M., Chenier, P., Ma, J., Harooni, M., & Kovacevic, R. (2014). Welding of Aluminum Alloys to Steels: An Overview. *Journal for Manufacturing Science and Production*, *14*(2), 59–78. https://doi.org/10.1515/jmsp-2014-0007

[12] U.R. Kattner, In: binary alloy phase diagrams. ASM International, Materials Park, OH, USA (1990).

[13] Meco, S., Pardal, G., Ganguly, S., Williams, S., & McPherson, N. (2015). Application of laser in seam welding of dissimilar steel to aluminium joints for thick structural components. *Optics and Lasers in Engineering*, *67*, 22–30. https://doi.org/10.1016/j.optlaseng.2014.10.006

[14] Song, J. L., Lin, S. B., Yang, C. L., Ma, G. C., & Liu, H. (2009). Spreading behavior and microstructure characteristics of dissimilar metals TIG welding–brazing of aluminum alloy to stainless steel. *Materials Science and Engineering: A*, *509*(1–2), 31–40. https://doi.org/10.1016/j.msea.2009.02.036

[15] Zhang, H., & Liu, J. (2011). Microstructure characteristics and mechanical property of aluminum alloy/stainless steel lap joints fabricated by MIG welding–brazing process. *Materials Science and Engineering: A*, *528*(19–20), 6179–6185. https://doi.org/10.1016/j.msea.2011.04.039

[16] Aslanlar, S.; Ogur, A.; Ozsarac, U.; Ilhan, E. Welding time effect on mechanical properties of automotive sheets in electrical resistance spot welding. Mater. Des. 2008, 29, 1427–1431.

[17] Qiu, R., Iwamoto, C., & Satonaka, S. (2009). Interfacial microstructure and strength of steel/aluminum alloy joints welded by resistance spot welding with cover plate. *Journal of Materials Processing Technology*, *209*(8), 4186–4193. https://doi.org/10.1016/j.jmatprotec.2008.11.003

[18] Rossini, N. S., Dassisti, M., Benyounis, K. Y., & Olabi, A. G. (2012). Methods of measuring residual stresses in components. *Materials & Design*, *35*, 572–588. https://doi.org/10.1016/j.matdes.2011.08.022

[19] T. B. Massalski, H. Okamoto, and P. R. Subramanian, L. Kacprzak, Binary Alloy Phase Diagrams, Second Edition Volume 1, Ohio, ASM International, 1990, pp. 239-241.

[20] Gullino, A., Matteis, P., & D'Aiuto, F. (2019). Review of Aluminum-To-Steel Welding Technologies for Car-Body Applications. *Metals*, *9*(3), 315. https://doi.org/10.3390/met9030315

[21] Sierra, G., Peyre, P., Deschaux-Beaume, F., Stuart, D., & Fras, G. (2007). Steel to aluminium key-hole laser welding. *Materials Science and Engineering: A*, *447*(1–2), 197–208. https://doi.org/10.1016/j.msea.2006.10.106

[22] Fan, J., Thomy, C., & Vollertsen, F. (2011). Effect of Thermal Cycle on the Formation of Intermetallic Compounds in Laser Welding of Aluminum-Steel Overlap Joints. *Physics Procedia*, *12*, 134–141. https://doi.org/10.1016/j.phpro.2011.03.017

[23] Sierra, G., Peyre, P., Deschaux Beaume, F., Stuart, D., & Fras, G. (2008). Galvanised steel to aluminium joining by laser and GTAW processes. *Materials Characterization*, *59*(12), 1705–1715. https://doi.org/10.1016/j.matchar.2008.03.016

[24] Sierra, G., Peyre, P., Beaume, F. D., Stuart, D., & Fras, G. (2008). Steel to aluminium braze welding by laser process with Al–12Si filler wire. *Science and Technology of Welding and Joining*, *13*(5), 430–437. https://doi.org/10.1179/174329308X341852

[25] Tomokatsu Aizawa, Mehrdad Kashani, & Keigo Okagawa. (2007). Application of magnetic puse welding for aluminium alloys and SPCC steel sheets joints. *Welding Journal*, 119–124.

[26] Aizawa, T. (2003). Magnetic pressure seam welding method for aluminium sheets. *Welding International*, *17*(12), 929–933. https://doi.org/10.1533/wint.2003.3199

[27] Akramifard, H. R., Mirzadeh, H., & Parsa, M. H. (2014). Cladding of aluminum on AISI 304L stainless steel by cold roll bonding: Mechanism, microstructure, and mechanical properties. *Materials Science and Engineering: A*, *613*, 232–239. https://doi.org/10.1016/j.msea.2014.06.109

[28] Movahedi, M., Kokabi, A. H., & Seyed Reihani, S. M. (2011). Investigation on the bond strength of Al-1100/St-12 roll bonded sheets, optimization and characterization. *Materials & Design*, *32*(6), 3143–3149. https://doi.org/10.1016/j.matdes.2011.02.057

[29] KAWASE, H., MAKIMOTO, M., TAKAGI, K., ISHIDA, Y., & TANAKA, T. (1983). Development of Aluminum-clad Steel Sheet by Roll-bonding. *Transactions of the Iron and Steel Institute of Japan*, *23*(7), 628–632. https://doi.org/10.2355/isijinternational1966.23.628

[30] Kimapong, K., & Watanabe, T. (2004). Friction stir welding of aluminum alloy to steel. *Welding Journal*, 277.

[31] Chen, Y. C., Gholinia, A., & Prangnell, P. B. (2012). Interface structure and bonding in abrasion circle friction stir spot welding: A novel approach for rapid welding aluminium alloy to steel automotive sheet. *Materials Chemistry and Physics*, *134*(1), 459–463. https://doi.org/10.1016/j.matchemphys.2012.03.017

[32] Haddadi, F. (2016). Microstructure reaction control of dissimilar automotive aluminium to galvanized steel sheets ultrasonic spot welding. *Materials Science and Engineering: A*, *678*, 72–84. https://doi.org/10.1016/j.msea.2016.09.093

[33] Chen, Y.-C., Bakavos, D., Gholinia, A., & Prangnell, P. B. (2012). HAZ development and accelerated post-weld natural ageing in ultrasonic spot welding aluminium 6111-T4 automotive sheet. *Acta Materialia*, *60*(6–7), 2816–2828. https://doi.org/10.1016/j.actamat.2012.01.047

[34] Prangnell, P., Haddadi, F., & Chen, Y. C. (2011). Ultrasonic spot welding of aluminium to steel for automotive applications—microstructure and optimisation. *Materials Science and Technology*, *27*(3), 617–624. https://doi.org/10.1179/026708310X520484

[35] Tsujino, J., Hidai, K., Hasegawa, A., Kanai, R., Matsuura, H., Matsushima, K., & Ueoka, T. (2002). Ultrasonic butt welding of aluminum, aluminum alloy and stainless steel plate specimens. *Ultrasonics*, *40*(1–8), 371–374. https://doi.org/10.1016/S0041-624X(02)00124-5

[36] Acarer, M., & Demir, B. (2008). An investigation of mechanical and metallurgical properties of explosive welded aluminum–dual phase steel. *Materials Letters*, *62*(25), 4158–4160. https://doi.org/10.1016/j.matlet.2008.05.060

[37] Bang, H., Bang, H., Jeon, G., Oh, I., & Ro, C. (2012). Gas tungsten arc welding assisted hybrid friction stir welding of dissimilar materials Al6061-T6 aluminum alloy and STS304 stainless steel. *Materials & Design*, *37*, 48–55. https://doi.org/10.1016/j.matdes.2011.12.018

[38] Mori, K., & Abe, Y. (2018). A review on mechanical joining of aluminium and high strength steel sheets by plastic deformation. *International Journal of Lightweight Materials and Manufacture*, *1*(1), 1–11. https://doi.org/10.1016/j.ijlmm.2018.02.002

[39] Mori, K., Kato, T., Abe, Y., & Ravshanbek, Y. (2006). Plastic Joining of Ultra High Strength Steel and Aluminium Alloy Sheets by Self Piercing Rivet. *CIRP Annals*, *55*(1), 283–286. https://doi.org/10.1016/S0007-8506(07)60417-X

[40] Mori, K., Abe, Y., & Kato, T. (2014). Self-pierce riveting of multiple steel and aluminium alloy sheets. *Journal of Materials Processing Technology*, *214*(10), 2002–2008. https://doi.org/10.1016/j.jmatprotec.2013.09.007

[41] Busse, S., Merklein, M., Roll, K., Ruther, M., & Zürn, M. (2010). Development of a mechanical joining process for automotive body-in-white production. *International Journal of Material Forming*, *3*(S1), 1059–1062. https://doi.org/10.1007/s12289-010-0953-3

[42] Abe, Y., Mori, K., & Kato, T. (2012). Joining of high strength steel and aluminium alloy sheets by mechanical clinching with dies for control of metal flow. *Journal of Materials Processing Technology*, *212*(4), 884–889. https://doi.org/10.1016/j.jmatprotec.2011.11.015

[43] Abe Y, Matsuda A, Kato T, & Mori KI. (2008). Plastic joining of aluminium alloy and high strength steel sheets by mechanical clinching. *Steel Res Int Spec Ed*, 649–657.

[44] Abe Y, Taromaru K, Kato T, & Mori K. (2011). Improvement of joinability in mechanical clinching of sheets using step punch. *Steel Research International*, 667–672.

[45] Hamedon, Z., Mori, K., & Abe, Y. (2014). Hemming for Joining High Strength Steel Sheets. *Procedia Engineering*, *81*, 2074–2079. https://doi.org/10.1016/j.proeng.2014.10.288

[46] Ubertalli, G., Ferraris, M., & Bangash, M. K. (2017). Joining of AL-6016 to Al-foam using Zn-based joining materials. *Composites Part A: Applied Science and Manufacturing*, *96*, 122–128. https://doi.org/10.1016/j.compositesa.2017.02.019

[47] Standards. (n.d.). *Table comparing sandpaper grit standard in Europe and USA*. Https://Www.Mibnet.Se/Home-Improvement/Sandpaper-Grit-Size-Comparison-between-European-and-Us-Standards.Html.

[48] Purdue University. (n.d.). *Scanning Electron Microscope*. https://www.purdue.edu/ehps/rem/laboratory/equipment%20safety/Research%20Equipment/sem.html.

[49] Tan, C., Zang, C., Xia, H., Zhao, X., Zhang, K., Meng, S., Chen, B., Song, X., & Li, L. (2018). Influence of Al additions in Zn–based filler metals on laser welding–brazing of Al/steel. *Journal of Manufacturing Processes*, *34*, 251–263. https://doi.org/10.1016/j.jmapro.2018.06.008

[50] Springer, H., Kostka, A., Payton, E. J., Raabe, D., Kaysser-Pyzalla, A., & Eggeler, G. (2011). On the formation and growth of intermetallic phases during interdiffusion between low-carbon steel and aluminum alloys. *Acta Materialia*, *59*(4), 1586–1600. https://doi.org/10.1016/j.actamat.2010.11.023

[51] Jia, L., Shichun, J., Yan, S., Cong, N., junke, C., & Genzhe, H. (2015). Effects of zinc on the laser welding of an aluminum alloy and galvanized steel. *Journal of Materials Processing Technology*, *224*, 49–59. https://doi.org/10.1016/j.jmatprotec.2015.04.017

[52] Fitzpatrick, M. E., Fry, A. T., Holdway, P., Kandil, F. A., Shackleton, J., & Suominen, L. (2018). Determination of residual stresses by X-ray diffraction. *Measurement Good Practice Guide*.